

STATE OF CALIFORNIA DEPARTMENT OF TRANSPORTATION
TECHNICAL REPORT DOCUMENTATION PAGE
 TR0003 (REV. 10/98)

1. REPORT NUMBER CA18-3023	2. GOVERNMENT ASSOCIATION NUMBER	3. RECIPIENT'S CATALOG NUMBER
4. TITLE AND SUBTITLE Capacities of Pin and Hanger Assemblies, Phase 1	5. REPORT DATE January 2018	6. PERFORMING ORGANIZATION CODE OSU
	7. AUTHOR(S) Jacob Montgomery, Christopher Higgins and Judy	8. PERFORMING ORGANIZATION REPORT NO. OSU / CA18-3023
9. PERFORMING ORGANIZATION NAME AND ADDRESS Oregon State University School of Civil and Construction Engineering 101 Kearney Hall Corvallis, OR 97331	10. WORK UNIT NUMBER	11. CONTRACT OR GRANT NUMBER 65A0608
	12. SPONSORING AGENCY AND ADDRESS California Department of Transportation Engineering Service Center 1801 30 th Street, MS 9-2/5i Sacramento, California 95816 California Department of Transportation Division of Research and Innovation, MS-83 1727 30 th Street, 2 nd Floor Sacramento CA 95816	13. TYPE OF REPORT AND PERIOD COVERED Final Report 1/1/2017 – 12/31/2017
15. SUPPLEMENTAL NOTES Prepared in cooperation with the State of California Department of Transportation.		
16. ABSTRACT Pin and hanger assemblies are a common type of connection used in past engineering practice for steel girder bridges. The connections are considered fracture critical and nonredundant because connection failure can lead to collapse of the bridge. Despite the critical nature of these connections, current specification-based rating methods lack clarity for evaluation of existing bridges. Additionally, inconsistencies exist between different methodologies used in bridge rating and design. In this report a literature review is conducted to identify the available knowledge and experimental data for the elements that comprise pin and hanger connections. Relevant past experimental data are only identified for the hangers plates. The experimental data identified for hanger plates are compared against in-service hangers and found to be of smaller scale but to have similar proportions. The data are used to check the sufficiency of existing evaluation methods and new resistance factors are calibrated for prediction methods consistent with LRFR methods. Recommendations are made in the form of specification changes to improve rating methods for hanger plates and knowledge gaps for the remaining connection components are discussed.		
17. KEY WORDS Pins and Hangers, Hanger Plates, Resistance Factor Calibration	18. DISTRIBUTION STATEMENT No restrictions. This document is available to the public through the National Technical Information Service, Springfield, VA 22161	
19. SECURITY CLASSIFICATION (of this report) Unclassified	20. NUMBER OF PAGES 172	21. PRICE

Disclaimer

This document is disseminated in the interest of information exchange. The contents of this report reflect the views of the authors who are responsible for the facts and accuracy of the data presented herein. The contents do not necessarily reflect the official views or policies of the State of California or the Federal Highway Administration. This publication does not constitute a standard, specification or regulation. This report does not constitute an endorsement by the California Department of Transportation of any product described herein.

For individuals with sensory disabilities, this document is available in Braille, large print, audiocassette, or compact disk. To obtain a copy of this document in one of these alternate formats, please contact: the Division of Research and Innovation, MS-83, California Department of Transportation, P.O. Box 942873, Sacramento, CA 94273-0001.

Capacities of Pin and Hanger Assemblies, Phase 1

Jacob Montgomery, Christopher Higgins, Ph.D., and Judy Liu, Ph.D

School of Civil and Construction Engineering
Oregon State University

January 2018

School of Civil and Construction Engineering
College of Engineering
Oregon State University
Corvallis, OR 97331

ACKNOWLEDGEMENTS

This work was funded by the California Department of Transportation under Contract #65A0608. Thank you to Pavan Patel for his early work on the investigation and implementation of the calibration process.

TABLE OF CONTENTS

	<u>Page</u>
LIST OF FIGURES	5
LIST OF TABLES	8
Chapter 1 – Introduction	10
1.1 Background	10
1.2 Objectives	13
1.3 Organization	14
Chapter 2 – Literature Review	15
2.1 Introduction	15
2.2 Design and Rating Specification Review	16
2.2.1 Standard Specifications	16
2.2.2 AASHTO Rating Methods	28
2.2.3 Alternate Rating Methods	42
2.3 Field Performance and Inspection	52
2.3.1 Askeland, et al. (1987)	52
2.3.2 Kulicki et al. (1990)	54
2.3.3 South et al. (1992)	55
2.3.4 Miller and Chaney (1994)	56
2.3.5 Finch et al. (1994)	56
2.3.6 Juntunen (1998)	57
2.3.7 Jansson (2008)	59
2.3.8 Moore et al. (2004)	60
2.3.9 Discussion	61
2.4 Experimental Studies	62

2.4.1 Hanger Plates.....	62
2.4.2 Pins	82
2.4.3 Beam Ends.....	88
2.5 Materials.....	96
2.5.1 AISC Design Guide 15.....	97
2.5.2 Mechanical and Corrosion Wear of Sliding Interface.....	97
2.6 Literature Review Conclusion.....	100
Chapter 3 – Analysis of Hanger Plate Ultimate Strength Predictions	103
3.1 Introduction.....	103
3.2 Data Review	103
3.3 Caltrans Inventory.....	104
3.4 Failure Modes.....	110
3.5 Review of Caltrans’ Rating Methods.....	112
3.5.1 Caltrans LFR Method.....	113
3.5.2 Caltrans LRFR Method	116
3.6 Analysis by Failure Mode.....	119
3.6.1 Failure Behind the Pin.....	119
3.6.2 Fracture on Net Section.....	124
3.6.3 Dishing	127
3.6.4 Dishing Proportional Limit.....	129
3.7 Discussion	133
Chapter 4 – Calibration of Resistance Factors for LRFR.....	135
4.1 Introduction.....	135
4.2 Load and Resistance as Random Variables.....	135
4.3 Load Variability	137

4.3.1 Load Statistical Properties	137
4.3.2 Load Mean and Standard Deviation	139
4.4 Resistance Statistical Properties	142
4.5 Reliability Index	144
4.6 Monte Carlo Simulation	146
4.7 Calibration Results	149
Chapter 5 – Conclusion and Recommendations	153
5.1 Summary and Conclusions	153
5.2 Recommendations for Future Work	156
References	157
Appendices	162
Appendix A – Historic Steel Specification (Brockenbrough, 2002)	163
Appendix B – Example Calibration Simulation	169

LIST OF FIGURES

<u>Figure</u>	<u>Page</u>
Figure 1-1: Pin and hanger assembly example.	11
Figure 2-1: Hanger plate sections.	20
Figure 2-2: Pin plates at pinned truss joints.....	22
Figure 2-3: AISC hanger diagram (AISC, 2016).....	45
Figure 2-4: Coped beam end geometries (AISC 2017).	47
Figure 2-5: Eurocode general hanger geometry (Eurocode 2005).....	50
Figure 2-6: Type B geometric requirements (Eurocode, 2005).....	51
Figure 2-7: Cracked MoDOT pin removed from service.	53
Figure 2-8: Instrumentation diagram (Juntunen, 1998).	58
Figure 2-9: Quebec bridge hanger specimen.	63
Figure 2-10: Dishing failure (Johnston, 1939).....	64
Figure 2-11: Splitting failure (Blake, 1981).	64
Figure 2-12: Net section failure (Blake, 1981).	64
Figure 2-13: Johnston’s hanger notation (Duerr, 2006).....	66
Figure 2-14: Shear planes for pin tear out.	70
Figure 2-15: Tolbert and Hackett amplification factor.	70
Figure 2-16: Tolbert and Hackett reduction factor.	71
Figure 2-17: Pin tear out failure (Blake, 1981).....	73
Figure 2-18: Accuracy of hanger plate strength predictions (Duerr and Pincus, 1985). ..	74
Figure 2-19: Test setup (Rex and Easterling, 1996).	76
Figure 2-20: Hoblit and Melcon pin load distribution (1953).	83
Figure 2-21: Hoblit and Melcon bearing factor (1953).	84

LIST OF FIGURES (Continued)

<u>Figure</u>	<u>Page</u>
Figure 2-22: Four-point pin load distribution (Blake, 1974).	85
Figure 2-23: Pin interaction equation comparisons (Kulicki, 1983).....	87
Figure 2-24: Example local web buckling (Yam and Chung, 2012).	89
Figure 2-25: Cheng et al., (1984) coped beam notation.	89
Figure 2-26: Example plate girder specimen (Cheng et al., 1984).	91
Figure 2-27: Cheng et al. (1984) test setup.....	92
Figure 2-28: Coped end reinforcement methods (Cheng et al., 1984).....	93
Figure 2-29: Test setup used by Aalberg (2014).	95
Figure 3-1: Thickness of Caltrans' hanger inventory with experimental data.....	105
Figure 3-2: Edge distance behind the pin of Caltrans' hanger inventory with experimental data.	106
Figure 3-3: Effective width of Caltrans' hanger inventory with experimental data.	106
Figure 3-4: Pin Diameter of Caltrans' hanger inventory with experimental data.....	107
Figure 3-5: Ratio of a to D_p of Caltrans' hanger inventory with experimental data.	108
Figure 3-6: Ratio of be to D_p of Caltrans' hanger inventory with experimental data. ..	108
Figure 3-7: Ratio of a to be of Caltrans' hanger inventory with experimental data.	109
Figure 3-8: Yield stress of Caltrans' hanger inventory with experimental data.	110
Figure 3-9: Hanger plate failure modes.	111
Figure 3-10: Ratio of measured and predicted strength for Caltrans LFR methods across all specimens.....	115
Figure 3-11: Ratio of measured and predicted strength for Caltrans' LFR method with non-dishing specimens.....	116

LIST OF FIGURES (Continued)

<u>Figure</u>	<u>Page</u>
Figure 3-12: Ratio of measured and predicted strength for Caltrans' LRFR methods across all specimens.....	117
Figure 3-13: Ratio of measured and predicted strength for Caltrans LRFR methods with non-dishing specimens.....	118
Figure 3-14: Splitting verses shear failure example (Luley, 1942).	120
Figure 3-15: Ratio of measured and predicted strength for failure behind the pin prediction methods.....	123
Figure 3-16: Ratio of measured and predicted strength for fracture on net section prediction methods.....	125
Figure 3-17: Ratio of measured and predicted strength for dishing prediction analysis.	129
Figure 3-18: Effective width to thickness ratios compared to bearing stresses.....	131
Figure 3-19: Dimension behind the pin to plate thickness ratios compared to bearing stresses.	132
Figure 3-20: Normalized dimensions for plate behind pin from Duerr (2006) with bearing stress.....	133
Figure 4-1: Random variable probability density function (PDF).....	137
Figure 4-2: Example reliability index for a normal PDF.....	145
Figure 4-3: Example calibration probability plot using 100,000 simulations.	148
Figure 4-4: Example of best-fit line using lower 5% of data from Monte Carlo simulations.	149

LIST OF TABLES

<u>Table</u>	<u>Page</u>
Table 2-1: Allowable stresses for carbon steel (AASHO, 1931).....	18
Table 2-2: Allowable stresses for carbon steel (AASHO, 1935).....	19
Table 2-3: Material allowable stresses (AASHO, 1941).	19
Table 2-4: Fatigue categories in 1965 AASHO Standard Specifications.	23
Table 2-5: Road types in 1965 AASHO Standard Specifications.	24
Table 2-6: Pin specific steel specifications.	26
Table 2-7: Summary of structural steel specifications.....	27
Table 2-8: Relevant MBE allowable stresses.	30
Table 2-9: Minimum yield stress of pins by year (AASHTO MBE, 2014).....	33
Table 2-10: Performance of capacity equations (Duerr, 2006).....	79
Table 2-11: Dimensional range of collected data.	81
Table 3-1: Range of data for hanger tests corresponding to AAHTO pin hole dimensional tolerances.	104
Table 3-2: Range of Caltrans' reported hanger plate inventory.	110
Table 3-3: Hanger data by failure mode.	112
Table 3-4: Statistics for Caltrans rating methods.....	118
Table 3-5: Example of similarity between splitting and shear failure behind the pin hole (Luley, 1942).....	120
Table 3-6: Splitting specimens compared against splitting and tear out prediction methods.	121
Table 3-7: Tear out specimens compared against splitting and tear out prediction methods.	121
Table 3-8: Statistics for failure behind the pin prediction methods.....	123

LIST OF Tables (Continued)

<u>Table</u>	<u>Page</u>
Table 3-9: Statistics for net section fracture prediction methods.	125
Table 3-10: Relative performance of specimen DP 1-A for alternate rating methods. ..	127
Table 3-11: Statistical results for dishing prediction methods.....	129
Table 4-1: HL-93 statistical live load parameters (Kulicki et al., 2007).	139
Table 4-2: Load statistics used for calibration.....	139
Table 4-3: Resistance statistics used for calibration.....	143
Table 4-4: Calibrated resistance factors for failure behind the pin.....	150
Table 4-5: Calibrated resistance factors for fracture on net section.	150
Table 4-6: Calibrated resistance factors for dishing.	151

Chapter 1 – Introduction

1.1 Background

Between the 1930's and the early 1980's transportation agencies from many states frequently constructed steel girder bridges with a connection detail known as a pin and hanger assembly or connection. These connections were used to connect main bridge girder segments at locations away from piers. Unlike typical girder splices, this detail was designed to allow free girder end rotation and act as a hinge. The geometry of these hinges allowed for longitudinal displacements making it convenient to install a deck expansion joint above them. A typical example of one of these assemblies is shown in Figure 1.1. These assemblies, at a minimum, consisted of two pins and two plates (referred to as hangers or links) connecting the coped ends of two longitudinal bridge girders. The top girder, referred to as the cantilever girder, in these assemblies was designed to be fully supported by adjacent piers. The lower girder, known as the suspended girder, was typically designed to be simply supported by the pin and hanger connection.

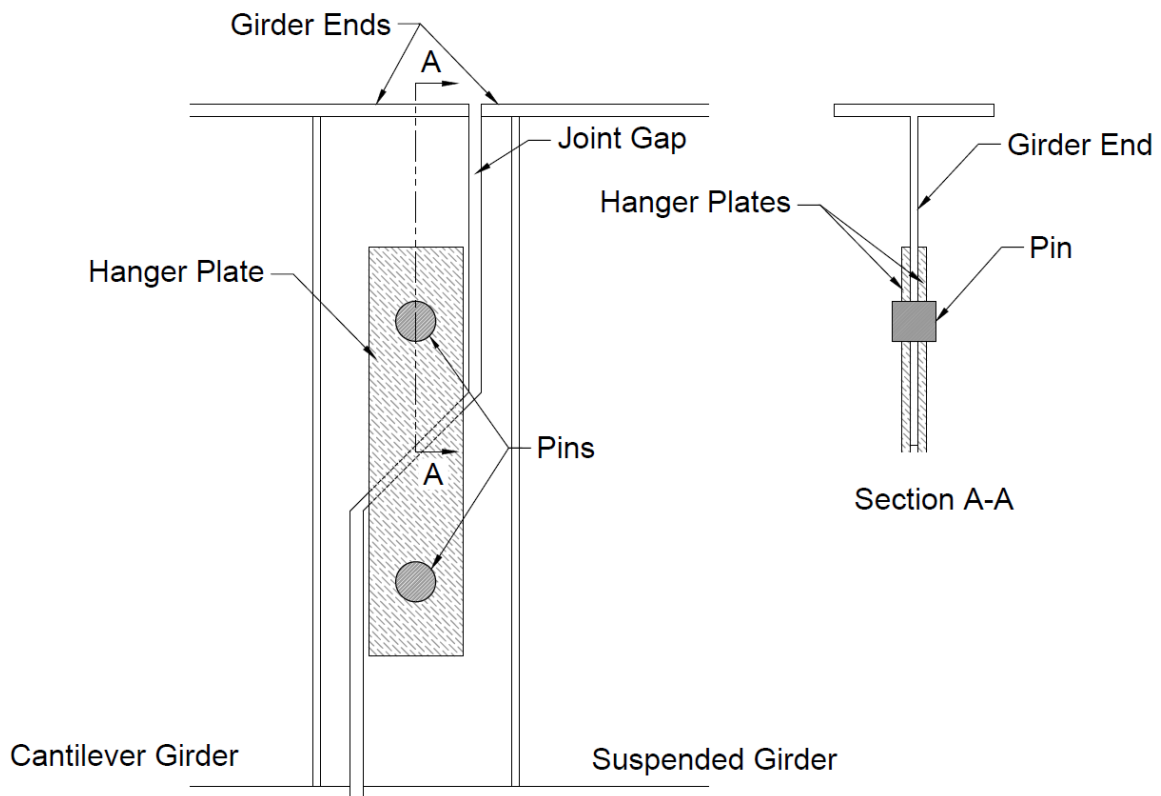


Figure 1-1: Pin and hanger assembly example.

These assemblies came under greater scrutiny after the failure of one of these assemblies led to the 1984 collapse of the Mianus River Bridge in Connecticut. Though this collapse was attributed to poor maintenance rather than insufficient member capacity (NTSB, 1984), it highlighted the hazard these assemblies can pose to the full structure. This hazard is due to the reliance of the suspended girder on this assembly and the lack of redundancy within this assembly. If any one element in this assembly (pin, hanger plate or girder end) fails, the system can fail. This is particularly dangerous in two girder bridges, like the Mianus River Bridge, where these assemblies are fracture critical, meaning that the failure of one element will lead to structural collapse.

Despite the importance of these assemblies, the methods for rating the connection components that comprise them are not always clear or consistent. Historically, there are three different design/rating methodologies allowed by the American Association of State Highway and Transportation Officials (AASHTO). These methods are Allowable Stress Design (ASD), Load Factor Design (LFD) and Load and Resistance Factor Design (LRFD). Of these methods LFD and LRFD are still used for rating, while the majority of pin and hanger bridges currently in service were designed using ASD. When comparing these methods, it is apparent that the treatment of pin and hanger assemblies are inconsistent across the different methodologies. Additionally, when looking at these methodologies individually it is not always clear what checks are required for the purpose of bridge rating.

The California Department of Transportation (Caltrans) has a large inventory of pin and hanger bridges, many of which are fracture critical. In rating their existing bridges, Caltrans has noted the inconsistencies in the different design methodologies and the lack of clarity in rating of pin and hanger assemblies. Caltrans, understanding the importance of these assemblies to the overall performance of a bridge, commissioned this study to clarify the rating methods for these assemblies and to make improvements with existing data, where possible.

1.2 Objectives

This report will describe the first phase of a project for which the ultimate goal is to develop new methods for rating the different components within pin and hanger assemblies. The general objective of this first phase is to conduct a thorough review of the literature on pin and hanger assemblies and to identify what future work is needed to advance rating of pin and hanger connections. There was sufficient information on hanger plates identified in the literature review to conduct a review of current rating methods and resistance factors were calibrated for new and existing hanger plate rating methods that are consistent with the LRFR framework. Below are specific objectives for this research:

- Identify failure modes of different elements of the pin and hanger assemblies
- Identify potential rating methods for the different elements within assemblies
- Collect relevant experimental data from previous studies
- Evaluate the sufficiency of existing rating methods for hanger plates
- Review existing and alternative rating methods against the experimental data for hanger plates
- To the extent possible, calibrate rating methods for hanger plates for use within the AASHTO Load and Resistance Factor framework

1.3 Organization

This report consists of five different chapters with the first being the introduction. The second chapter is a comprehensive literature review. This literature review will be presented in four sections: specifications, field performance, past experimental studies, and historic materials. The next two chapters describe an investigation into capacity prediction and resistance factor calibration for hanger plates. In the final chapter results are summarized and recommendations made for future work.

Chapter 2 – Literature Review

2.1 Introduction

The ultimate goal of this investigation is to provide better bridge rating of existing pin and hanger connection components which includes and extends methods in the present AASHTO LFD, LRFD Bridge Design Specifications, and the AASHTO Manual for Bridge Evaluation (MBE). This literature review was conducted to gain a better understanding of the existing body of knowledge and to guide future investigation. Both historic and current specifications relevant to pin and hanger assemblies were reviewed. The specifications reviewed included the historic editions of the AASHTO Standard Specifications period between 1931 and 1973, the 2011 AASHTO MBE, 2002 AASHTO Standard Specifications and 2014 AASHTO LRFD. Additionally the AREMA Manual for Railway Engineering, the AISC Steel Design Specifications and Eurocode 3 were reviewed. These specifications are not typically used in the United States for highway bridge design but were reviewed to gain insight into alternate design methods. Reports related to the in-service performance of these assemblies were reviewed to identify their typical performance issues. A review of existing nondestructive evaluation methods used to assess the condition of pin and hanger assemblies was conducted. Existing experimental and theoretical studies conducted on hanger plates, pins and girder ends were investigated and their results documented. Finally, additional historic material was reviewed along with the basic principles of wear.

2.2 Design and Rating Specification Review

This section reviews previous design and construction specifications, current specifications for bridge rating, and relevant non-bridge specifications as they relate to pin and hanger assemblies in bridges. This review is intended to improve understanding of the evolution in design and construction of these connections, document available rating methods, and investigate other specification-based design methods that could be applied to pin and hanger assemblies.

2.2.1 Standard Specifications

Since its introduction in 1931 and until the introduction of the AASHTO LRFD Bridge Design Specifications in 1994, the AASHTO/AASHO (the precursor to AASHTO) Standard Specifications for Highway Bridges has been the most influential document for the design of most bridges in the United States. For this review, relevant sections from the construction, design, and material sections of the original 1931 AASHO Standard Specifications (AASHO, 1931) were summarized. The 10 following editions of these same specifications (AASHO, 1935, 1941, 1944, 1949, 1953, 1957, 1961, 1965, 1969, 1973) were then reviewed and the relevant additions and revisions were documented.

2.2.1.1 Review of AASHO Construction Sections

In the construction section of the 1931 edition of the AASHO Standard Specifications, requirements were provided for both the fabrication of pins and pin holes. Pins were specified to be turned smooth and free of flaws, all pins over 7 in. diameter were required to be forged and annealed. Any pins over 9 in. diameter were specified to have holes no less than 2 in. diameter drilled through their centers. Holes for pins in pin connected members were required to be bored to the specified diameter with the final surface produced by a finishing cut. The distance from outside to outside of pin holes in tension members was not to vary from the specified dimension by more than $1/32^{\text{th}}$ in. Pin holes were allowed to be oversized by a maximum of $1/50^{\text{th}}$ in. for pins 5 in. diameter and smaller, and $1/32^{\text{th}}$ in. for pins larger than 5 in.

In 1957, the article describing pin fabrication was altered to require all pins under 7 in. diameter to be either forged and annealed or made out of cold finished carbon steel shafting. All pins over 7 in. diameter were still required to be forged and annealed. Then in 1969, this article increased the allowable diameter for non-forged pins from 7 in. to 9 in. In 1959, roughness requirements for the surfaces of pins and pin holes were standardized to comply with American Standards Association (ASA) 125. This roughness level was described in ASA B 46.1-55. In 1969, this requirement was revised to United States of America Standards Institute (USASI) 125 and then again to American National Standards Institute (ANSI) 125, both referencing B46.1.

2.2.1.2 Review of AASHO Design Sections

The design section of the 1931 edition of the AASHO Standard Specifications gives provisions for the design of pins, pin connected members, and pin plates. Additionally, this section provides allowable stresses (F_a) for use in the design of elements. In 1931, the only structural steel for which allowable stresses were provided was carbon steel (ASTM A7). In this specification, different allowable stresses were given for dead load and live load, with the allowable stress for live load being $2/3$ that for dead load. Table 2.1 provides relevant prescribed allowable stresses applicable to pin and hanger assemblies. It is noted in these specifications that the allowable stresses for cast steel were to be $3/4$ of that for structural steel.

Table 2-1: Allowable stresses for carbon steel (AASHO, 1931).

	Live Load (psi)	Dead Load (psi)
Axial Tension/Net section	16,000	24,000
Stress in extreme fiber of pins	24,000	36,000
Shear in pins	12,000	18,000
Bearing on pins	24,000	36,000
Shear in Girder Web Gross Section	10,000	15,000

In the 1935 edition of the AASHO Standard Specifications, the allowable stresses (F_a) are simplified to eliminate the differing allowable stresses for live load and dead load. These simplified allowable stresses are shown in Table 2.2.

Table 2-2: Allowable stresses for carbon steel (AASHO, 1935).

	F_a (psi)
Axial Tension/Net section	18,000
Stress in extreme fiber of pins	27,000
Shear in pins	13,500
Bearing on pins	27,000
Shear in Girder Web Gross Section	11,000

In 1941, the allowable stress for pin bearing is broken into two categories: non-rotating pins and rotating pins. The pins subject to rotation had lower allowable stresses. These new allowable stresses are shown in Table 2.3 for the three structural steels included in the specifications at the time. In this same year, the cast steel allowable stresses were amended so that the allowable stresses for compression and bearing were equal to carbon structural steel. All other allowable stresses for cast steel remained at $\frac{3}{4}$ that of carbon structural steel.

Table 2-3: Material allowable stresses (AASHO, 1941).

	Carbon Steel		Silicon Steel		Nickel Steel	
	F_a/F_y	F_a (psi)	F_a/F_y	F_a (psi)	F_a/F_y	F_a (psi)
Axial Tension/Net section	0.55	18,000	0.53	24,000	0.55	30,000
Stress in extreme fiber of pins	0.82	27,000	0.80	36,000	0.80	44,000
Shear in pins	0.41	13,500	0.40	18,000	0.40	22,000
Bearing on pins	0.73	24,000	0.71	32,000	0.73	40,000
Bearing on pins subject to rotation	0.36	12,000	0.36	16,000	0.33	18,000

For pin design, the 1931 AASHO Specification states that pins are to be sized to resist the shear and moment produced by the connected members. In the section “net section at pin holes,” the region around the pin hole was to be sized based on the net section away from the pin hole (Section A-A in Fig. 2-1) for design of pin-connected riveted tension members. The net section across the pin hole (Section B-B in Fig. 2-1) was not to be less than 140% of the net Section at A-A. Additionally, the net section beyond the pin hole (Section C-C in Fig. 2-1) was not to be less than 100% of the net section at Section A-A. In 1941, a new requirement was added to this provision specifying that the ratio between a member’s net width (taken along Section B-B from Fig. 2-1) and thickness was not to exceed 8. In the 1949 edition, the reference to rivets in this provision was removed.

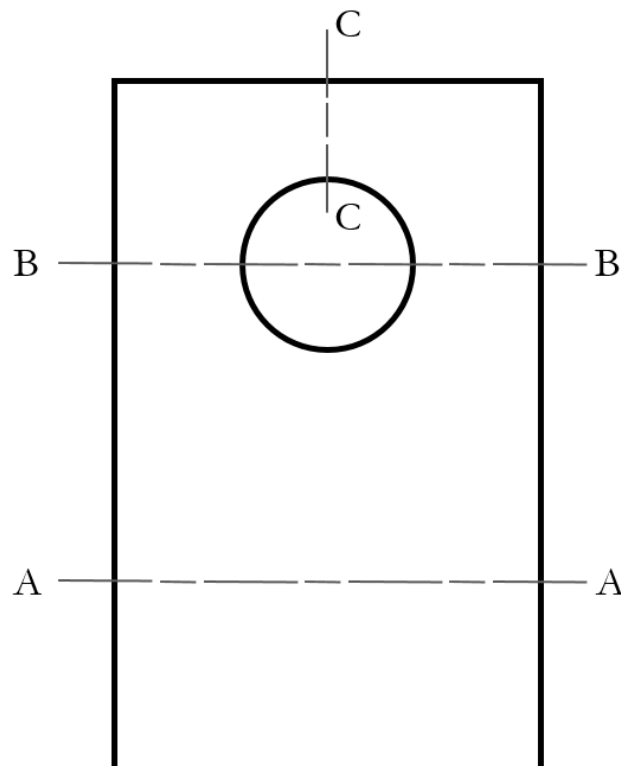


Figure 2-1: Hanger plate sections.

The 1931 edition of the AASHO Standard Specifications mandated that bearing stress was to be calculated using the effective bearing area of the pin. This effective bearing area was determined by multiplying the diameter of the pin by the thickness of the connected member in bearing. The 1965 edition clarified that when the pin and the connected member were made of different materials, the allowable bearing stress would be controlled by the material with the lower allowable bearing stress.

The specifications allowed, when necessary to obtain the required section or bearing area, the installation of symmetric pin plates on the connected members. These plates were to be as wide as any outstanding flanges on the member, if the member was built-up and had angles for flange elements, then at least 1 pin plate was required to cover the vertical legs of the flange angles. Pin plates were to be connected to the main element with enough rivets to transmit the bearing forces applied by the pin. These rivets were to be placed to uniformly distribute this load over the full section. In the 1941 edition, the reference to flange angles was removed. A new requirement was added that prescribed at least one of the full-width pin plates extend to the far edge of the stay plate and the remainder of the pin plates extend not less than 6 in. beyond the stay plate's near edge.

The applicability of the above pin plate provisions to the pin plates often used in pin and hanger assemblies is not clear. Only the rivet requirements appear applicable. The provisions appear more relevant to pin plates found on pin connected trusses, as illustrated in Fig. 2-2.



Figure 2-2: Pin plates at pinned truss joints.

Fatigue design was introduced in the 1965 AASHTO Standard Specifications. The fatigue provisions imposed an allowable fatigue stress on bridge elements subject to repeated variations, or reversals, of stress. The allowable fatigue stress was given as:

$$F_r = \frac{k_1 f_{ro}}{1 - k_2 R} \quad [2 - 1]$$

where k_2 and f_{ro} (psi) were tabulated values that depended on the element category, stress type and number of load cycles, R was the ratio between the minimum and maximum stress seen by the member and k_1 was given as:

$$k_1 = 1.0 + \alpha \left(\frac{F_u}{58,000} - 1 \right) \geq 1.0 \quad [2 - 2]$$

where F_u was the members ultimate strength (psi) and α was a tabulated value that depended on the element category, stress type, and number of load cycles. Of the element categories given and stress types provided by the provision, the most applicable for pin and hanger assemblies was category C, base metal adjacent to bearing type fasteners in tension, and category I, bearing type fasteners in shear. These two categories were applicable to hangers and pins, respectively. For both of these categories α was equal to zero, so F_r can be simplified to:

$$F_r = \frac{f_{ro}}{1 - k_2 R} \quad [2 - 3]$$

f_{ro} and k_2 for categories C and I are given in Table 2.4. These values varied depending on the number of stress cycles seen by the member. For design purposes, the number of cycles was based on the type of loading inducing the maximum stress and the type of road being considered. The tabulated cycle numbers provided by the specifications are shown in Table 2.5.

Table 2-4: Fatigue categories in 1965 AASHTO Standard Specifications.

Category	Maximum Stress Type	100,000 Cycles		500,000 Cycles		2,000,000 Cycles	
		f_{ro}	k_2	f_{ro}	k_2	f_{ro}	k_2
C	Tension	20,500	0.55	17,200	0.62	15,000	0.67
I	Shear	F_v	0.50	13,500	0.50	11,200	0.50

Table 2-5: Road types in 1965 AASHO Standard Specifications.

Case	Type of Road	0-14' incl. (H Loading)	14' to 44' incl. (HS Loading)	Over 44' (Lane Loading)
I	1. Freeways 2. Expressways 3. Major Highways and Streets	2,000,000	500,000	100,000
II	Other Highways and Streets not included in Case I	500,000	100,000	100,000

In the 1973 edition, Load Factor Design (LFD) was introduced as an alternative design methodology to Allowable Strength Design (ASD). This design methodology used similar design provisions to the Allowable Stress Design but substituted yield stress for the allowable stresses and then used load factors to amplify the service loads. There were no specific provisions for pins or pin connected members in the LFD portion of the AASHO Standard Specifications.

2.2.1.3 Review of AASHO Material Sections

The 1931 edition of the AASHO Standard Specifications provided for the use of three (3) material specifications for the fabrication of pins: ASTM A7 structural carbon steel, ASTM A20 Carbon Steel Forgings, and ASTM A27 Carbon Steel Castings, Class B medium grade.

In the 1935 edition, references to ASTM A20 and A27 were eliminated. These references were replaced with expanded steel forging and steel casting material sections that included fabrication and testing requirements. The forging section required minimum

tensile and yield strengths of 60 ksi and 33 ksi, respectively. The casting section required minimum tensile and yield strengths of 70 ksi and 38 ksi, respectively.

In the 1941 edition, silicon (ASTM A94) and nickel (ASTM A8) steel were introduced as alternatives to carbon structural steel. The maximum thicknesses of 1 1/8 in. and 1 in. were set for silicon and nickel steel plates, respectively. In the allowable stress section for both of these steels, allowable stresses were provided for pins. The steel forgings material section of this edition added a reference to ASTM A235 Class C1. In the casting section, the reference to ASTM A27 Grade B-1 for carbon steel castings returned and the reference to ASTM A221 Class A for chromium alloy steel castings was added. The fabrication and testing requirements, added in the previous edition, for forgings and castings were removed.

In the 1949 edition, the ASTM Specification for chromium alloy steel castings was changed to ASTM A296, grade 10 and the grade for carbon steel castings was changed to Grades 65-35. Additionally, structural low-alloy steel (ASTM A242) was introduced with the maximum thickness of 1 1/8 in. specified for steel plates. Allowable stresses for up to 2 in. thick material were provided, these allowable stresses included those for pins. In the following edition (1953), the allowable stresses for pin shear and bending were removed from the low alloy steel section.

In the 1957 edition, pin shear and bending returned and the allowable stresses for low alloy steel and the restriction on plate thickness were removed. In this same edition, cold-finished steel shafting (ASTM-A108/AASHO M169) (grades 1016-1030) was added as a permissible pin material specification for pins under 7 in. diameter. Cold finished

steel shafting was required to have a minimum Rockwell Scale B hardness of 80 or minimum tensile strength of 66 ksi and yield strength of 33 ksi was required.

In the 1961 edition, ASTM A440 and A441 were added as optional low alloy steel specifications. Allowable stresses were provided for both materials up to 4 in. thick, including allowable stresses specific to pins. Allowable stresses were provided for A441 up to 8 in. but stresses for pins were not provided for these thicker sections.

In the 1965 edition, silicon steel, nickel steel and A7 steel were removed from the specifications. ASTM A36 low carbon structural steel was added, complete with allowable stresses for pins. Additionally, a new material section specific to pins, rollers and expansion rockers was created. This new section included all of the material specifications shown in Table 2.6. It was noted that pins may conform to one of these specifications in addition to those listed in the structural steel section.

Table 2-6: Pin specific steel specifications.

Specification (ASTM #) (Year Added)	Restrictions	F_y (psi)
Carbon Steel Forgings (ASTM A235-C1) (1941)	Dia. \leq 20"	33,000
Cold Finished Carbon Steel Bars (ASTM A108) (1957)	Dia. \leq 7"	36,000*
Cold Finished Carbon Steel Bars (ASTM A108) (1965)**	Dia. \leq 9"	50,000
Carbon Steel Forgings (ASTM A235-E) (1965)	Dia. \leq 20"	37,500
Carbon Steel Forgings (ASTM A235-G) (1965)	Dia. \leq 10"	50,000
Alloy Steel Forgings (ASTM A237-A) (1965)	Dia. \leq 20"	50,000

*Minimum yield strength required only if minimum Rockwell Scale B Hardness of 80 was not met.

**Revised cold finished carbon steel bar specification. No Rockwell Scale B Hardness Requirements.

In the 1969 edition of the AASHTO Standard Specifications, high yield strength quenched and tempered alloy steel was introduced (ASTM A514 and A517). Allowable stresses for this material were given for material up to 4 in. thick, including for pin specific allowable stresses. Additionally, new ASTM specifications A572 and A588 were added to the low alloy steel section. ASTM A588 and ASTM A572 provide allowable stresses for material up to 8 in. and 4 in. thick respectively. Allowable stresses were provided for pins. Table 2.7 provides a summary of the material specifications allowed by the AASHTO Standard Specifications during the period reviewed. Appendix A provides a more detailed summary of the specification in Tables 2.6 and 2.7.

Table 2-7: Summary of structural steel specifications.

Steel Specification (ASTM #) (Time Range)	F_y (psi)	F_u (psi)
Structural Carbon Steel (ASTM A7) (1931)	30,000	55,000
Structural Carbon Steel (ASTM A7) (1935-1961)	33,000	60,000
Structural Silicon Steel (ASTM A94) (1941-1961)	45,000	70,000
Structural Nickle Steel (ASTM A8) (1941-1961)	55,000	90,000
Structural Carbon Steel (ASTM A36) (1965)	33,000	60,000
High Strength Low Alloy Steel (ASTM A242) (1949), (ASTM A440/A441) (1961), (ASTM A572/A588) (1969)	42,000 - 50,000	63,000 - 70,000
High Yield Strength Quenched & Tempered Alloy Steel (ASTM A514/A517) (1969)	90,000 - 100,000	105,000 - 115,000

2.2.2 AASHTO Rating Methods

The 2011 AASHTO Manual for Bridge Evaluation (MBE) with interim revisions through 2016 (AASHTO, 2011) provides current rating methods for existing bridge elements. The MBE uses Rating Factors (RF) to describe whether a bridge has sufficient capacity to carry a given rating load. The equation for this rating factor depends on the rating methodology used. A general rating equation can be described by:

$$RF = \frac{C - \sum(\gamma_p * PL)}{\gamma_{LL}(LL + IM)} \quad [2 - 4]$$

where C is the capacity of the bridge (controlled by its weakest member), PL are the permanent loads, LL is the live load, IM is the impact loading and γ_p & γ_{LL} are load factors whose values vary based on rating method and type of permanent load. If a bridge has a rating factor greater than 1, it has sufficient capacity to carry the load for which it is being rated. While both capacity and load effects influence rating, the focus of this review is on resistance models.

The MBE allows rating to be performed using one of three methodologies, allowable stress rating (ASR), load factor rating (LFR) and load and resistance factor rating (LRFR). In this section, the rating provisions for pin and hanger assemblies for these three rating methodologies will be reviewed. The MBE acts as a companion document to the design specifications, providing addendums to design provisions, when necessary, to make them applicable for rating. For this reason, the applicable design codes for each of these methodologies will be referenced in tandem with the MBE in this review. In addition to the national design specifications, the LFR rating method using Caltrans' Bridge Design Specifications will be summarized for future comparison.

In general, there are two levels for which a bridge can be rated: inventory or operational. Inventory corresponds to a higher level of reliability equal to that of design, while the operational level rating is less conservative but generally considered acceptable. ASR achieves these different rating levels by providing allowable stresses equal to design levels for inventory rating and increased allowable stresses for operational rating. Alternatively, LFR and LRFR achieve this difference in rating level by decreasing load factors for operational rating.

2.2.2.1 ASD (2002 AASHTO Standard Specifications & 2011 MBE)

Allowable strength design (ASD), also referred to as working stress design (WSD), was the first design methodology employed by AASHTO for bridge design and rating. The most current specifications for design and rating using this methodology are the 17th edition of the AASHTO Standard Specifications for Highway Bridges (AASHTO, 2002) and the 2nd edition of the AASHTO Manual for Bridge Evaluation (AASHTO, 2011) respectively. When using ASD, the stress in an element, at service level loads is limited to an allowable stress. Some relevant allowable stresses at inventory and operational reliability levels are reported in Table 2-8.

Table 2-8: Relevant MBE allowable stresses.

	Operational	Inventory/Design
Axial Tension (no holes or open holes greater than 1 ¼")	$0.75F_y$	$0.55F_y$
	$0.60F_u$	$0.46F_u$
Axial Tension on Net Section (for riveted/bolted members)	$0.67F_u$	$0.50F_u$
Stress in extreme fiber of pins	$0.90F_y$	$0.80F_y$
Shear in pins	$0.55F_y$	$0.40F_y$
Bearing on pins	$0.90F_y$	$0.70F_y - 0.80F_y$
Bearing on pins subject to rotation	$0.55F_y$	$0.33F_y - 0.40F_y$
Shear on Gross Section	$0.45F_y$	$0.33F_y$

2.2.2.1.1 Pin Rating

The ASD section of the MBE does not address rating of pins. Therefore, the design specification given in the AASHTO Standard Specification are used for rating of these elements. The design provisions for pins has remained essentially unchanged since 1931. Article 10.25.3 of the AASHTO Standard Specifications simply states that pins are to be sized for the maximum shear and moment produced by the connected members.

2.2.2.1.2 Hanger Plate Rating

The rating of hanger plates is not specifically addressed in the ASD portion of the MBE, and the design specifications for hangers have not seen any consequential change since 1949. The design provisions provided in article 10.25.1 of the AASHTO Standard Specifications rely on dimensional requirements for hanger plate design.

2.2.2.1.3 Bearing Rating

AASHTO Standard Specification Article 10.32.4 prescribes allowable bearing stresses to the connection elements (plates and pins). The bearing stresses were shown in Table 2-8.

2.2.2.1.4 Girder End Rating

The only guidance provided in the AASHTO Standard Specification for design or rating of coped girder ends such as those of pin and hanger assemblies is a general note in Article 10.12. This article states that all flexural elements are to be designed using the moment of inertia method. The complex nonuniform stress distributions in the girder ends from the concentrated pin loading makes application of flexural and shear design provisions and their interactions uncertain.

2.2.2.2 LFD (2002 AASHTO Standard Specifications & 2011 MBE)

The Load Factor Design (LFD) methodology was added to the AASHTO Standard Specifications in 1973, Similar to the ASD method the most current guidance for this methodology is provided in the 17th Edition of the AASHTO Standard Specifications (AASHTO, 2002) and the 2011 MBE (AASHTO, 2011). In this method, members are designed to ultimate capacity and the design loads are increased beyond service levels. Ultimate capacity design is accomplished in general by substituting the allowable stress from ASD with the material yield stress. In addition to this general rule, specific provisions are given for areas of design where this increase in stress is not

sufficient to capture the ultimate limit state of a member. The LFD/LFR portions of the MBE and AASHTO Standard Specifications do not provide any specific provisions for the design of pins, hangers or their bearing. New provisions are provided for design of shear in girders in Article L6B2.2 of the MBE which states that Article 10.48.8.1 of the AASHTO Standard Specifications is to be used.

2.2.2.3 LRFD (2014 AASHTO LRFD & 2011 MBE)

In 1994, AASHTO adopted the load and resistance factor design (LRFD) method as an alternative to the LFD and ASD methods presented in the AASHTO Standard Specifications. The most recent version is the 7th Edition of the AASHTO LRFD Bridge Design Specifications (AASHTO, 2014). The LRFR portion of the MBE uses much of the AASHTO LRFD provisions and applies factors to both the member resistances and the load effects to establish rating factors for bridge components. Additionally, in this section Caltrans' current LRFR rating methods will be reviewed were appropriate.

2.2.2.3.1 Pin Rating

Article 6A.6.12.4 of the MBE specifies that pins are to be checked for combined flexure and shear as specified in the ASHTO LRFD Specifications. AASHTO LRFD uses plastic analysis to calculate the ultimate capacity of pins in shear and bending. To do this Article 6.7.6.2.1 of the AASHTO LRFD Specifications specifies pin capacity to be checked using the interaction equation

$$\frac{6M_u}{\phi_f D^3 F_y} + \left(\frac{2.2V_u}{\phi_v D^2 F_y} \right)^3 \leq 0.95 \quad [2 - 5]$$

where D is the pin diameter (in), M_u and V_u are the factored moment and shear load effects due to factored loads (kip-in and kips respectively) and F_y is the pin material yield stress (ksi). ϕ_f and ϕ_v are resistance factors for shear and flexure respectively, both of which are equal 1.0.

Additionally, Article 6A.6.2.2 of the MBE provides minimum pin strength based on year of construction as shown in Table 2-9.

Table 2-9: Minimum yield stress of pins by year (AASHTO MBE, 2014).

Year of Construction	Minimum Yield Point, F_y , ksi
Prior to 1905	25.5
1905 through 1935	30
1936 through 1963	33
After 1963	36

2.2.2.3.2 Hanger Rating

The LRFR section of the AASHTO MBE furnishes 3 provisions in Section 6A.6.6.1 for the rating of hangers. The first two provisions are the similar to those provided by the ASD specification requiring 140% and 100% of the net area away from the hole, across the hole (perpendicular to the load) and beyond the hole, respectively. The third provision specifies a proportional reduction of the net area used for capacity calculations if one of the first two provisions is not met.

Article 6A.6.6 of the MBE specifies that members and splices subject to axial tension are to be checked against Article 6.8.2 of the AASHTO LRFD Design Specifications. Article 6.8.2 of the AASHTO LRFD Design Specifications requires members to be checked for tensile yield as:

$$P_r = \phi_y F_y A_g \quad (kips) \quad [2 - 6]$$

and tensile rupture as:

$$P_r = \phi_u R_p U F_u A_n \quad (kips) \quad [2 - 7]$$

where A_g is the gross section area in tension (in.²), A_n is the net section area in tension (in.²) and U is the shear lag reduction factor. ϕ_y and ϕ_u are the tension yield and fracture resistance factors and are equal to 0.95 and 0.80 respectively. The specifications require that, when determining the gross section area, holes larger than those typically used for bolts are to be deducted. The commentary confirms that this includes pin holes.

Based on Caltrans interpretation of these articles, two rating checks are performed. The first checks for yield on the section across the pin, this check is the same as that shown in equation 2-6 with the gross area taken as the full cross-section of the hanger minus cross-sectional area of the pin hole. The next check used by Caltrans combines the dimensional requirements described in Section 6A.6.6.1 of the MBE and the tensile rupture check shown equation 2-7 the produce:

$$P_r = \phi_u W_e t F_u \quad (kips) \quad [2 - 8]$$

were W_e , the effective section, is given by the lesser of:

$$W_e = \frac{2b_e}{1.4} \quad (\text{in}) \quad [2 - 9]$$

$$W_e = a \quad (\text{in}) \quad [2 - 10]$$

2.2.2.3.3 Bearing Rating

Article 6A.6.12.4 of the MBE specifies that pins are to be checked for bearing according to Article 6.7.6.2.2 of the AASHTO LRFD Specifications as:

$$(R_{pB})_n = 1.5tD_pF_y \quad (\text{kips}) \quad [2 - 11]$$

and

$$(R_{pB})_r = \phi_b(R_{pB})_n \quad (\text{kips}) \quad [2 - 12]$$

to describe the factored pin bearing resistance where t is the thickness of the connected member (in.), D_p this the pin diameter (in.) and the bearing resistance factor, ϕ_b , is equal to 1.0. In the commentary, the coefficient of 1.5 is allowed to be halved to 0.75 for the design of new pins subject to significant rotation in order to account for wear over the life of the pin. This provision mimics the reduced bearing stress allowed for pins subject to rotation in the original ASD methodology. The commentary states that only the 1.5 coefficient should be used for the rating of existing pins regardless of pin rotation.

Additionally, Article 6.8.7.2 of the AASHTO LRFD design specifications states that the nominal bearing of a pin plate is computed as:

$$P_r = \phi_b P_n = \phi_b A_b F_y \quad (\text{kips}) \quad [2 - 13]$$

where F_y is the yield stress of the plate (ksi) and A_b is the projected bearing area of the pin on the plate (in^2) and is given by:

$$A_b = D_p t \quad (\text{in}^2) \quad [2 - 14]$$

where t is the thickness of the connected plate (in.), D_p this the pin diameter (in.).

2.2.2.3.4 Connection Rating

The AASHTO LRFD Specifications contain two additional provisions for design of connections that could be applicable to rating pin and hanger assemblies. The first provision is for block shear tear out and the second is for shear yield and rupture. The provision for block shear is contained in Article 6.13.4 of AASHTO LRFD Specifications which requires web connections of coped beams and tension elements to be checked for block shear capacity as:

$$R_r = \phi_{bs} R_p (0.58 F_u A_{vn} + U_b F_u A_{tn}) \leq \phi_b R_p (0.58 F_y A_{vg} + U_b F_u A_{tn}) \quad (\text{kips}) \quad [2 - 15]$$

where F_u is the tensile strength of the connected material (ksi), F_y is the yield strength of the connected material (ksi), A_{vg} is the gross area of the connected member along the assumed failure path in shear (in^2), A_{vn} is the net area of the connected member along the assumed failure path in shear (in^2), A_{tn} is the net area of the connected member along the assumed failure path in tension (in^2), U_{bs} is a capacity reduction factor that is to be set to 0.5 for non-uniform tensile stress and 1.0 otherwise, R_p is a reduction factor that is to be set to 0.9 if the connector holes were punched full size and 1.0 otherwise and ϕ_b is the resistance factor for block shear and equal to 0.80. When calculating block shear

capacity, all possible failure paths through the connection should be considered. All portions of the failure surface parallel to the load are assumed to be in shear and all those perpendicular to the load are assumed to be in tension.

Article 6.13.5.3 of AASHTO LRFD Design Specifications requires connection elements to be checked for shear yield as:

$$R_r = \phi_v 0.58 F_y A_{vg} \quad (\text{kips}) \quad [2 - 16]$$

and shear rupture as:

$$R_r = \phi_{vu} R_p 0.58 F_u A_{vm} \quad (\text{kips}) \quad [2 - 17]$$

where the resistance factors ϕ_v and ϕ_{vu} equal 1.0 and 0.80 respectively.

Caltrans applies both of these methods in the rating of the hanger plates and the girder ends. For the hanger plates shear yield (Eqn 2-16) and shear rupture (Eqn 2-17) are checked with the assumption that shear planes will form at either side of the pin. This assumption produces a shear area equal to:

$$A_{vm} = A_{vg} = 2 \left(a + \frac{D_p}{2} \right) t \quad (\text{in}) \quad [2 - 18]$$

where a is the clearance between the back of the pin and the end of the hanger plate. For the rating of beam ends, shear is checked on multiple failure planes with rivets holes deducted from the net section.

2.2.2.3.5 Girder Rating

The AASHTO LRFD Specifications include revised provisos for the design of I sections for flexure and shear. As discussed previously the nonuniform stress conditions at the girder ends from the concentrated pin loading makes application of these design equations uncertain.

2.2.2.4 Caltrans' Rating Methods and Bridge Design Specifications (BDS)

The Caltrans' 2004 Bridge Design Specifications (Caltrans, 2004) was reviewed. These specifications contain provisions based on the ASD and LFD design methodologies. This review will focus on the LFD portion of these specifications because it was more recently used by Caltrans for rating pin and hanger assemblies.

2.2.2.4.1 Pin Rating

Similarly, to the AASHTO Standard Specification, Article 10.25.2 of the BDS specifies that pins are to be sized to resist shear and bending. For the calculation of pin bending capacity Caltrans treats the pin as a braced non-compact section (Article 10.48.2 of the BDS). This specifies the section capacity as:

$$M_u = F_y * S_{xt} \quad (kip * in) \quad [2 - 19]$$

where F_y is equal to the pin yield strength (ksi) and S_{xt} is the elastic section modulus of the pin ($in.^3$).

Shear capacity of pins is taken from Section 10.48.8.1 of the BDS where pins are treated as stout beams. The shear capacity of a pin is effectively computed as:

$$V_u = 0.58F_y A_p \quad (kips) \quad [2 - 20]$$

where A_p is the cross-sectional area of the pin (in^2).

2.2.2.4.2 Hanger Rating

Two checks for the tension failure beside the pin hole are in the BDS. The first check determines the capacity due to yield on the gross section (A_g). The gross section is computed as the hanger cross-section less the pin hole diameter times the thickness of the plate. While this deduction is not mentioned in the LFD code it is consistent with similar specifications in both the ASD and LRFD design methods. The nominal capacity for yielding on the gross section is computed as:

$$P_{u1} = F_y A_g \quad (kips) \quad [2 - 21]$$

The second check, based on section 10.12.3 of the BDS, determines the capacity due to rupture on net section of the hanger. For this application, the net section is the same as the gross section discussed previously. Based on the ASD and LRFD code requirement that the net section at the pinhole be 140% of the required net section away from the pin hole, the net area at the pin hole is divided by 1.4 which gives the capacity as:

$$P_{u2} = F_u \frac{A_n}{1.4} \quad (kips) \quad [2 - 22]$$

where F_u is the tensile stress of the hanger material (ksi) and A_n is the net area of the hanger across the pin hole (in^2). In addition to these provisions, which are specific to hanger plates, additional provisions applicable to both hanger plates and girder ends are discussed in the following two sections.

2.2.2.4.3 Bearing

The BDS uses the same bearing capacity equation specified in the ASD portion of the Standard Specifications but substitutes yield stress, per BDS Sections 10.32.4.1 and 10.46, for the allowable bearing stress. This gives the bearing capacity as:

$$P_u = F_y A_b \quad (\text{kips}) \quad [2 - 23]$$

where P_u is the bearing capacity (kips) and A_b is the projected bearing area (in^2) of the pin as described in Eqn. 2-14.

2.2.2.4.4 Block Shear and Shear Yielding

Section 10.19.4.1 of the BDS requires that all web connections of coped beams, tension members and tension connections to be checked for block shear rupture. Block shear rupture is defined in the BDS as failure when the net section of one segment ruptures and the gross section of a perpendicular segment yields. The capacity for this failure is described by the set of equations as:

$$T_{bs} = \phi_b (0.58 F_y A_{vg} + F_u A_{tn}) \quad (\text{kips}) \quad [2 - 24]$$

when

$$A_{tn} \geq 0.58 A_{vm}$$

and

$$T_b = \phi_b (0.58 F_u A_{vm} + F_y A_{tg}) \quad (\text{kips}) \quad [2 - 25]$$

when

$$A_{tn} < 0.58A_{vn}$$

where A_{vg} is the gross area of the failure plane in shear (in²), A_{vn} is the net area of the failure plane in shear (in²), A_{tg} is the gross area of the failure plane in tension (in²), A_{tn} is the net area of the failure plane in tension (in²), and ϕ_{bs} is the capacity reduction factor for block shear and is equal to 0.8.

In addition to block shear, shear yielding is checked along potential shear failure planes. This is done by modifying the girder plastic shear capacity from BDS Article 10.48.8.1 This equation is modified by replacing the girder web area with the gross area of the shear planes being investigated (A_{vg}) which gives the shear capacity as:

$$V_p = 0.58F_y A_{vg} \quad (kips) \quad [2 - 26]$$

Caltrans applies these two provisions to check for pin tear out in both beam ends and hanger plates. The application of these provision are similar to Caltrans' LRFR method discussed in section 2.2.2.3.4.

2.2.2.4.5 Girder Rating

The shear capacity of I shaped girders is described in BDS Section 10.48.8. This section matches the girder shear design given in the LFD portion of the AASHTO Standard Specifications. In the Caltrans rating example, the portion of the web reinforced by pin plates is treated as unstiffened web with the web thickness being the combination of plate girder web and pin plates. When pin plates do not extend all the way to the adjacent stiffener, the pin plate is treated as a stiffener and the shear capacity of the unreinforced web panel is treated as a stiffened end panel.

2.2.3 Alternate Rating Methods

In this section, alternate design specifications not commonly used for the design or rating of highway bridges in the United States are reviewed. The intent of this is to present possible alternative equations that could be adapted for rating purposes.

Specifications reviewed include the American Railway Engineering and Maintenance-of-Way Association's (AREMA) Manual for Railway Engineering (AREMA, 2016), The 15th Edition of the American Institute of Steel Construction's (AISC) Steel Construction Manual (AISC, 2017), AISC 360-16 Specifications for Structural Steel Buildings (AISC, 2016) and Eurocode 3.

2.2.3.1 AREMA

The AREMA Manual utilizes allowable stress design and is fairly consistent with the ASD specifications present in AASHTO's Standard Specifications. The hanger dimensional requirements and pin design are exactly the same and the allowable stresses differ only slightly. The only significant difference is that AREMA does not reduce the allowable bearing stress for pins subject to rotation.

2.2.3.2 AISC

The 2017 version of the American Institute for Steel Construction (AISC) Steel Construction Manual and 2016 AISC Specifications for Structural Steel Buildings were reviewed. While the structures for which these specifications were developed are subject to very different loading conditions and generally consist of smaller members than bridges, relevant resistance models were considered.

2.2.3.2.1 Hanger Plates

Within the AISC Specifications, four (4) equations are given for the design of connected members. The first equation (given in Section D5-1(a)) provides a capacity for tension rupture on the net effective area beside the pin hole as:

$$P_n = F_u(2tb_e) \quad (kips) \quad [2 - 27]$$

where F_u is the ultimate tensile stress of the hanger plate (ksi) and b_e , the effective width (in^2) defined as:

$$b_e = 2t + 0.63 \quad (in) \quad [2 - 28]$$

where t is the hanger thickness (in) and b_e must be less than the actual hanger width minus the pin hole dimension (in). The second design equation (given in section D5-1(b)) describes the capacity for shear rupture beyond the pin as:

$$P_n = 0.6F_uA_{sf} \quad (kips) \quad [2 - 29]$$

with A_{sf} , the area of shear planes (in^2), defined as:

$$A_{sf} = 2t(a + d/2) \quad (\text{in}^2) \quad [2 - 30]$$

where a (in) is the shortest distance from the edge of pin hole to the edge of the member measured parallel to the direction of force, and d (in) is the diameter of the pin. AISC defines the bearing capacity (J7(a)) for the components of a pin connected assembly as:

$$P_n = 1.8F_y A_b \quad (kips) \quad [2 - 31]$$

where F_y is the yield stress of the material (ksi), and A_b the projected bearing area of the pin (in²) which is given by equation 2-14. Finally, the AISC Specifications require yielding to be checked on the gross hanger section.

Similar to the AASHTO Specifications, the AISC Specifications require hangers to meet specific dimensional requirements as shown in Fig. 2-3. Firstly, the plate width must be greater than two times the effective width (b_e) plus the diameter of the pin. Secondly, the least distance behind the pin hole, a , is not to be less than 1.33 times the effective width. The corners of hangers are allowed to be clipped at 45° angles assuming the clearance between the pin hole and the clipped edge, c , is greater than or equal to the a .

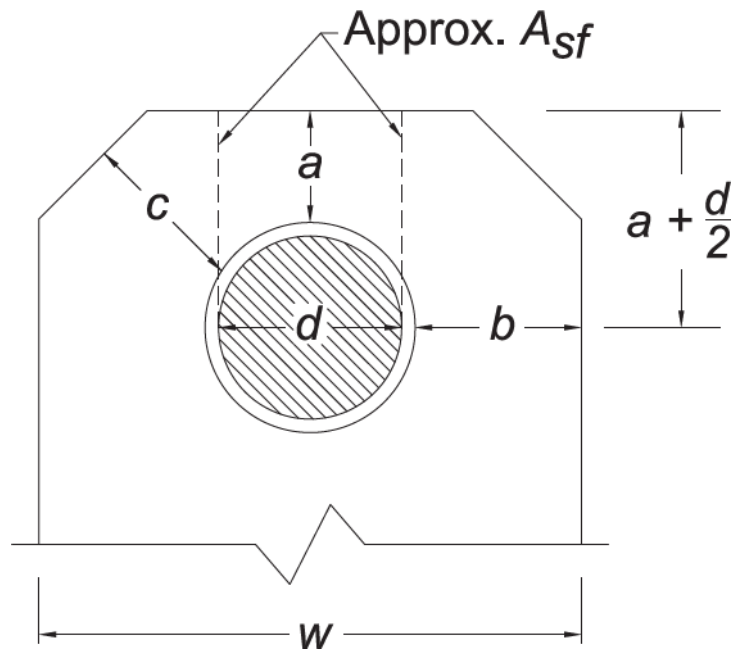


Figure 2-3: AISC hanger diagram (AISC, 2016).

2.2.3.2.2 Beam Ends

Part 9 of the AISC Steel Construction Manual provides specific guidance for the design of coped beam ends not included in any of the AASHTO Specifications. The behavior of the coped section is controlled by the web slenderness ratio, λ , and its relationship to the compact web slenderness limit, λ_p as:

$$\lambda = \frac{h_r}{t_w} \quad [2 - 32]$$

and

$$\lambda_p = 0.475 \sqrt{\frac{k_1 E}{F_y}} \quad [2 - 33]$$

where t_w is the web thickness (in), h_r is the total height of the coped section (in), where E is the modulus of elasticity (ksi), F_y is the yield stress of the web material (ksi) and where k_1 is the modified plate buckling coefficient as:

$$k_1 = fk \quad [2 - 34]$$

but always greater than 1.61. In equation 2-34, k is the web plate buckling coefficient and given as:

$$k = 2.2 \left(\frac{h_o}{c} \right)^{1.65} \quad \text{when } \frac{c}{h_o} \leq 1.0 \quad [2 - 35]$$

or

$$k = 2.2 \left(\frac{h_r}{c} \right) \quad \text{when } \frac{c}{h_o} > 1.0 \quad [2 - 36]$$

and f is the buckling adjustment factor that is given as:

$$f = 2 \left(\frac{c}{d} \right) \quad \text{when } \frac{c}{d} \leq 1.0 \quad [2 - 37]$$

or

$$f = 1 + \left(\frac{c}{d} \right) \leq 3 \quad \text{when } \frac{c}{d} > 1.0 \quad [2 - 38]$$

where, c is the length of the coped section, and d is the full beam depth. These coped sections dimensions are illustrated in Fig. 2-4. When $\lambda \leq \lambda_p$ the nominal flexural capacity (kip-in), M_n , is equal to plastic flexural moment (kip-in), M_p , of the coped section which is given as:

$$M_n = M_p = F_y Z_{net} \quad (\text{kip} * \text{in}) \quad [2 - 39]$$

where Z_{net} is the plastic section modulus of the coped section (in^3). When $\lambda_p \leq \lambda \leq 2\lambda_p$ then the nominal moment capacity is computed as:

$$M_n = M_p - (M_p - M_y) \left(\frac{\lambda}{\lambda_p} - 1 \right) \quad (\text{kip} * \text{in}) \quad [2 - 40]$$

where M_y , the flexural yield moment, is given as:

$$M_y = F_y S_{net} \quad (\text{kip} * \text{in}) \quad [2 - 41]$$

where S_{net} is the elastic section modulus of the coped section (in^3). When $\lambda > 2\lambda_p$ then

the nominal moment capacity is computed as:

$$M_n = F_{cr} S_{net} \quad (\text{kip} * \text{in}) \quad [2 - 42]$$

where F_{cr} , the critical web buckling stress (ksi), is computed as:

$$F_{cr} = \frac{0.903Ek_1}{\lambda^2} \quad (\text{ksi}) \quad [2 - 43]$$

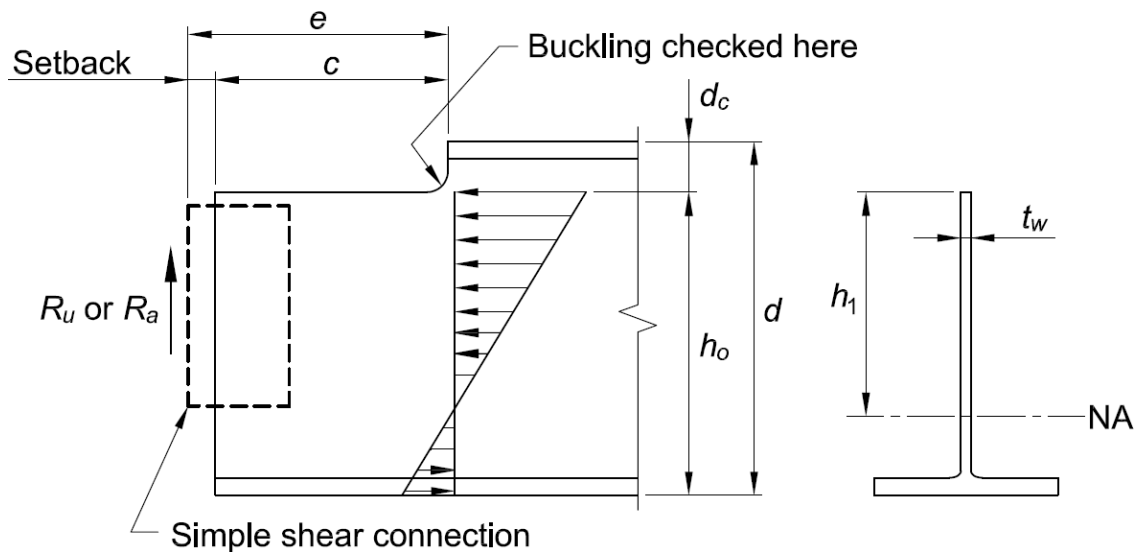


Figure 2-4: Coped beam end geometries (AISC 2017).

2.2.3.3 Eurocode 3

Eurocode 3 is a comprehensive set of design specifications used in the European Union for the design of both buildings and bridges. Part 1-8 of these design specifications provides design provisions for connections in steel structures. Section 3.13 of Part 1-8 includes methods for the design of pins and pin connected members. Eurocode 3 uses a similar LRFD format the AASHTO LRFD Specification, with resistance factors denoted by the greek letter gamma.

2.2.3.3.1 Pins

Similar to the AASHTO-LRFD Specifications, Eurocode 3 requires pins be designed for shear, bearing, bending, and combined bending and shear. One unique aspect to the Eurocode pin design methodology is that for bending and bearing, pins are designed at both strength and service load levels. The service level design is only specified for those pins that are intended to be removed.

The factored pin shear capacity is given as:

$$V_r = \frac{0.6AF_u}{\gamma_{M2}} \quad (kips) \quad [2 - 44]$$

where A is the cross-sectional area of the pin (in^2), F_u is the pin tensile strength (ksi) and γ_{M2} is the resistance factor.

The factored strength level bearing capacity for both pins and pin connected members is given as:

$$P_r = \frac{1.5tdF_y}{\gamma_{M0}} \quad (kips) \quad [2 - 45]$$

where t is the thickness of the pin connected member (in), d is the pin diameter (in) F_y is the yield stress of either the pin or the pin connected member (ksi) and γ_{M0} is the resistance factor. The service level bearing capacity (kip) is given as:

$$P_b = \frac{0.6tdF_y}{\gamma_{M6,ser}} \quad (\text{kips}) \quad [2 - 46]$$

The factored strength level bending capacity for pins is given as:

$$M_r = \frac{1.5S_x F_y}{\gamma_{M0}} \quad (\text{kip} * \text{in}) \quad [2 - 47]$$

where S_x is the elastic section modulus for the pin (in^3) the F_y is the yield stress of the pin (ksi) and $\gamma_{M6,ser}$ is a resistance factor. The service level bending strength (kip*in) is given as:

$$M_s = \frac{0.8S_x F_y}{\gamma_{M6,ser}} \quad (\text{kip} * \text{in}) \quad [2 - 48]$$

The combined shear and bending capacity of a pin is described by the interaction equation:

$$\left[\frac{M_u}{M_r} \right]^2 + \left[\frac{V_u}{V_r} \right]^2 \leq 1 \quad [2 - 49]$$

where M_u and V_u the strength level moment and shear loads seen by the pin and M_r and V_r are the moment and shear pin capacities as described by Eqn. 2-47 and Eqn. 2-45.

2.2.3.3.2 Hangers

The Eurocode design methodology for pin connected members relies entirely on dimensional requirements. These specifications only consider one general geometry as

shown in Fig. 2-5. Within this general geometry, two separate design methods are specified for Type A and Type B hangers. These hanger types are differentiated by the location of the end radius in relation to the pin hole.

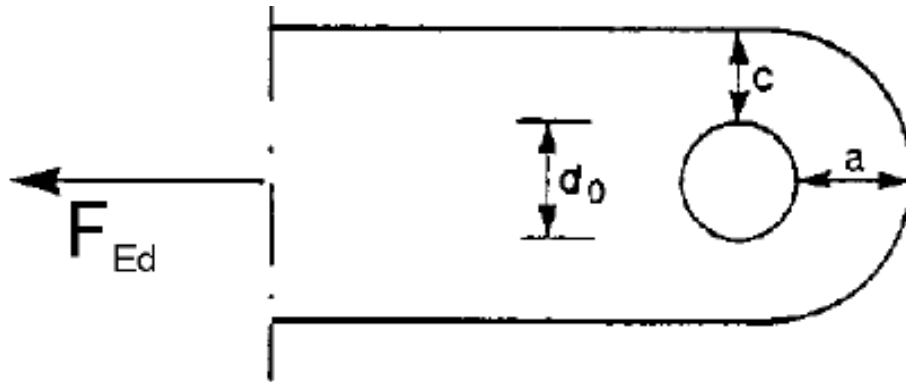


Figure 2-5: Eurocode general hanger geometry (Eurocode 2005).

A Type A hanger has its end radius concentric with its pin hole. For the design of these hangers, first a , the clear distance between the outside of the pin hole the end of the hanger, is determined as:

$$a \geq \frac{P_u \gamma_{MO}}{2tF_y} + \frac{2d_o}{3} \quad (in) \quad [2 - 50]$$

where, t is the hanger thickness (in), d_o is the pin hole diameter (in), F_y is the hanger material yield stress (ksi) and P_u is the strength level force (kip) seen by the hanger plate. Next c , the clear distance between the outside of the pin hole and the side of the hanger, is determined as:

$$c \geq \frac{P_u \gamma_{MO}}{2tF_y} + \frac{d_o}{3} \quad (in) \quad [2 - 51]$$

A Type B hanger has the center point of its end radius beyond the center of the pin hole. The design of Type B hangers is based on stricter geometric requirements that are mostly based on the pin hole diameter. These requirements can be seen in Fig. 2-6. Additional requirements for plate thickness and pin hole diameter are given as:

$$t \geq 0.7 \sqrt{\frac{P_u \gamma M O}{F_y}} \quad (\text{in}) \quad [2 - 52]$$

and

$$o \leq 2.5t \quad (\text{in}) \quad [2 - 53]$$

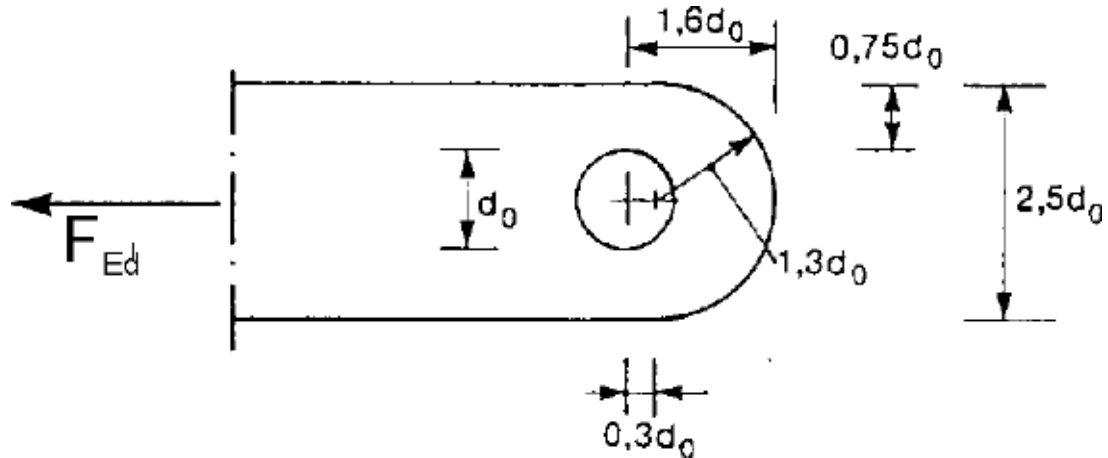


Figure 2-6: Type B geometric requirements (Eurocode, 2005).

2.3 Field Performance and Inspection

Since the Mianus River Bridge collapse in 1983 transportation agencies have conducted numerous investigations into pin and hanger assemblies. The majority of these studies focused on documenting other failures of these assemblies along with ultrasonic testing of in-service pins. This section reviews the body of knowledge on field performance of failures and pin materials. Additionally, this section reviews guidance provided for field inspection of pins.

2.3.1 Askeland, et al. (1987)

On March 16th, 1987, a 35 ft suspended span on I-55 nearly collapsed when fracture occurred in 4 of the 12 pins on the bridge. Full collapse was only prevented when the suspended span caught on the lower flange of the adjacent spans girders.

In a report detailing this near collapse, Askeland et al. describe the examination and metallurgical report on 4 cracked pin samples from two separate Missouri bridges. A photograph of one of these samples is shown in Figure 2-7.



Figure 2-7: Cracked MoDOT pin removed from service.

The pins that were removed from the bridge showed up to 0.25 in. deep wear marks along with a thick layer of corrosion residue along the surface of the pin and imbedded within the cracks. Scanning electron microscopy (SEM) of the corrosion residue revealed high levels of chloride and iron. Cracking was concentrated at locations of significant wear although one crack was found at a location where minimal wear was present. All locations were said to be corroded enough to lock the pin and hanger assembly. Analysis of the ferrite crystals showed localized plastic deformation around the cracks. The report concluded that the excessive wear was due to corrosion at the interface of the web/hanger plate and the pin and that cracking was caused by fixation of the pin due to corrosion. Crack growth was caused and accelerated by a combination of torsion overload and continued corrosion i.e. stress corrosion. This report deemed that cracking was not induced by the wear marks but rather by locked pin rotation.

Limited information was provided regarding the geometry of the pin and hanger assemblies or the bridges themselves. Based on the photographs provided, the I-55 pins appear to be approximately 2.5 in. diameter, and pins from the Clinton Bridge were approximately 2.75 in. diameter. Additionally, the bridges were said to be 20 years old, placing their construction in the late 1960s.

2.3.2 Kulicki et al. (1990)

Kulicki et al (1990) provided a summary of corrosion effects on steel bridges and recommended specifications for the evaluation of the corrosion effects. Within this report a brief review of earlier pin and hanger assembly failures was provided. A list of maintenance related failure modes was compiled. Pin related failure modes included failure due to shifting hanger plates which increased the moment arm on the pin, cracking due to excessive wear that reduced the pin section, and excessive torsional loading induced by pin fixity. Hanger plate related failure modes included cracking at the net section due to fatigue and cracking at the gross section due to bending stresses induced by fixity. Limited information was given for the determination of loads effects due to assembly fixity. For live load effects, field measurements were recommended. For temperature effects, the report recommended predicting the expected loads using the relative movement anticipated in the girder ends due to temperature change and the hanger geometry. Ultimately repair or replacement of an assembly was recommended if it was identified as fixed.

2.3.3 South et al. (1992)

This report describes the Illinois Department of Transportation's (IDOT) ultrasonic inspection of 130 bridges containing 3,165 pins. While the UT methods used appeared effective in identifying the existence of flaws they had difficulty relating their readings to flaw size. Of the pins inspected no cracks were identified. The pin with the lowest indication reading had wear grooves of $3/8^{\text{th}}$ of an inch on a 2.5 in. pin.

Another key aspect of this report was an investigation into methods of detecting pin fixity and quantifying the forces developed in a fixed assembly. In order to detect the degree of fixity of a pin, IDOT tested multiple methods such as attaching paper gages, paint strips and paint scratch pointer gages at the pin to hanger interface. Unfortunately, due to the limited longevity of the paint strips and paper gages and the relative insensitivity of all these methods, none were recommended. Additionally, electronic rotation sensors and instrumentation of the hanger plates with strain gages to measure bending stress were investigated. Both systems were found to be sensitive and provide useful data but IDOT recommended strain gauges over the rotation sensors based on their lower cost and the usefulness of data for further stress analysis.

To quantify forces caused by fixed hangers, three (3) finite element models of different bridges were produced. The pins were modeled as rotationally fixed and torque values at these locations due to temperature change and horizontal live load were recorded. For the girder bridge considered within this modeling study, effects of temperature change were small compared to live load effects. The maximum stress

induced by temperature change on the fixed bridge was well within the pin capacity while the live load induced stress far exceeded the yield stress of the pin.

2.3.4 Miller and Chaney (1994)

Between 1988 and 1991 The Pennsylvania Department of Transportation (PennDOT) underwent a major UT inspection and repair project on its 23-fracture critical pin and hanger bridges. During this project, 315 pins were inspected. Of this population, 24 pins were identified by UT inspection as containing defects and 13 of these were later independently verified. Only one pin was found to have an internal crack like discontinuity. This paper reviewed 4 bridges in detail, information on others is provided in a table at the end of the paper. Material specification information was provided for the pins for most of the bridges. Seventeen (17) of these bridges had A235 (forged carbon steel pins), two (2) had A237 (forged alloy steel), and one (1) had A-36 (mild carbon steel).

2.3.5 Finch et al. (1994)

This paper describes the UT inspection of 192 pins on 16 fracture critical pin and hanger bridges conducted by LA-DOTD/FHAW in Louisiana. This inspection, combined with previous LA-DOTD inspections (bring the total number of inspected pins to over 300), found only one (1) pin with a minor flaw and only 2% with minor wear marks (considered as being under 1/16 in.). No information was provided about the material or

bridge geometries. Additionally, it is unclear how many pins were removed to verify the UT results.

This report concluded that most pins within pin and hanger assemblies appeared to be immune to cracking. Those that could be subjected to cracking were frozen pins, those undergoing stress corrosion, or from poor fabrication. This conclusion was based on the assumptions of high dead to live load ratios in these elements, the high dislocation density of forged steel blunting cracks, and that pins are generally shear controlled members with minimal bending.

2.3.6 Juntunen (1998)

Juntunen (1998) investigated the condition of Michigan's pin and hanger assemblies in his report. The condition rating of the population was reviewed, live load stresses were measured, fatigue evaluations were done, and problems with pin and hanger assemblies documented within the Michigan Department of Transportation (MDOT) inventory.

Juntunen reported on 3 issues found within the MDOT pin and hanger bridge inventory. The most common issue found was that of corroded hanger plates. It was noted that this issue could lead to pin fixity (inducing torque in the pin and bending in the hanger plate), section loss, and lateral pressure caused by pack rust leading to dishing deformation in pin caps. Additionally, the phenomena of beam ends bearing on each other was described. This issue was said to cause buckling in the beam webs thereby inducing lateral pressure on the hanger plate. On one occasion, this phenomenon pushed

a hanger plate off the pin. The final issue described was the fracture of a link plate on the M-36 bridge over the Tittabawassee River near Saginaw, MI. This fracture occurred on a 14 girder span with a longitudinal open joint running down the center of the bridge. The fracture was found in the net section across the pin hole. The beam ends were observed to be in contact and the assembly was heavily corroded.

This report describes the instrumentation of hanger plates on three (3) bridges and stresses were briefly recorded at the gross section, the net section and behind the pin. The hanger instrumentation diagram is shown in Figure 2-8. An effective stress value at net section, adjusted to remove stress concentration effects, was calculated and compared to the calculated effective stress using AASHTO Fatigue Guide and WIM data. Finite and safe fatigue lives for these assemblies were calculated and the assembly geometries were compared to those required to satisfy the AASHTO fatigue design criteria in both the AASHTO Standard Specifications and AASHTO LRFD Design.

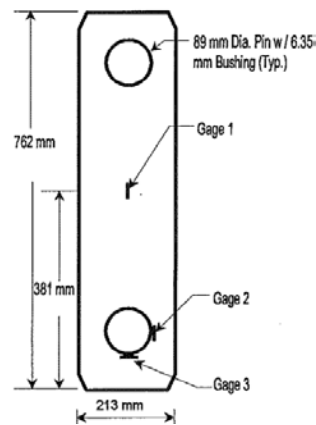


Figure 2-8: Instrumentation diagram (Juntunen, 1998).

2.3.7 Jansson (2008)

The hanger plates on an I-94 bridge in Michigan constructed in 1964 had only 40% of the AASHTO specified area behind the pin hole. These hanger plates were identified as undersized and removed from service in 2007. Based on this occurrence, Jansson investigated the performance of hangers with undersized sections behind the pin hole. In this investigation, two tests were performed on instrumented plates. The tests were not conducted to failure. One of the plates tested was designed with the AASHTO specified section behind the pin hole and the other used the same undersized section as that observed in the hanger plate removed from service. These tests were then used to verify non-linear FEA models.

Based on FEA models, Jansson developed equations to determine the stress concentrations behind the pin and at the net section depending on the amount of material behind the pin. Jansson revisited the “General Yield” criteria originally discussed by Johnston in 1939 (Johnston, 1939). General yielding in the hanger was defined as the point where the slope of the load vs pin displacement curve was one-third of its original slope. Using the FEA models discussed above, Jansson developed another equation to describe this general yield based on the area of the section behind the pin hole. This general yield equation was computed as:

$$F_{gy} = \phi_g \frac{P_u}{2A_n} \quad (ksi) \quad [2 - 54]$$

where σ_g is the hanger general yield stress, P_u is the factored load seen by the hanger assembly (kips), A_n is the net section area of the hanger plate body (in²) and ϕ_g is an end length adjustment factor and is given by:

$$\phi_g = 1.2579 - 73.7781R^{-1} - 4913.3525R^{-2} \quad [2 - 55]$$

where R is the ratio between the actual area beyond the pin hole and that prescribed by the code. Jansson recommended that those hangers whose general yield stress exceeds their material yield stress be removed from service.

2.3.8 Moore et al. (2004)

This guide provides a summary of traditional ultrasonic pin and hanger inspection techniques. Information reported includes general equipment information, flaw sizing techniques, discussion of acoustic coupling and inspection data collection. Additionally, this guide describes the results of laboratory tests on pins removed from service and with manufactured cracks. This study investigated ultrasonic beam diffraction, distance amplitude correction, the sensitivity of angle and straight beam transducers, the effectiveness of defect sizing techniques and the phenomena of acoustic coupling. The results for the beam diffraction and distance amplitude experiments found the wave behavior performed as anticipated. For the sensitivity testing all cracks were able to be identified by both transducers (0 and 14) but for the smallest crack, the inspector had to be informed of the crack location in order to identify it with the 0-degree transducer. Defect sizing using a procedure similar to the 6-dB drop method was found to be reasonably accurate with an average of 23.5% error. Finally, evidence of acoustic coupling was observed under the controlled laboratory conditions and shown to be a function of the load on the pin. Acoustic coupling, is the appearance of an impedance in ultrasonic test results caused by high stress in the pin. Due to the high stress at the shear

planes in these pins this phenomenon creates the appearance of a crack in the pin at the location where cracks would normally be anticipated.

2.3.9 Discussion

Based on this review, the most prominent issue for in-service pin and hanger assemblies is that of assembly fixity. As discussed in Kuliciki (1990), due to its severity, pin fixity should be prevented and assemblies that exhibit fixity should be replaced as soon as possible. Due to the difficulty in identifying the occurrence and degree of pin fixity (as discussed in South et al., 1992) it may be reasonable to have a susceptibility check for bridges. Bridges that are unusually susceptible due to their geometry could be inspected more frequently for the effects of full or partial fixity.

An important detail identified in this review is the relationship between corrosion and wear on these assemblies. This adds another variable, in addition to material properties and loading, to consider in future wear investigation and possibly testing. What was not reported in detail was documentation of pin materials.

The experience described in Jansson (2008) shows that hangers not meeting current AASHTO dimensional requirements can survive in service for an extended duration. In his report, Jansson appeared to treat the general yield of the hanger as a strength limit state.

Standard ultrasonic testing is the chief method for pin inspection and standard procedures have been developed for inspection of pins. This standardization has increased the reliability and accuracy of both crack identification and crack sizing in pins.

Unfortunately, it is apparent that there remain some limits to this technology. One of these limits is acoustic coupling which reduces the reliability of this method and can lead to false identifications in cracked pins. Newer technologies, such as phased array UTM may improve these methods but are not described in the literature.

2.4 Experimental Studies

In this section relevant experiment and analytical studies of hanger plates, pins and beam ends were reviewed. Special attention is given to collecting existing experimental test data, noting failure modes and documenting capacity equations.

2.4.1 Hanger Plates

Of the three main elements within pin and hanger assemblies, the hanger plates have by far received the most experimental investigation. In this section, the descriptions of various experimental studies and analyses on hanger plates are reviewed. Special attention was given to collecting specimen dimensions for future comparison to the Caltrans inventory. When reviewing these studies, the primary focus was on identifying ultimate failure modes and reporting available capacity predictions. It should be noted that a considerable amount of work has been performed to identify and quantify the stress concentrations that develop at the sides and behind the pin hole. Much of this work is not reported here as the current research aims at determining ultimate limit states for hangers and local yielding at stress concentrations is not considered as an ultimate limit state for this work.

2.4.1.1 The Quebec Bridge (1919)

This report documents some of the earliest destructive tests on hanger like links. The significance of these tests was their use of 12 in. diameter pins, this is the largest pin size of any study reviewed. The specimens were rectangular bars with 4 slightly elongated holes placed along the length of the hanger, a representation of one of these specimens is shown in Figure 2-9. The additional holes along the length of these plates contaminates the deformation data from these tests but should not affect the ultimate load.

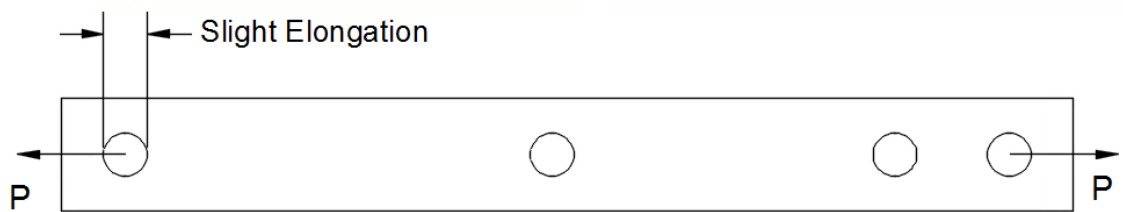


Figure 2-9: Quebec bridge hanger specimen.

In the Quebec Bridge tests, ten hangers were tested to failure and 3 different failure modes were described: dishing, net section failure and splitting. Dishing failures were described as instability of the material behind the pin hole causing the portion of the hanger behind the pin to deform out-of-plane. When dishing occurred, the strength of the hanger plate was greatly decreased. Figure 2-10 shows an image of a hanger in the early stages of a dishing failure. Examples of the other failure modes observed are shown in Figures 2-11 and 2-12.



Figure 2-10: Dishing failure (Johnston, 1939).

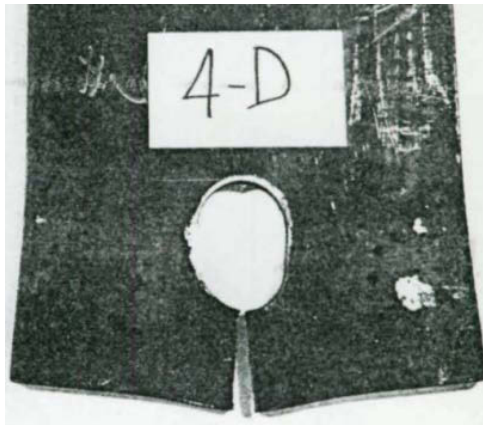


Figure 2-11: Splitting failure (Blake, 1981).

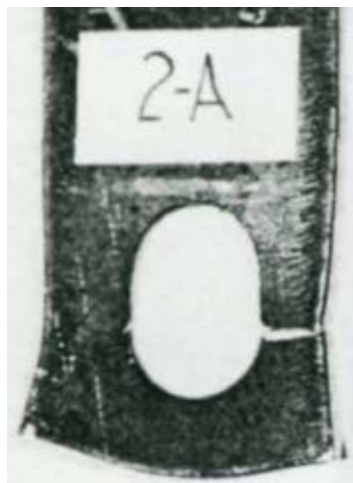


Figure 2-12: Net section failure (Blake, 1981).

Six of the hangers were smaller scale specimens with plate thickness of 3/8 in., widths varying from 9 to 13 in. and they were loaded through 5 in. diameter pins. The second set consisted of full size hangers with thicknesses varying from 1.5 to 2 in. and widths varying from 26 to 28 in. Of the small-scale specimens, four dished and the remaining 2 specimens were restrained behind the pin to prevent dishing and failed via fracture at the net section and splitting behind the pin hole. Of the large-scale specimens one split behind the hole. The remainder fractured at the net section with one plate fracturing next to one of the unloaded holes. None of the large specimens were restrained against dishing, and the 1.5 in. thick plates showed some lateral deformation prior to failure.

2.4.1.2 Johnston (1939)

Johnston (1939) describes one of the earliest and most referenced hanger plate test series consisting of 106 hanger plate specimens. Additionally, Johnston developed a notation for hanger plate specimens shown in Figure 2-13. Where b is the total plate width (in.), D_h is the pin hole diameter (in), D_p is the pin diameter (in), c is the pin clearance (in), t is the plate thickness (in), b_e is the effective width on one side of the hole (in) and a is the edge distance behind pin.

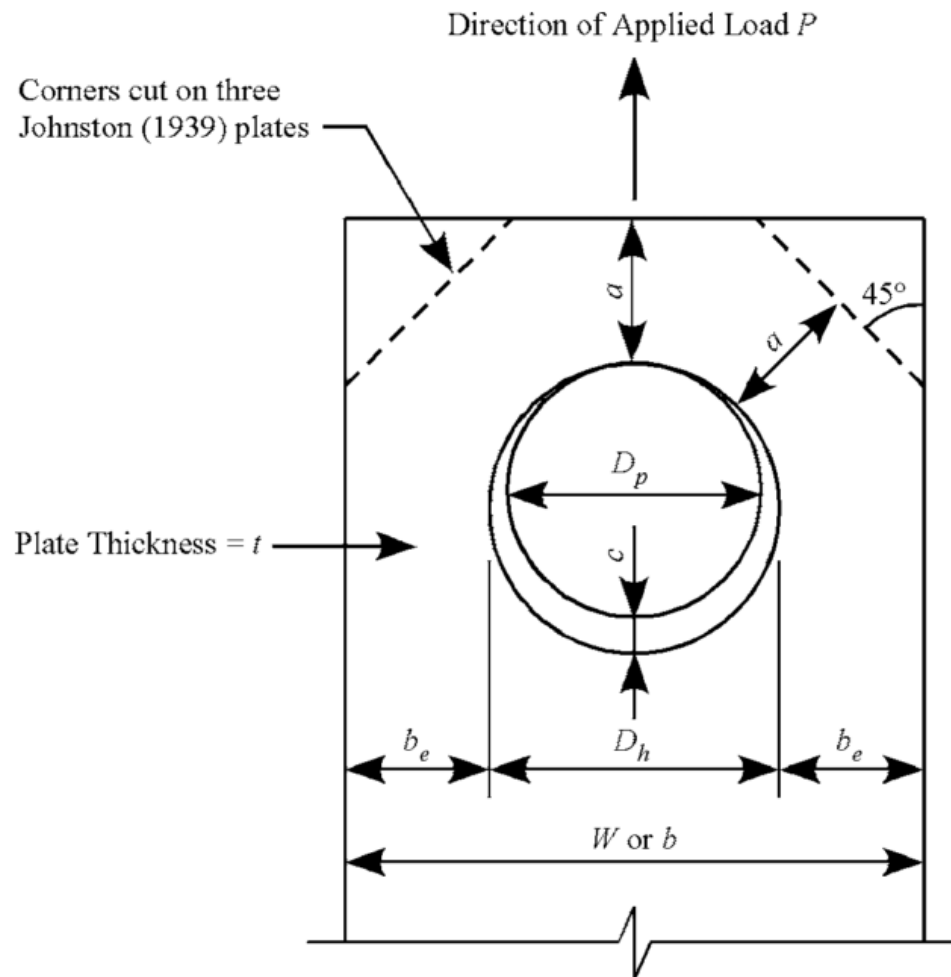


Figure 2-13: Johnston's hanger notation (Duerr, 2006).

The specimens tested in this study were relatively small having thicknesses ranging from $1/8$ in. to $3/4$ in. and widths ranging from 6 in. to 10 in. Johnston described 3 failure modes seen in these test: dishing, net section failure, and failure below the hole. The first two failures modes appear to be the same as those described in in The Quebec Bridge Report (1919). Johnston described his third failure mode as “crushing and shearing failure below the pin, in some cases followed by a tearing fracture in “hoop” tension after considerable deformation”. This description certainly points to at least some specimens failing by splitting behind the hole yet doesn't rule out some of these

specimens failing by a shear tear out failure mode described in later studies. Using the notation from Figure 2-13, Johnston presents empirically derived equations for the three failure modes observed in these studies. Originally these equations were written to provide an average pin bearing stress at which failure would occur. For the purposes of this paper these equations were converted to give total load on the hanger at failure. This conversion was done by assuming the average pin bearing stress is given by:

$$F_b = \frac{P_u}{D_p t} \quad (\text{kips}) \quad [2 - 56]$$

where P_u is the ultimate load of the hanger (kips) and F_b is the average pin bearing stress (ksi). For dishing failures, plate strength (kips) was described as:

$$P_{u,d} = (20 + 315 \left(\frac{t}{D_h} \right) + 75 \left(\frac{t * b_e}{D_h^2} \right) + 20 \left(\frac{a}{D_h} \right) - 20 \left(\frac{a}{D_h} \right)^2) D_p t \quad (\text{kips}) \quad [2 - 57]$$

For net section failures, plate strength (kips) was described as:

$$P_{u,t} = 2F_u D_p t \left(\frac{b_e}{D_h} \right) \quad (\text{kips}) \quad [2 - 58]$$

where F_u is the tensile stress (ksi) of plate material. Finally, for failure behind the pin, the plate strength (kip) was described by:

$$P_{u,b} = F_u D_p t \left[1.13 \left(\frac{a}{D_h} \right) + \frac{0.92 \left(\frac{b_e}{D_h} \right)}{1 + \left(\frac{b_e}{D_h} \right)} \right] \quad (\text{kips}) \quad [2 - 59]$$

The plate ultimate strength would be determined by the least value of $P_{u,d}$, $P_{u,t}$ and $P_{u,b}$.

Additionally, Johnston documented the “general yield point” of the hanger plates tested. This general yield was defined as the point at which the slope of the load vs.

deformation curve became a third of its initial slope. Johnston developed an empirical equation to describe this limit as:

$$P_{gy} = \frac{F_y D_p t}{2} \left[3 \left(\frac{a}{D_h} \right) - \left(\frac{a}{D_h} \right)^2 - 2 \left(\frac{c}{D_h} \right) \right] \quad (\text{kips}) \quad [2 - 60]$$

where P_{gy} is the applied load (kips) at the point of general yield in the plate, and F_y is yield stress of the plate material. Deformation for these tests were measured from the back of the pin to a fixed location on the interior of the hanger plate approximately 3 inches from the pin. Due to the empirical nature of all of these equations, Johnston recommends their use to hanger plates of similar dimensions to those tested.

2.4.1.3 Luley (1942)

This report describes the destructive testing of 16 hanger plate specimens made from 4 different materials: mild carbon steel, low alloy steel, silicon steel, and an aluminum alloy. These specimens were designed, using equations from Johnston (1939), to fail by either fracturing at the net section or splitting behind the hole with half designed to fail each way. All 12 of the steel hanger plates failed in the manner anticipated. The capacities agreed reasonably well with those predicted, ranging from 93% to 110% of the predicted capacity for failure on the net section and from 92% to +101% for failure behind the hole. This report also discusses the “general yield” concept but using the 0.2% offset criterion.

2.4.1.4 Tolbert and Hackett (1970)

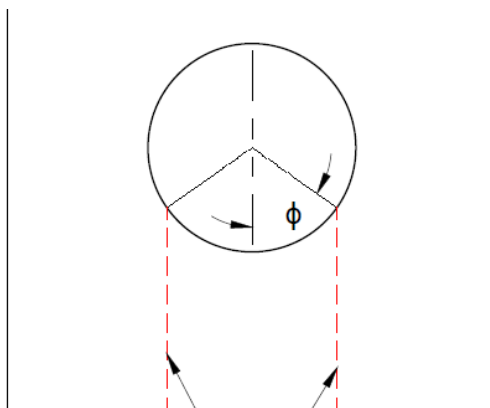
Tolbert and Hackett (1970) describe the testing of 13 specimens with the intent of investigating the effect of pin hole clearance on the elastic stress distribution and ultimate strength of lifting lugs. The specimens in this study are all 0.10 in. thick with 1 in. diameter pin holes. In 5 of these tests, pin size is varied from a 0.5 in. to 1 in. diameter (neat fit) to observe the effects of pin clearance. In the remainder of the tests, neat fit pins were used and net section and area behind the pin were altered. Of these specimens, 11 failed behind the pin and 2 failed via dishing. It is not noted whether the plates that failed behind the pin failed through tear out or splitting.

Tolbert and Hackett (1970) proposed an equation to predict the ultimate force in the plate through a modified shear rupture equation as:

$$P_{u,s} = A * V_u * C_a * C_r \quad (kips) \quad [2 - 61]$$

where $P_{u,s}$ is the ultimate pin load (kips), V_u is the ultimate shear stress of the hanger plate (ksi), C_a is a width variation amplification factor, C_r is a pin clearance reduction factor and A is the total area of shear planes (in²).

The locations of shear planes are described by an angle (ϕ in Figure 2-14) from the plate center line. Based on observations during testing it was noted that this angle was frequently between 45 and 55 degrees. Using 45 degrees was recommend for simplicity. The adjustment factors for pin clearance and plate width were provided through charts and are provided in Fig. 2-15 and Fig. 2-16 In Fig. 2-15 D is the hole diameter (in.) and W is the total plate width (in.). Eqn. 4-6 was described as only applicable to plates with overall widths at least twice the distance from center of the pin hole to the back of plate.



Shear Planes

Figure 2-14: Shear planes for pin tear out.

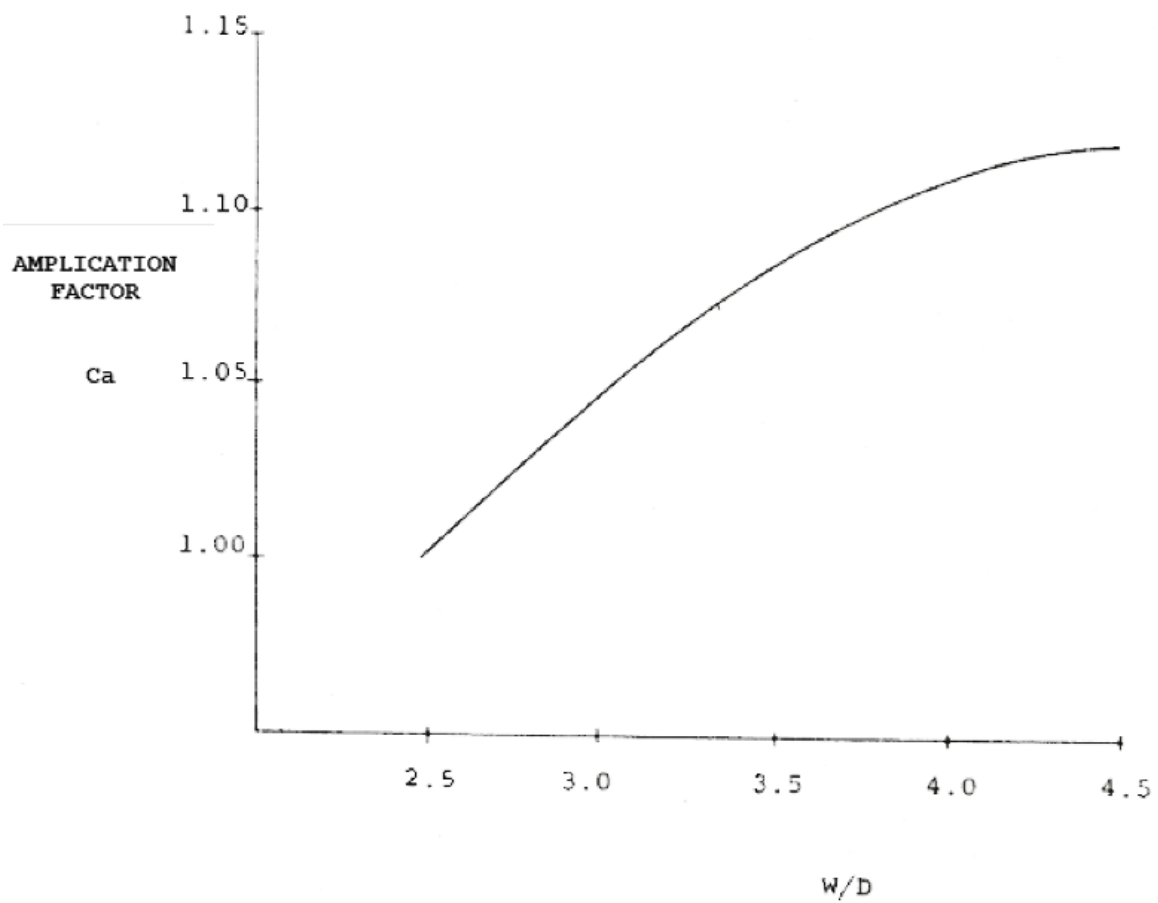


Figure 2-15: Tolbert and Hackett amplification factor.

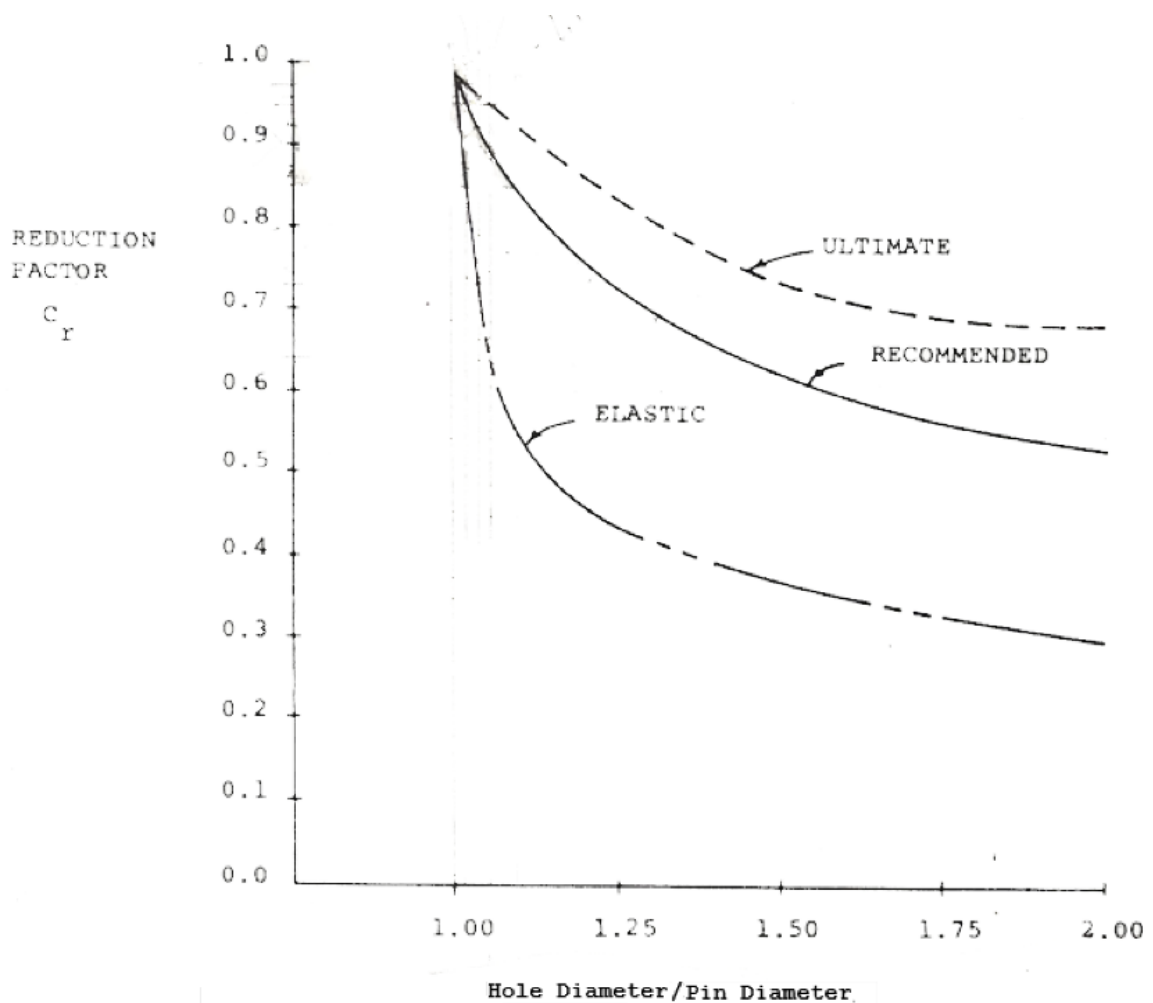


Figure 2-16: Tolbert and Hackett reduction factor.

2.4.1.5 Blake (1981)

This report describes the specimens, methods, and results from tests of 23 specimens to failure. The specimens in this test program were loaded through pins with diameters ranging from 2.5 in. to 3.5 in., plate thicknesses ranging from $\frac{1}{4}$ to 2 in., and plate widths ranging from 6 to 23.75 in. Specimens were tested with tight spacers that left only a $\frac{1}{16}$ th inch gap between the spacers and the test specimen at the pin. These spacers likely prevented any possible dishing during these tests. In this experimental

study, three (3) different failure modes were observed: failure at the net section, single shear pull through, and double shear pull through. An example of double shear pull through is provided in Fig. 2-17. While no interpretations of these results were made in this report, Duerr (1985) describes that these results were analyzed by T.R. Higgins and two capacity equations were developed. The plate capacity for failure on net section was described by:

$$P_{u,t} = 2t b_{eff} F_u \quad (\text{kips}) \quad [2 - 62]$$

where F_u is the ultimate tensile stress of the steel plate (ksi), t is the plate thickness (in) and b_{eff} , the effective width, is given by:

$$b_{eff} = 2t + 0.625 \leq b_e \quad (\text{in}) \quad [2 - 63]$$

Plate capacity for failure by shear beyond the pin was described as:

$$P_{u,s} = 2t \left(a + \frac{D_h}{2} \right) V_u \quad (\text{kips}) \quad [2 - 64]$$

where V_u is the ultimate shear stress of the steel plate (ksi) taken as $0.58 * F_u$.

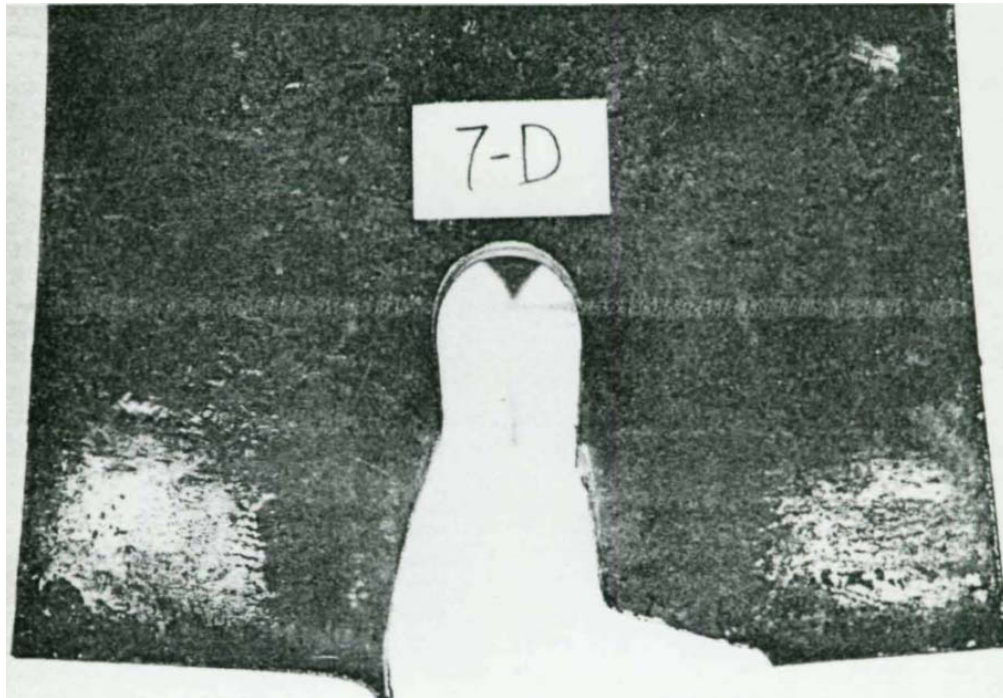


Figure 2-17: Pin tear out failure (Blake, 1981).

2.4.1.6 Duerr and Pincus (1985)

This report describes tests of 10 hanger specimens and 3 triangular shaped picking eye shapes. The application driving this research was the design of picking eyes for heavy lifting. Due to this application, the main variable changed in these tests was the pin clearance which varied from neat fit to 3 in.

A significant portion of this report was devoted to reviewing existing hanger strength equations with experimental results available in the literature. Of the sets of equations reviewed, including those produced by Johnston (1939), T.R. Higgins and Tolbert (1970). The equations from Johnston (1939) were found to agree best with the test data available at the time, predicting the correct failure mode 50 out of 57 times and the greatest degree of error being 30% and the second greatest being 16.7%. The T.R.

Higgins equations were found to be inaccurate for the data from Tolbert (1970) and Johnston (1939) with the greatest degree of error being 62.6% and the predicted mode of failure only being correct 15 out of 57 times. Duerr attributes this inaccuracy to the b_{eff} concept. The graphs shown in Figure 2-18 were presented to show ability of each of these methods to predict the available experimental results.

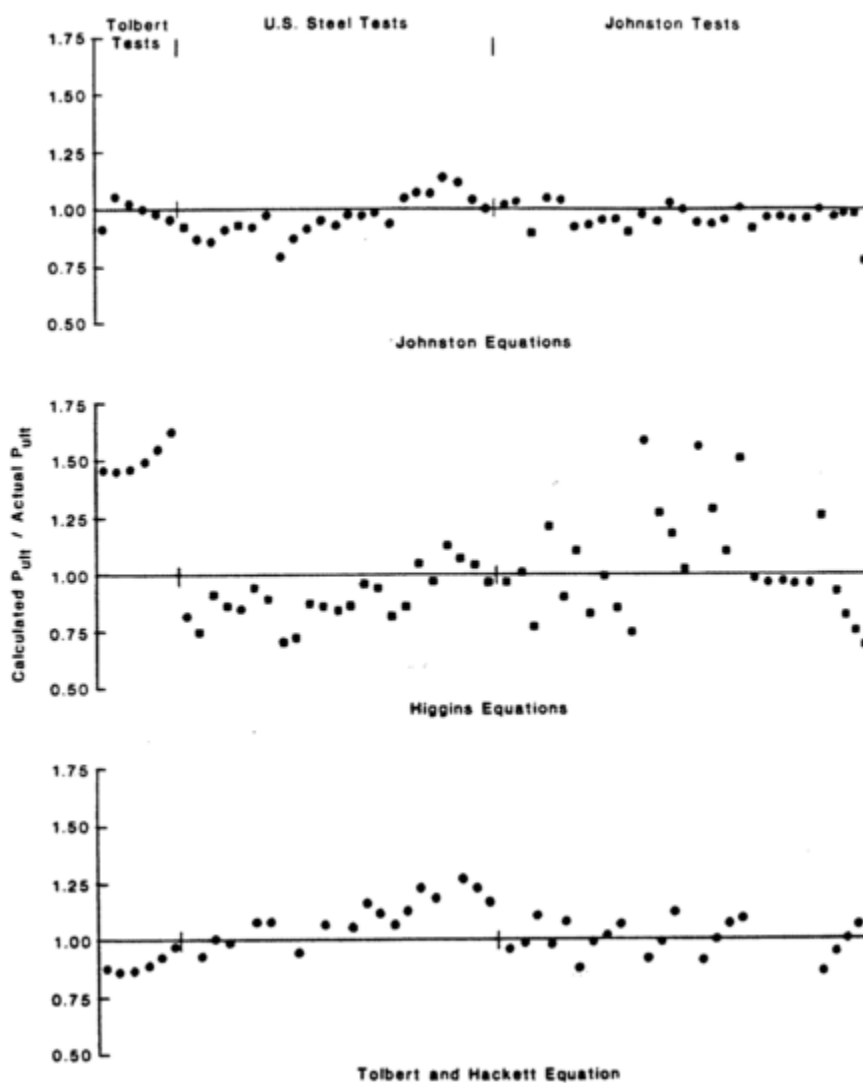


Figure 2-18: Accuracy of hanger plate strength predictions (Duerr and Pincus, 1985).

2.4.1.7 Rex and Easterling (2003) & Easterling (1996)

These tests were performed to investigate the bearing behavior of a single bolt in order to better understand the rotational behavior of semi-rigid column to beam connections in buildings. All though the focus of this research does not initially appear relevant to pin and hanger assemblies, a review of the test specimens and methods show strong similarities with previous hanger tests, see Figures 2-19(a) and (b). Because of the building oriented focus of these tests the specimen dimensions are smaller than those in most tests with pin diameters ranging only from 0.75 in. to 1 in., hanger plate thickness ranging from 0.25 in. to 0.75 in., and plate widths smaller than 5.5 in. Rex and Easterling noted 4 varieties of failure: tear out, splitting, dishing, and bearing (excessive deformation at the pin). For this test series, bearing failure was defined as plate deformation exceeding 0.5 in. with no substantial loss in load capacity. Of the 48 specimens tested 13 failed by bearing, 1 failed from tear out, 6 failed by splitting, 11 failed by dishing, and the remainder were not tested to failure.

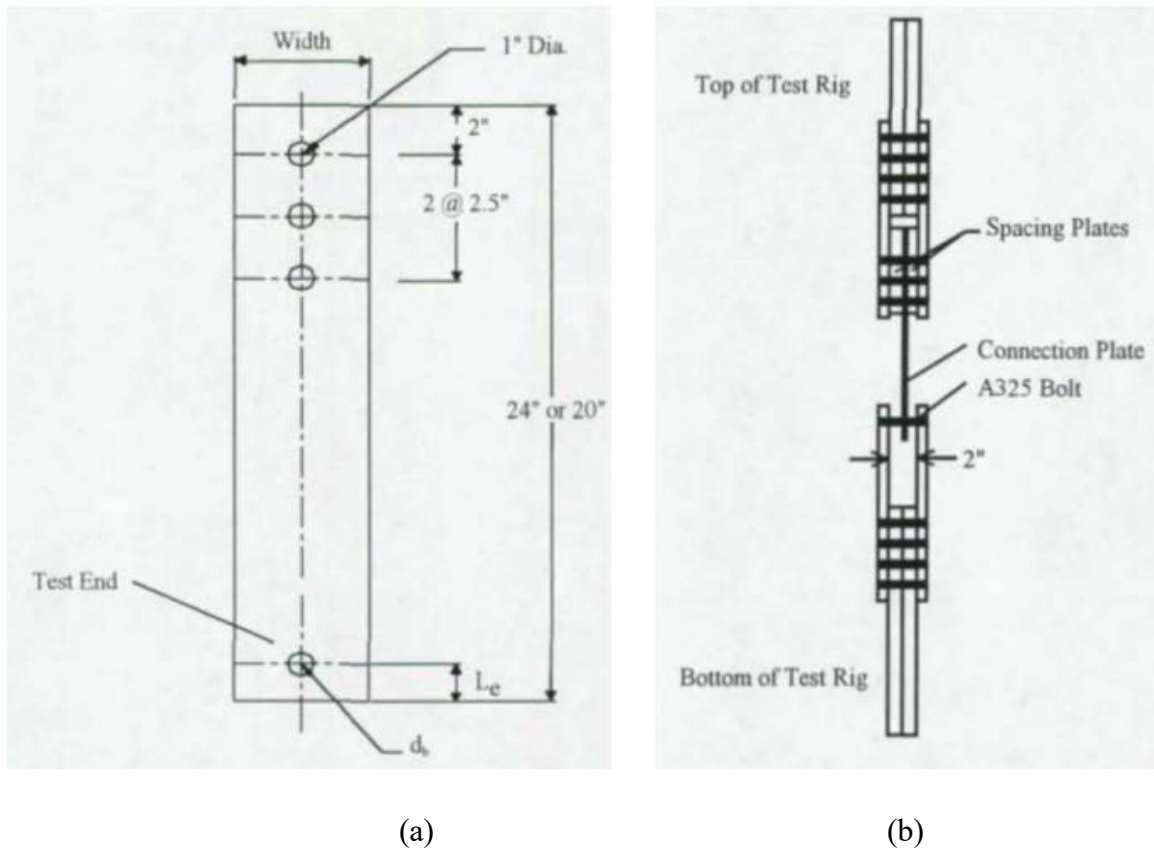


Figure 2-19: Test setup (Rex and Easterling, 1996).

Existing capacity equations for tear out and bearing failure of bolt connected material from AISC LRFD (1993), Fisher and Struik (1974), AISC LRFD (1999) and Eurocode 3 (1993) were reviewed and compared to test data. Of the equations reviewed, AISC LRFD (1993) was found to best predict the capacities of the specimens.

2.4.1.8 Duerr (2006)

In this journal article, design equations and data gathered by Johnston (1939), Tolbert (1970), Blake (1981), Duerr and Pincus (1985) and Easterling (1996) were reviewed. Based on this review, capacity equations for the ultimate failure modes of fracture on net section, splitting behind the pin, double plane shear, and dishing were recommended. For fracture on the net section Duerr recommended the plate strength be calculated as:

$$P_{u,t} = f_t * 2 * b_{eff} * t * C_r \quad (\text{kips}) \quad [2 - 65]$$

where P_n is the predicted capacity of the hanger plate for the failure mode of fracture on net section (kip), b_{eff} is the reduced effective width (in.) and is described by:

$$b_{eff} = b_e * 0.6 * \frac{f_t}{F_y} * \sqrt{\frac{D_h}{b_e}} \leq b_e \quad (\text{in}) \quad [2 - 66]$$

Similar to Tolbert and Hackett (1970), C_r is a pin clearance reduction factor that is described by:

$$C_r = 1 - 0.275 \sqrt{1 - \frac{D_p^2}{D_h^2}} \quad [2 - 67]$$

For splitting behind the hole, Duerr recommended continuing to use the empirical equation from Johnston (1939) but reorganized it to be in terms of load rather than bearing stress and adds the pin clearance reduction factor as:

$$P_{u,b} = F_u * C_r \left[1.13a + \frac{0.92(b_e)}{1 + \left(\frac{b_e}{D_h}\right)} \right] t \quad (\text{kips}) \quad [2 - 68]$$

where P_b is the nominal capacity of hanger plate for the failure mode of splitting behind the hole (kips). For double plane shear, Duerr recommended using an equation similar to that developed by Tolbert and Hackett (1970):

$$P_{u,b} = 2 * A_{bp} * V_u \quad (\text{kips}) \quad [2 - 69]$$

where P_b is the nominal capacity of hanger plate for the failure mode of double plane shear failure (kips), V_u is the ultimate shear strength of the steel plate (ksi), and A_{bp} is the total area of shear planes (in^2), this is determined similarly to “A” from Tolbert and Hackett (1970), but ϕ , the angle describing the locations of shear planes (see Figure 2-13), is given in degrees by:

$$\phi = 55 * \frac{D_p}{D_h}$$

Finally, Duerr recommended a new equation to describe dishing strength as:

$$P_{u,d} = W_{eff} * t * F_{cr} \quad (\text{kips}) \quad [2 - 70]$$

where F_{cr} is the critical dishing stress (ksi) and is described by either

$$F_{cr} = \left[\frac{1 - \frac{(K * L/r)^2}{2 * C_c^2}}{1 - \nu^2} \right] * F_y \quad (\text{ksi}) \quad [2 - 71]$$

or

$$F_{cr} = \frac{\pi^2 * E}{(1 - \nu^2) * (K * L/r)^2} \quad (\text{ksi}) \quad [2 - 72]$$

where

$$C_c = \sqrt{\frac{2 * \pi^2 * E}{F_y}} \quad [2 - 72]$$

and

$$K = 2 * \sqrt{\frac{b_e}{a}} \quad [2 - 73]$$

Eqn. 2-71 is used for E_r if $KP/r < C_c$ and Eqn. 2-72 is used otherwise. These equations for the critical dishing stress are intended to account for inelastic and elastic behavior respectively. The effective width of dishing section, W_{eff} (in), is given by the lesser of

$$W_{eff} = D_p + a \quad (\text{in}) \quad [2 - 74]$$

$$W_{eff} = D_h + 1.25 * b_e \quad (\text{in}) \quad [2 - 75]$$

No resistance factors for these strength equations were developed but the table providing the performance of these equations is shown in Table 2-10.

Table 2-10: Performance of capacity equations (Duerr, 2006).

	Net section tension ^a	Beyond splitting ^b	Double plane shear ^c	Dishing ^d
Number of specimens	12	48	18	80
Minimum Test/Prediction	0.985	0.809	0.735	0.651
Maximum Test/Prediction	1.071	1.144	1.040	1.387
Average Test/Prediction	1.042	1.024	0.952	0.961
Standard deviation	0.029	0.082	0.086	0.170
Coefficient of variation	0.028	0.080	0.090	0.177

^aTest data from Johnston (1939), Blake (1981), Duerr and Pincus (1985).

^bTest data from Johnston (1939), Tolbert (1970), Blake (1981), Duerr and Pincus (1985), and Rex and Easterling (2003).

^cTest data from Tolbert (1970), Blake (1981), Duerr and Pincus (1985), and Rex and Easterling (2003).

^dTest data from Johnston (1939), Duerr and Pincus (1985), and Rex and Easterling (2003).

2.4.1.9 Duerr (2008)

This journal article reviews and justifies revisions to the ASME standard for Design of Below-the-Hook Lifting Devices (BTH-1) (ASME, 2006) describing the design of pinned connections. The majority of these specifications were based on equations provided in Duerr (2006). The development of safety factors for these specifications and their respective reliability factors was described. One aspect of these design specifications not based on Duerr (2006) is the specification for allowable bearing stress as:

$$F_p = \frac{1.25 * F_y}{FS} \quad (kips) \quad [2 - 76]$$

where FS is a safety factor. The coefficient of 1.25 is to be reduced 50% for members subjected to more than 20,000 cycles of rotation to reduce wear and galling. Duerr notes that this coefficient is somewhat arbitrary and that development of a higher coefficient would require additional investigation.

2.4.1.10 Discussion

Based on the test specimens described in the literature, the dimension ranges were compiled in Table 2-11. As can be seen in this table, the range of specimen dimensions seems to be reasonably wide, but it should be noted that most of the test data was from the smaller sized components. Only (Blake 1981) and the Quebec Bridge (1919) included large scale hanger plates (over $\frac{3}{4}$ in. thick and widths greater than 12 in.) and even within these studies, the large-scale specimens make up the minority (only 10 specimens). This is particularly true for large size pins, as only 4 tests have been performed using pins of

3.5 in. diameter. These large pin tests were not only the oldest found in the literature, they were also conducted on hangers containing additional holes between the loaded pin holes. After the completion of the Caltrans pin and hanger inventory this range will be compared to existing pin and hanger assemblies to see if the existing data represents the inventory of in service hanger plates.

Table 2-11: Dimensional range of collected data.

	Plate Thickness, (t) (in)		Pin Diameter, (D_p) (in)		Pin Clearance, (c) (in)		Effective Width, (b_e) (in)		Clearance Back of Pin, (a) (in)		Total Specimens Tested
	min	max	min	max	min	max	min	max	min	max	
Quebec	0.38	2.00	5.0	12.0	0.03	0.06	2.0	8.1	3.8	12.1	10
Johnston	0.13	0.75	3.0	3.0	0.00	0.20	1.5	3.5	1.0	3.2	106
Luley	0.50	0.51	2.0	2.0	0.00	0.00	2.0	3.0	1.0	1.5	12
Tolbert	0.10	0.10	0.5	1.0	0.00	0.50	0.8	1.8	0.4	0.8	13
Blake	0.25	2.00	2.5	3.0	0.13	0.13	1.4	10.1	1.3	6.8	23
Duerr	0.50	0.50	2.0	2.8	0.01	3.02	1.3	1.5	1.4	2.3	8
Rex	0.25	0.75	0.8	1.0	0.06	0.06	3.5	5.4	1.0	3.0	18
Range	0.10	2.00	0.5	12.0	0.00	3.02	0.8	10.1	0.4	12.1	190

Based on preliminary review of the available data, there appears to be sufficient data from destructive tests of hanger plates to calibrate rating equations and resistance factors for these elements. The equations presented in Duerr (2006) could provide a starting point to develop rating equations within the AASHTO-LRFR framework, with the next step being the development of appropriate resistance factors for bridge rating. Depending on the comparability of Caltrans' inventory and the dimensional range of existing test results, tests may be needed to validate the approach of an appropriate size range.

2.4.2 Pins

During this literature review no physical pin tests resembling pins found in pin and hanger assemblies were found. Tests documented in Burr (1909) were reviewed, but the pins within these tests were only 1 in. diameter and had a minimum span of 8 in. and therefore hold little relevance for this research. In lieu of physical pin tests, the literature on theoretical ultimate capacity of pins and the load distribution over the length of the pin were reviewed and summarized below.

2.4.2.1 Hoblit and Melcon (1953)

In Hoblit and Melcon (1954) an attempt was made to quantify the effect of pin flexural deformation on the bearing stress distribution along the length of a pin. This concept was based on the idea that a pin bearing along a long flat surface will try to deflect upwards at its center causing it to bear more heavily on the outside edges of the bearing surface. This would shift the bearing stress from an evenly distributed load along the length of the pin to a distribution that decreases towards the center of the bearing surface and peaks at the outside faces. Hoblit and Melcon describe this by localizing bearing stress to patches at the outside faces of the plate as shown in Figure 2-20. The method for calculating a bearing area reduction factor, γ , used a chart repeated here in Figure 2-21. It should be noted that these results were stated to be supported by experimental studies but this data is not reported. Additionally, Hoblit was an engineer at

Lockheed Aircraft Corporation, so data used derivation of this equation was likely from smaller pins found in aircraft.

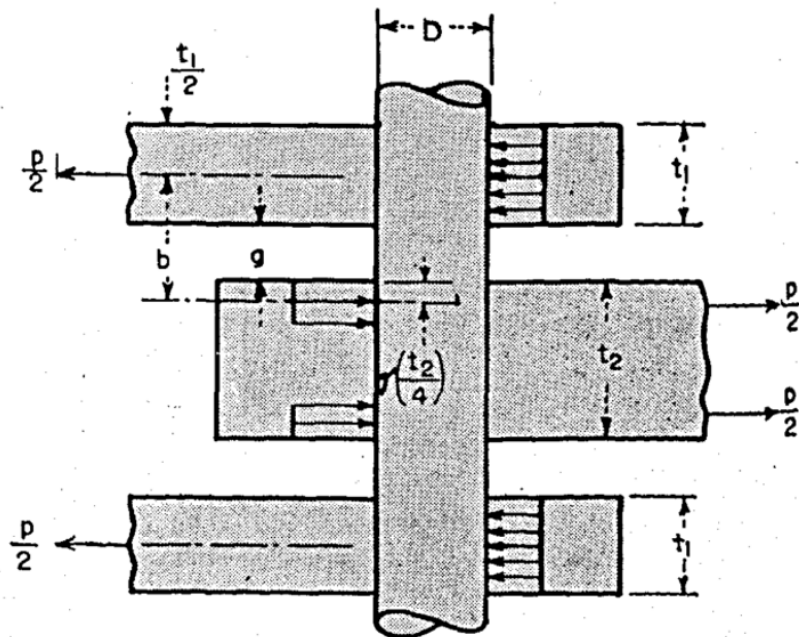


Figure 2-20: Hoblit and Melcon pin load distribution (1953).

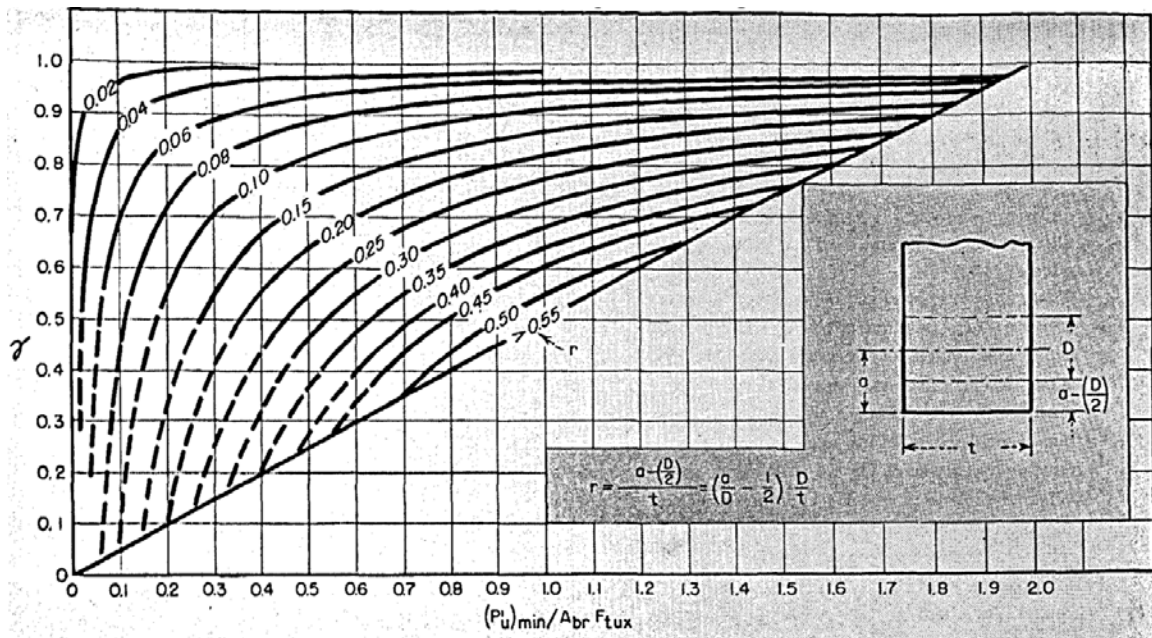


Figure 2-21: Hoblit and Melcon bearing factor (1953).

2.4.2.2 Blake (1974)

Blake (1974) presents a 4-point bending model as a load distribution method for plate forces acting on pins. He derived the distribution by dividing the uniformly distributed load along the bearing surfaces of a pin into 4 equivalent point loads. For each hanger plate, a single point load was placed at the centerline of the plate and for the beam web, two concentrated point loads were placed at a location a quarter of the web width away from each of the web faces. This distribution method is illustrated in Figure 2-22. Blake then uses this model and concepts of elastic stress distribution (also shown in Figure 2-22) to justify the common practice of checking shear and bending capacities of pins independent of one another.

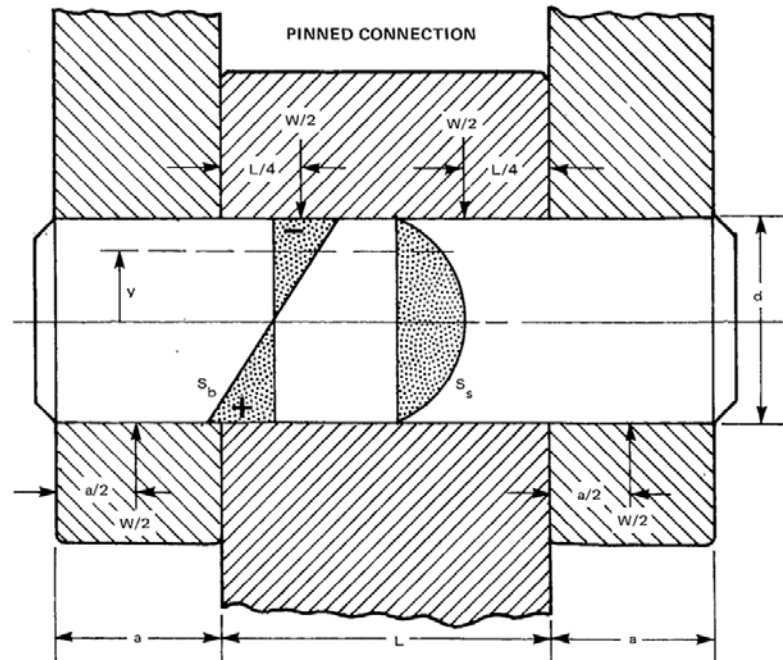


Figure 2-22: Four-point pin load distribution (Blake, 1974).

2.4.2.3 Kulicki (1983)

In this paper Kulicki developed a LFD design method for the Greater New Orleans Bridge. Of specific relevance to this project is the development of a moment-shear interaction equation for pins with plastic stress distributions. Kulicki used a computer program to track the development of plasticity across pin sections due to both shear and moment. This program assumed that those sections that had yielded due to shear resisted no moment and those sections yielded due to bending resisted no shear. Based on results from this model an interaction equation was developed as:

$$\frac{M}{M_p} + \left(\frac{V}{V_p}\right)^3 = 1.0 \quad [2 - 77]$$

where M is the applied moment at a section (kip-in), V is the applied shear at a section (kips), M_p is the plastic moment capacity of the pin (kip-in) and is described by:

$$M_p = F_y \left(\frac{D^3}{6} \right) \quad (\text{kip} \cdot \text{in}) \quad [2 - 78]$$

and V_p is the plastic shear capacity of the pin (kip) and is described by:

$$V_p = \left(\frac{\pi * D^2}{4} \right) * \frac{F_y}{\sqrt{3}} \quad (\text{kips}) \quad [2 - 79]$$

This interaction equation was compared to previous interaction equations developed for solid beams by Hodge (1957) (shown Figure 2-23) and Drucker (1956) who provided an interaction equation as:

$$\frac{M}{M_p} + \left(\frac{V}{V_p} \right)^4 = 1.0 \quad [2 - 80]$$

Due a lack of available experimental data for verification, Kulicki proposed a lower bound interaction equation as:

$$\frac{M}{M_p} + \left(\frac{V}{V_p} \right)^3 = 0.95 \quad [2 - 81]$$

This equation was later adopted into the AASHTO LRFD Bridge Design Specifications (AASHTO, 2014). Figure 2-23 shows all four of these interaction equations along with results from Kulicki's program.

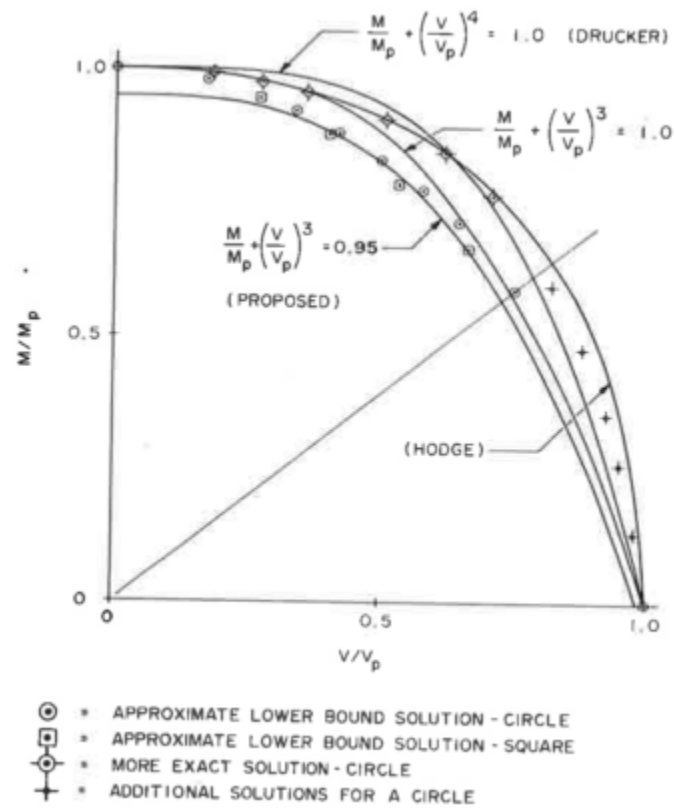


Figure 2-23: Pin interaction equation comparisons (Kulicki, 1983).

2.4.2.4 Conclusion

Based on the available literature, it is apparent that there is a lack of experimental data on large diameter pins similar to those contained in pin and hanger assemblies for bridges. Also Hoblit and Melcon (1954) and Blake (1974) show that there are multiple approaches to characterize the distribution of bearing stresses along the length of the pin but no data are available to support the formulations.

2.4.3 Beam Ends

Review of the literature for relevant past work on beams ends supporting pin and hanger assemblies reveals no specific past experimental or analytical investigations. The closest related work is on geometries found for coped beams used in buildings to connect main girders and subframing. Coped connections can exhibit lateral torsional buckling and local web buckling. Due to the presence of lateral bracing adjacent to girder ends in bridge pin and hanger assemblies, lateral torsional buckling will be less likely and was not included in this literature review.

2.4.3.1 Cheng et al. (1984)

This report details finite element modeling and physical tests to develop new design equations for both the local web buckling and lateral torsional buckling of coped beam ends. As discussed above only the local web buckling, shown in Figure 2-24, will be discussed here. Cheng et al. first develops the notation shown in Figure 2-25 describing the dimensions of a coped flange. In this figure, c is the coped length (in), d_c is the cope depth (in), h_o is the height of the remaining web (in) at coped section, d is the beam depth (in) and R is the applied shear (kips)



Figure 2-24: Example local web buckling (Yam and Chung, 2012).

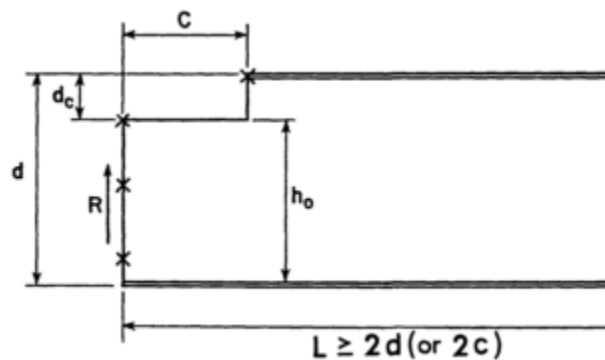


Figure 2-25: Cheng et al., (1984) coped beam notation.

Ten specimens were tested in the experimental program, of these 8 were rolled sections (12 and 18 in. deep) and two were small plate girders 26.5 in. deep. The specimens were laterally braced on the compression flange at the start of the coped section and on the web at the location of applied shear. Unlike in pin and hanger assemblies the shear force in these specimens was applied through connections welded to the web (see Figure 2-26). Three specimens used two angles welded to the side of the

web as their connectors while the remaining specimens used flat plates welded to the end of the web. These connectors were then attached to a reaction wall as shown in Figure 2-27. The intent of this test setup was to minimize the amount of in-plane restraint felt by the beam end.

Based on the results of these tests and the computer models, Cheng et al. found the existing code recommendations to be overly conservative and recommended an alternate equation to describe the elastic web buckling of coped beams as:

$$F_{cr} = \frac{k * \pi^2 * E}{12 * (1 - \nu^2)} * \left(\frac{t_w}{h_0} \right) \quad (\text{ksi}) \quad [2 - 82]$$

where F_{cr} is the critical buckling stress (ksi) of the girder web at elastic stress distributions, t_w is the web thickness and the buckling coefficients k is described as:

$$k = 2.2 * \left(\frac{h_r}{c} \right)^{1.65} \quad \text{when} \quad \frac{c}{h_0} \leq 1.0 \quad [2 - 83]$$

$$k = 2.2 * \left(\frac{h_r}{c} \right) \quad \text{when} \quad \frac{c}{h_0} \geq 1.0 \quad [2 - 84]$$

and the coefficient f is described as:

$$f = 2 \left(\frac{c}{d} \right) \quad \text{when} \quad \frac{c}{d} \leq 1.0 \quad [2 - 85]$$

$$f = 1 + \left(\frac{c}{d} \right) \quad \text{when} \quad \frac{c}{d} \geq 1.0 \quad [2 - 86]$$

Additionally, Cheng et al. determined that designing a coped beam end for both elastic web buckling and shear yield effectively precludes inelastic local buckling of the web.

Shear yielding is controlled by the equation:

$$R_y = 0.577 * F_y * h_0 * t_w \quad (\text{kips})$$

[2 - 87]

where R_y is the applied shear load (kips) at yielding failure.

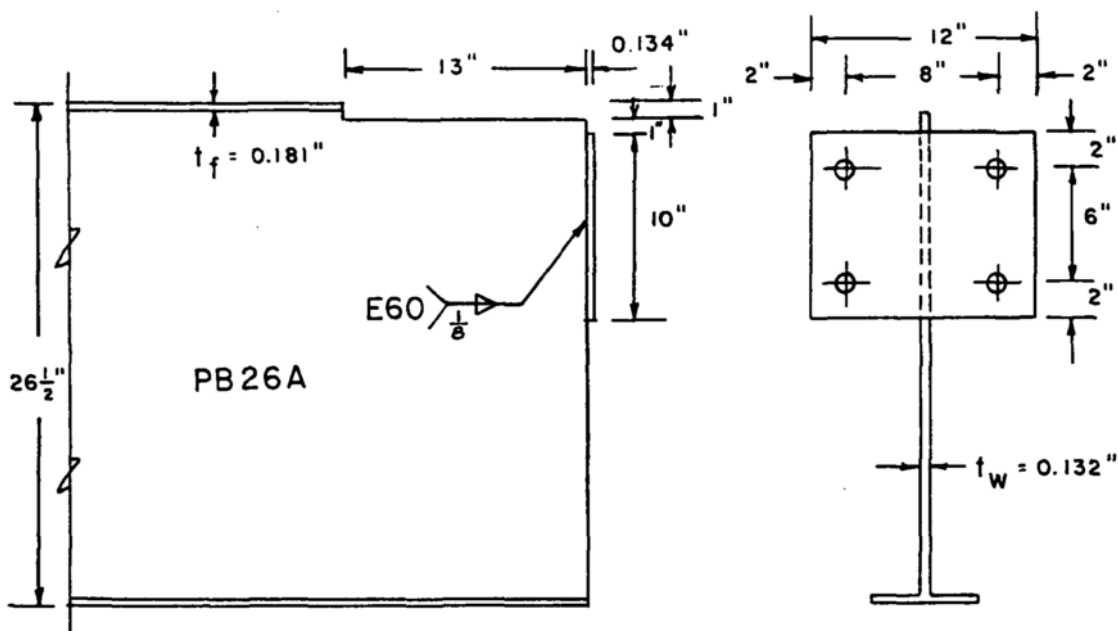


Figure 2-26: Example plate girder specimen (Cheng et al., 1984).

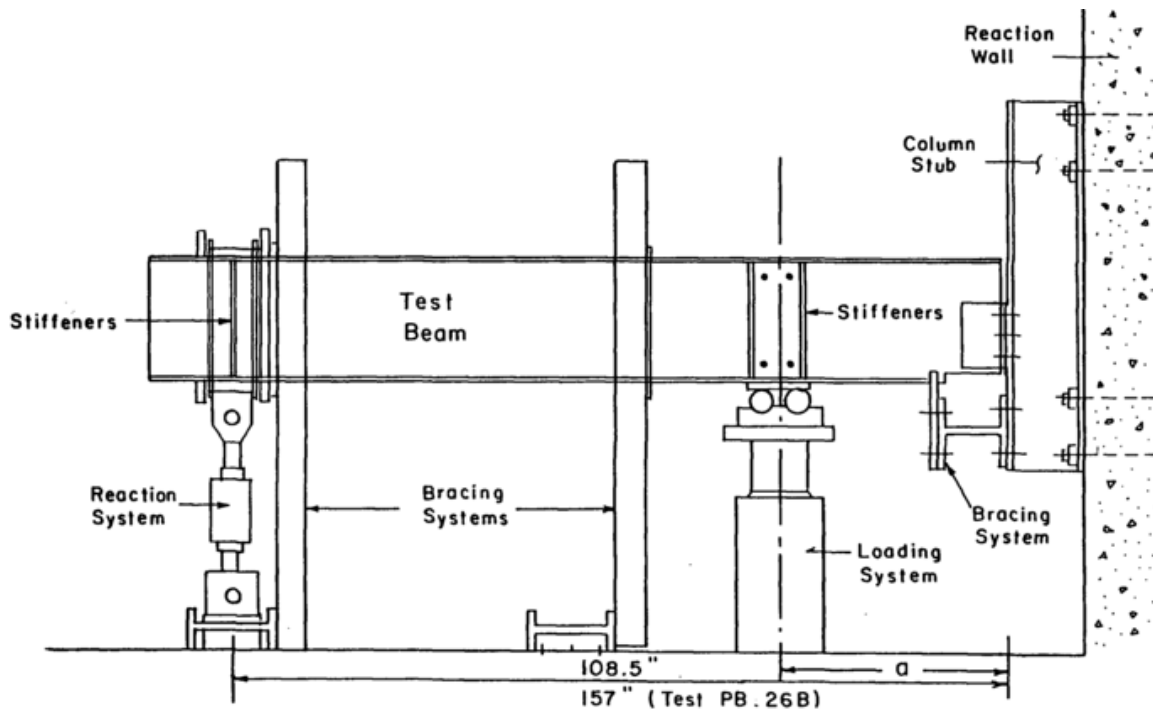


Figure 2-27: Cheng et al. (1984) test setup.

All of the specimens tested in this report were plain beam sections with no stiffeners or doubler plates. Cheng discusses three varieties of reinforcement for coped beams: horizontal stiffeners (A), horizontal and vertical stiffeners (B) and doubler plates (C) (see Figure 2-28). Based on results from the finite element model only, detail B was recommended for plate girders ($d/t_w > 60$). The other two details were recommended only for rolled sections due to their stouter webs.

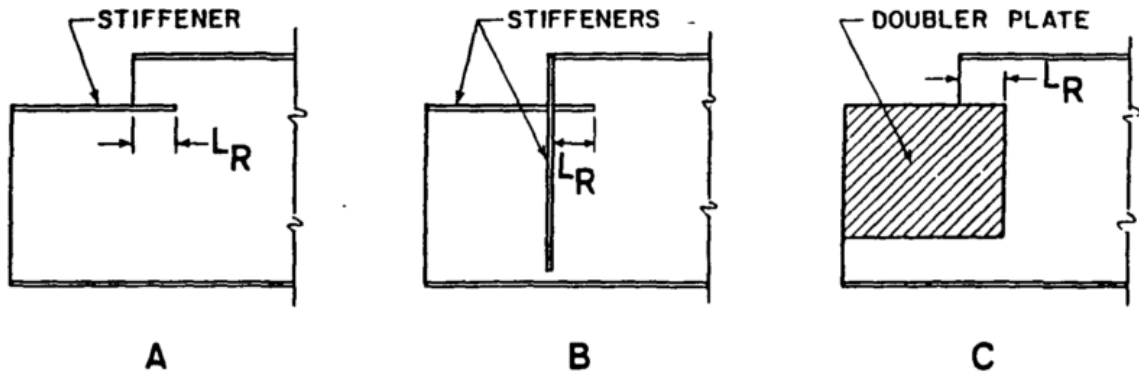


Figure 2-28: Coped end reinforcement methods (Cheng et al., 1984).

2.4.3.2 Yam et al. (2003)

Yam et al. (2003) describe the testing of four coped beam sections. These specimens were designed similar to those in Cheng et al. (1984) and consisted of (2) W16x26 and (2) W18x35 beam sections. The test setup was similar to Cheng et al. (1984) with welded end connections designed to simulate simply supported conditions. These tests were used to validate a finite element model and an equation to establish the resistance of the connection was developed as:

$$V_{cr} = \tau_{cr} * t_w (D - d_c) \quad (\text{kips}) \quad [2 - 88]$$

where V_{cr} is equal to the critical buckling shear (kips), D is the beam depth (in) and τ_{cr} is the critical shear stress (ksi), and is described by:

$$\tau_{cr} = \frac{k_b * \pi^2 * E}{12 * (1 - \nu^2)} * \left(\frac{t_w}{h_r} \right) \quad (\text{ksi}) \quad [2 - 89]$$

where k_s is the shear buckling coefficient, and is described as:

$$k_s = a * \left(\frac{h_o}{c} \right)^b \quad [2 - 90]$$

where the coefficients a and b are described as:

$$a = 1.38 - 1.79 \frac{d_c}{D} \quad [2 - 91]$$

and

$$b = 3.64 \left(\frac{d_c}{D} \right)^2 - 3.36 \left(\frac{d_c}{D} \right) + 1.55 \quad [2 - 92]$$

This new design equation was based on shear buckling of the girder web distinguishing it from that proposed by Cheng et al. (1984) which was based on flexural buckling theory. Additionally, this equation was shown to better predict the capacity with less conservatism, predicting the average capacity to be 98% of actual capacity.

2.4.3.3 Aalberg (2014)

The paper describes the tests of 6 stainless steel IPE300 beams (approximately 12 inches deep with ¼” webs) with 5 of them being coped. These beams were tested by applying a patch load to the bottom face of the uncoped flange in the manner shown in Figure 2-29. Four of the five coped beams failed by web buckling at the coped section while the final coped beam failed by local web crippling above the uncoped flange. Finite element models were created and results compared with test results. The results were also compared to existing coped beam capacity equations produced from Cheng et al. (1984)

and Yam et al. (2003) and other triangular brackets models. Yam et al.'s (2003) equations were shown to correspond most closely to the present experimental results.

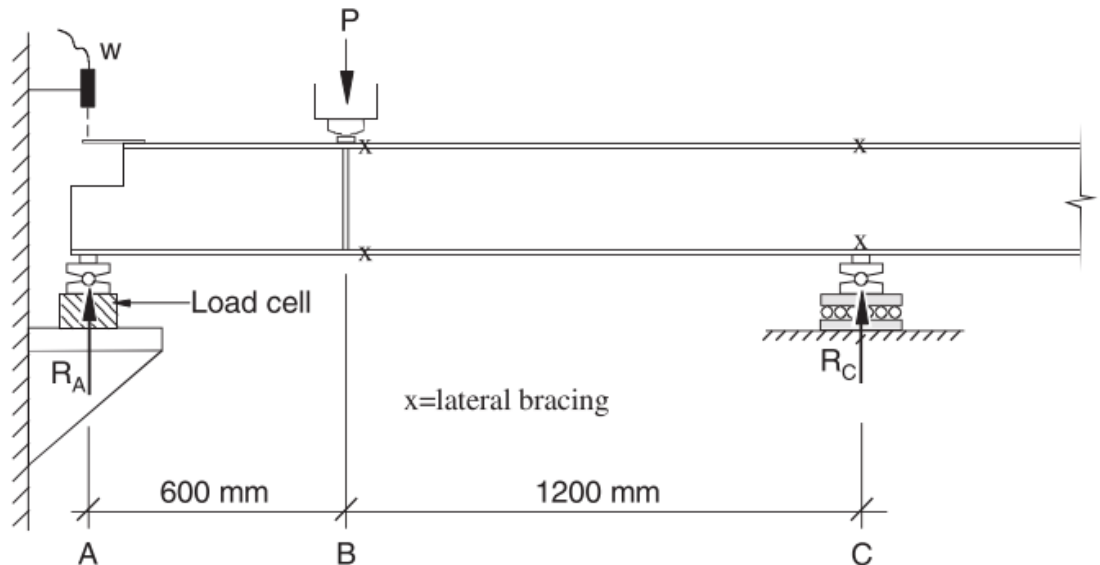


Figure 2-29: Test setup used by Aalberg (2014).

2.4.3.4 Yam et al. (2014)

Yam et al. (2014) reviews existing test data and experimentally derived equations relevant to the capacity of bolted coped beams. Failure modes considered include shear/flexural yielding at the coped section, elastic and inelastic buckling at the coped section, and block shear at the connection. In the investigation of the failure of coped beams at the coped section this paper reviews the work by Cheng et al. (1984), Yam et al. (2003), and Aalberg (2014). Based on the available data, the author found that the equations developed by Cheng and Yam both predicted the capacity of elastic web buckling at coped section fairly well but that Cheng's equations were overly

conservative. The author also noted that taking the lowest of the calculated buckling, flexural yielding, and shear yielding adequately eliminated inelastic buckling.

Block shear tests for single rows of bolts in coped sections were also reviewed and compared to existing code capacity equations. The AISC LRFD equation was seen to show good agreement with a mean predicted/test capacity of 1.15 and with a coefficient of variation of 0.106.

2.4.3.5 Conclusion

Based on the literature reviewed, the available experimental data consists of small coped ended beam specimens with connections that are very different from common bridge girder beam ends with pin and hanger assemblies. Significant differences exist in the manner of loading (doubler plates and single concentrated loading at the pin hole), connection geometry, and member size. These differences make application of current design equations uncertain for bridge girder ends supporting pin and hanger assemblies.

2.5 Materials

While materials were discussed in previous sections, this section will review information specific to materials that did not align with the previous sections. Specifically, the AISC Steel Design Guide 15 will be reviewed for insight into historic steel. Additionally, the basics of wear will be reviewed in order to try and better understand the discrepancy in allowable bearing stresses, noted in Section 2.2 of this paper.

2.5.1 AISC Design Guide 15

The AISC Design Guide 15: Rehabilitation and Retrofit Guide (AISC, 2002), provides information and guidance for engineers evaluating and rehabilitating historic steel buildings. Included in this document is a compilation of historic rolled steel shapes and their section properties. Also included in this document is a historic timeline of changes in ASTM specifications for steels used in steel buildings. A review of this timeline shows that some of the specifications documented were also specified for steel bridges. Additionally, it is noted that the information provided in the timeline is more complete than what can be found from the AASHTO specifications (Section 2.2). The relevant information from this timeline has been reproduced in Appendix A.

2.5.2 Mechanical and Corrosion Wear of Sliding Interface

As reviewed in Section 2.2 of this paper, there are significant inconsistencies among bridge specifications on what limits to apply to pin bearing stress. Of specific interest to this project is the treatment of bearing stress on pins subject to rotation. For the purpose of rating, the ASD portions of the AASHTO Standard Specifications (AASHTO, 2002) and the Manual for Bridge Evaluation (AASHTO, 2011) require this allowable bearing stress to be essentially halved. At the same time the AASHTO LRFD Specifications (AASHTO, 2014) specify, for the rating of existing pins, the same bearing stress for rotating and non-rotating pins. Presumably the different treatment of rotating pins is to reduce the effects of wear on the pin. The intent of this subsection is to

investigate the basic characteristics of wear as related to bearing stress for rating of pin and hanger assemblies.

The likely wear mechanism occurring in pin and hanger assemblies is a sliding wear mechanism, because of the relative sliding motion between the hanger, or beam web, and the pin. From the literature, only dry (unlubricated) sliding systems were reviewed. It was assumed that these systems were built unlubricated or that the life of any lubricant would be finite. The effects of corrosion on the sliding wear processes was also investigated.

Sliding wear is defined by ASTM G40 as “wear due to relative motion in the tangential plan of contact between two solid bodies” (ASTM, 2015). A special case of sliding wear specifically applicable to this pin and hanger assemblies is adhesive wear. A traditional description of this wear mechanism starts with the two solid bodies adhering at asperities (microscopic protrusions in the surface of the bodies) as they slide across each other. After significant plastic deformation, a portion of the softer body is torn off and joins the opposite body. Eventually this process leads to the dislocation of material off both bodies in the form of wear debris (Rigney, 1997). The equation most frequently referenced in the literature in relation to adhesive wear is from the 1950’s and credited to Archard (Archard, 1953):

$$Y = k * \frac{W * L}{H} \quad [2 - 93]$$

where Y is the wear volume, W is the applied load, L is the sliding distance, H is the hardness of the softer material, and k is the wear coefficient. Major implications of this equation are that the wear rate is controlled by the load and the hardness of the weaker

material, and that adhesive wear is a function of only four (4) variables. Adhesive wear is a complex and may be a function of more than twenty five (25) variables (Ludema, 1990). Welsh (1965) describes one occasion where slight changes in one of these variables can lead to jumps in wear rate.

Suh et al (1973) introduced an alternate wear theory specific to slow sliding bodies where heat is not accumulated. In this theory wear results from subsurface tearing and is considered more a function of the presences of large second phase particles and inclusions in the steel rather than just its hardness. Suh supports this theory in part by the observation that under slow sliding conditions, annealed iron had one third the wear rate of AISI 1020 steel despite only having one third of the hardness. However, Rigney (1997) brings into question the subsurface origin of the material fracture. Rigney (1997) also highlights the importance of the properties of the wear particles produced in the process, which in themselves can be a function of many factors.

The literature cited here is a small sample of the complexity inherent in adhesive wear. Because of this complexity, Ludema (1990) warns not to rely on any wear equation without simulative testing to support the behavior described by the equation. It should be noted that none of the documented tests found to date accurately describe the conditions occurring in the assemblies under investigation.

One form of adhesive wear that is of particular interest is to this project is galling. Galling is defined by ASTM G40 as “a form of surface damage arising between sliding solids, distinguished by macroscopic, usually localized, roughening, and the creation of protrusions above the original surface” (ASTM, 2015). Galling is of specific interest to this research due to the severity of the damage it causes, as well as significance as a

binary occurrence. This means that it either occurs or it does not, and its occurrence is based on reaching threshold stress and sliding distance (Waite et al., 2006). ASTM currently offers two standardized test methods for the occurrence of galling ASTM G98 (ASTM, 2002) and ASTM G196 (ASTM, 2016). But these tests are only recommended for preferential ranking of mating materials for the purpose of design (Waite et al., 2006). Situational specific tests are recommended to determine quantitative values for stresses at which galling occurs.

Corrosion can significantly affect the mechanism of sliding wear. Madsen (1990) observed that there can often be a synergistic effect between these two processes. This synergistic effect does not always occur in sliding scenarios. Trausmuth et al. (2014) observed no increase in the wear of one of their two low-alloyed steel samples when exposed to sliding wear within a corrosive environment. These specimens were of the same chemistry and only differed by heat treatment. Trausmuth et al. (2014) also documents surface softening of both specimens exposed to sliding corrosion wear. This is the opposite of what is normally seen in sliding wear, where strain hardening typically increase surface hardness.

2.6 Literature Review Conclusion

In this literature review, both historic and current specifications, relevant to pin and hanger assemblies, were reviewed. Additionally, reports related to the in-service performance of these assemblies and existing nondestructive evaluation methods used to assess the condition of pin and hanger assemblies were reviewed. Existing experimental

and theoretical studies conducted on hanger plates, pins and girder ends where investigated. The basic principles of wear were also reviewed. Based on the literature reviewed the following conclusions were drawn:

- The provisions available in the AASHTO Specifications for the analysis of girder ends in pin and hanger assemblies are based on Euler-Bernoulli beam theory. Based on the complex and non-uniform stresses created by the concentrated load exerted by the pin the application of these equations is questionable. To better understand the distribution and interaction of stresses in these girders ends experimental and analytical investigations are required.
- Given the lack of previous testing on large diameter pins, experimental data is necessary to support the pin interaction equation given in the AASHTO LRFD Specifications. This experimental data could allow for a less conservative interaction equation.
- The current hanger plate provisions provided in the AASHTO specifications appear to be most applicable for hanger plate sizing during design. These provisions do not seem as useful for the determination of the actual member capacity. More accurate rating methods are required for hanger plates.
- Outside of instrumentation there is currently a lack of good methods for determining complete or partial fixity in these assemblies. Additionally, while it is recommended that fixed assemblies be replaced, there is no guidance how to treat partially fixed assemblies.

- Specific wear testing of this assembly is necessary prior to determining if a reduced bearing stress, as used in the allowable stress portion of the AASHTO Standard Specification, should be used when rating these assemblies,
- Based on the experimental studies conducted on hanger plates, there appears to be enough data to develop rating equations and to calibrate resistance factors for their various failure modes.

Chapter 3 – Analysis of Hanger Plate Ultimate Strength Predictions

3.1 Introduction

From the literature review, a significant amount of information on the performance of hanger plates was identified. This information included various failure modes and test results for 190 experimental specimens. Additionally, several existing methods were identified that have been used to predict the strength of hangers for different failure modes. In this chapter, the empirical data for different hanger failure modes is reviewed and the specimen geometries and material properties are compared to those from a sample inventory of Caltrans' in-service hanger plates. Of the equations identified in the literature review, those from Caltrans' LFR and LRFR methods (Caltrans, 2016a) (Caltrans, 2016b), the AISC specifications (AISC, 2016), Johnston (1939) and Duerr (2006) considered in more detail. The equations are compared against experimental results in the literature and the predictive capabilities of the different methods are described statistically.

3.2 Data Review

In the literature review, data on 190 specimens was collected from seven separate experimental studies. These studies were conducted between 1919 and 1997. Of these specimens 14 were removed because they either did not achieve ultimate strength or their failure mode was not reported. Some data were removed when the specimens had small pins in oversized holes that exceed the tight pin hole clearance of typical bridge

construction. The review of historic and current AASHTO/AASHO specifications revealed that tolerances for the clearance between the pin and the pin holes were limited to 1/50th in. for pins under 5 in. diameter and 1/32nd in. for pins over 5 in. diameter. Caltrans' current rating methods also do not take clearance into account, likely due to the tight tolerances specified. Studies by Duerr and Pincus (1985) and by Tolbert (1970) both investigated hole clearance and showed that increased clearances decreased the hanger capacity. In order to prevent data from tests with unrealistically large pin hole clearances from negatively affecting predictive equations applicable to only tight tolerance pin holes, specimens that did not conform to the AASHTO requirements for clearance were removed. This left 80 remaining specimens from five (5) different experimental studies for use this investigation. The general dimensional ranges for these specimens are shown in Table 3-1.

Table 3-1: Range of data for hanger tests corresponding to AAHTO pin hole dimensional tolerances.

	b_e (in)	a (in)	D_p (in)	t (in)	F_y (ksi)	F_u (ksi)
Max	4.00	4.73	5.00	0.75	97.6	109.4
Min	0.75	0.37	1.00	0.10	28.4	46.8

3.3 Caltrans Inventory

The remaining data from the literature was compared to the hanger plates used on Caltrans' bridges. This comparison was conducted to determine applicability of the previous studies to Caltrans' inventory. To accomplish this comparison, Caltrans

reviewed their bridges and provided expert opinion on typical in-service pin and hanger assemblies within their inventory. To illustrate the representative details, ten (10) separate bridges were reported. The first step in this process was a comparison of hanger thickness (t), effective width (b_e), edge distance behind the pin hole (a) and the pin diameter (D_p). These comparisons are shown in histograms in Figures 3-1 through 3-4. The bars in these histograms represent the available experimental data while the vertical dashed lines represent hangers from Caltrans' inventory. This comparison showed that, based on overall scale, the experimental specimens were considerably smaller than the hangers within the Caltrans' inventory.

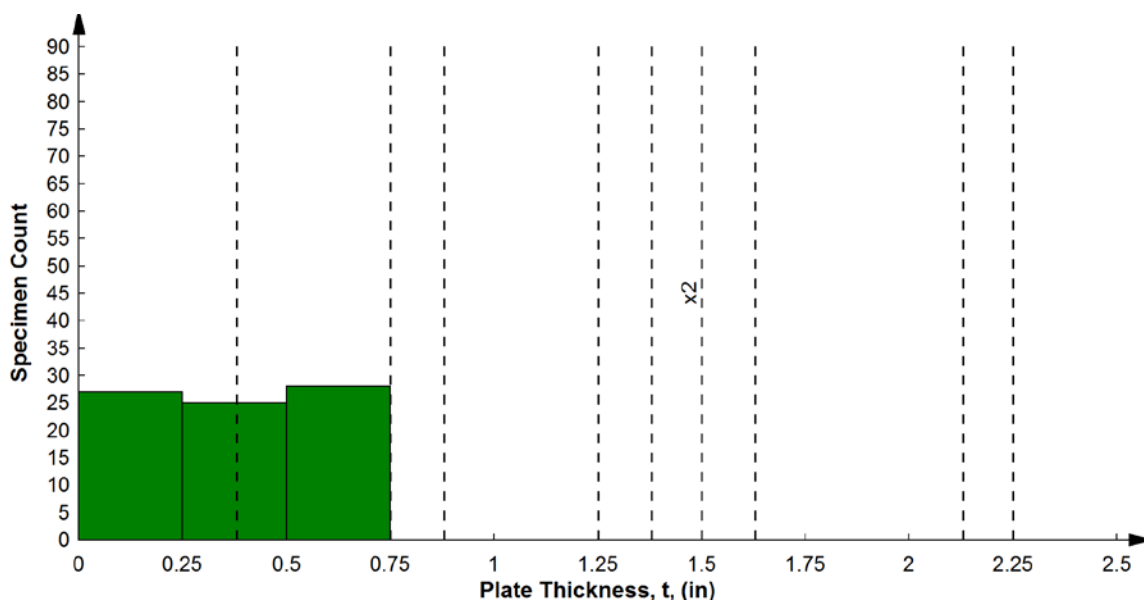


Figure 3-1: Thickness of Caltrans' hanger inventory with experimental data.

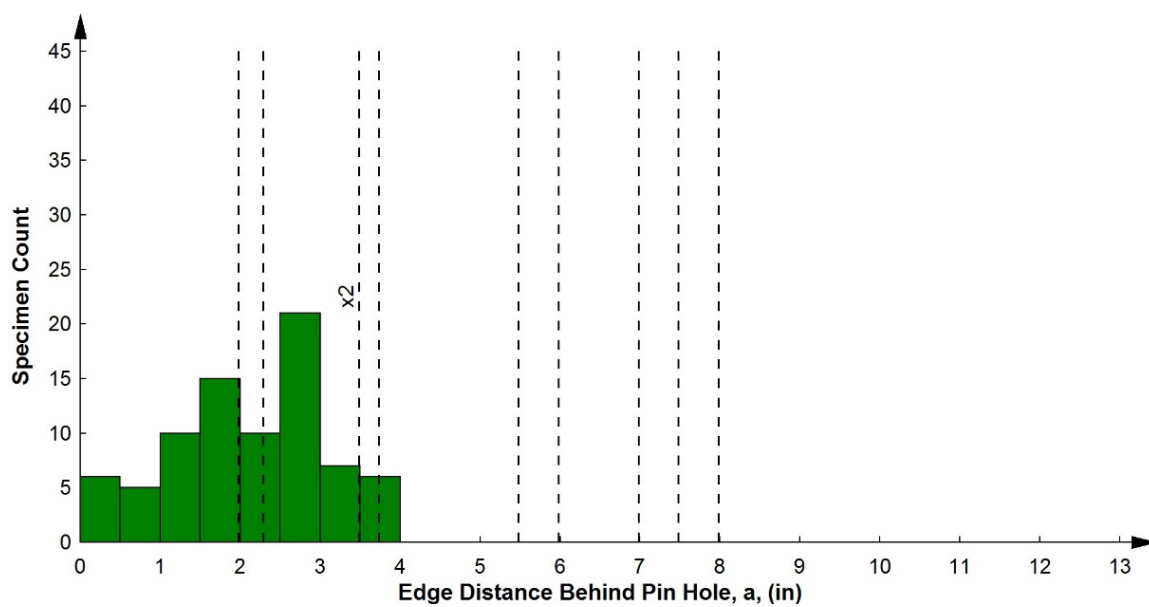


Figure 3-2: Edge distance behind the pin of Caltrans' hanger inventory with experimental data.

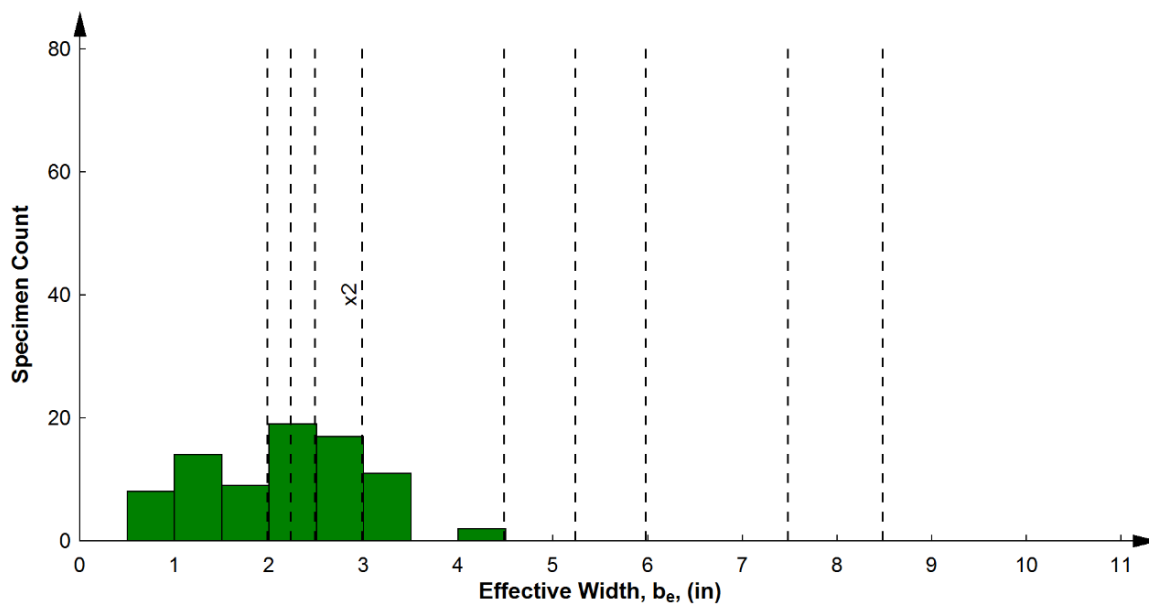


Figure 3-3: Effective width of Caltrans' hanger inventory with experimental data.

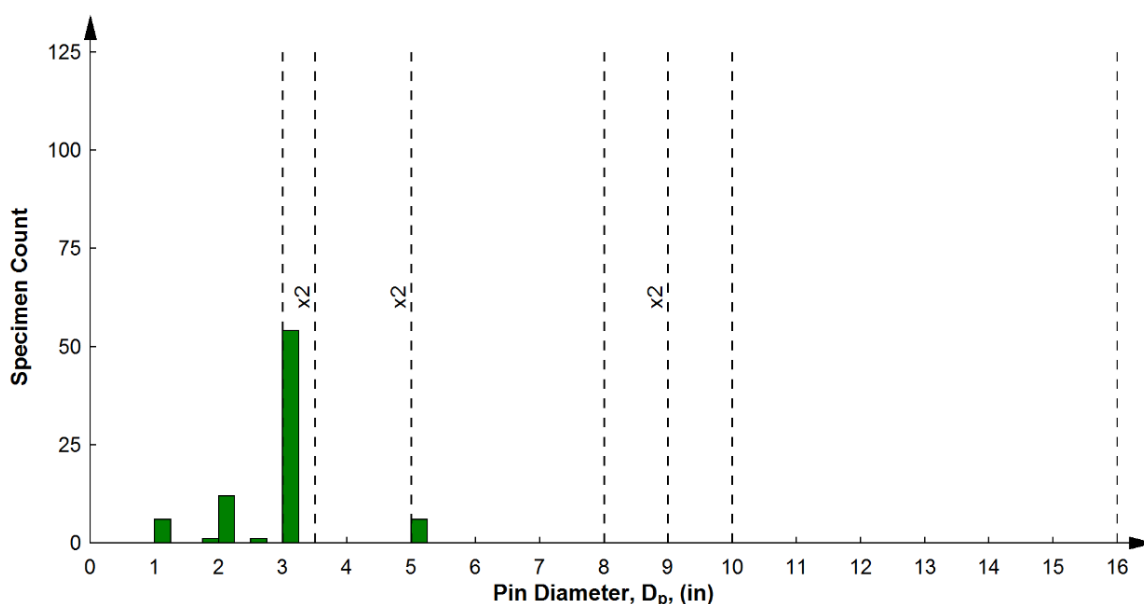


Figure 3-4: Pin Diameter of Caltrans' hanger inventory with experimental data.

Comparisons between the hanger and pin dimensional proportions was made. The proportions investigated were the ratio between:

- edge distance behind the pin hole to the diameter of the pin ($a: D_p$)
- effective width to the diameter of the pin ($b_e: D_p$)
- edge distance behind the pin hole to effective width ($a: b_e$).

The comparison of these proportions in Caltrans' inventory to those of the literature specimens is shown in histograms in Figures 3-5 through 3-7. This showed that the available specimens match well with Caltrans' inventory based on the relative sizes of elements (proportions). Given this, assuming that there are no scaling factors (which none are expected), the available data set appears sufficient for use in developing and calibrating rating methods for in-service bridge components.

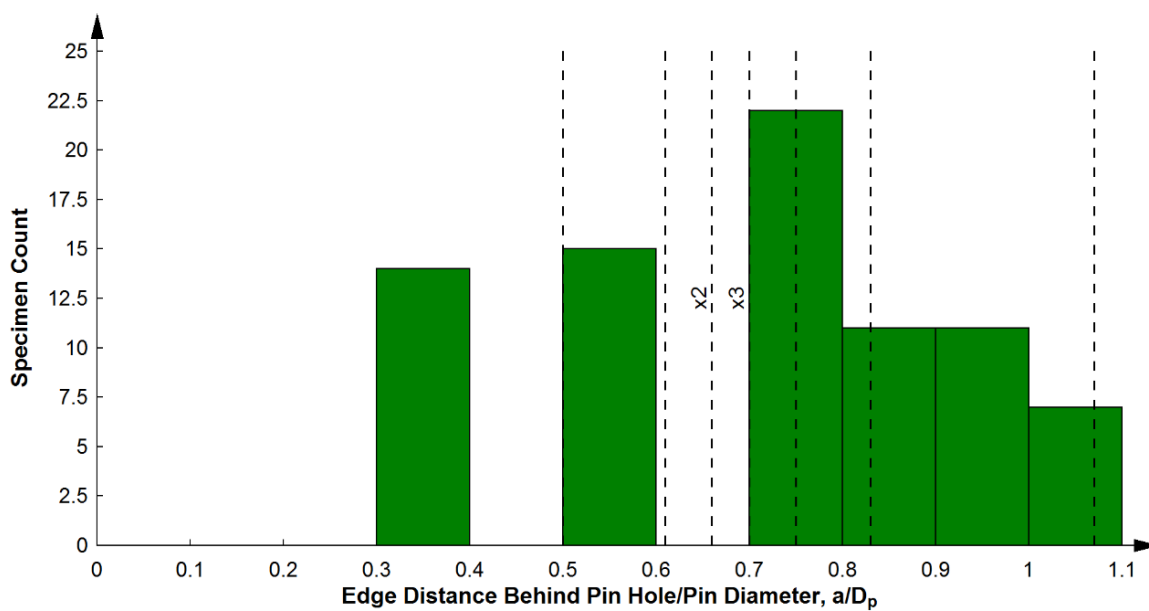


Figure 3-5: Ratio of a to D_p of Caltrans' hanger inventory with experimental data.

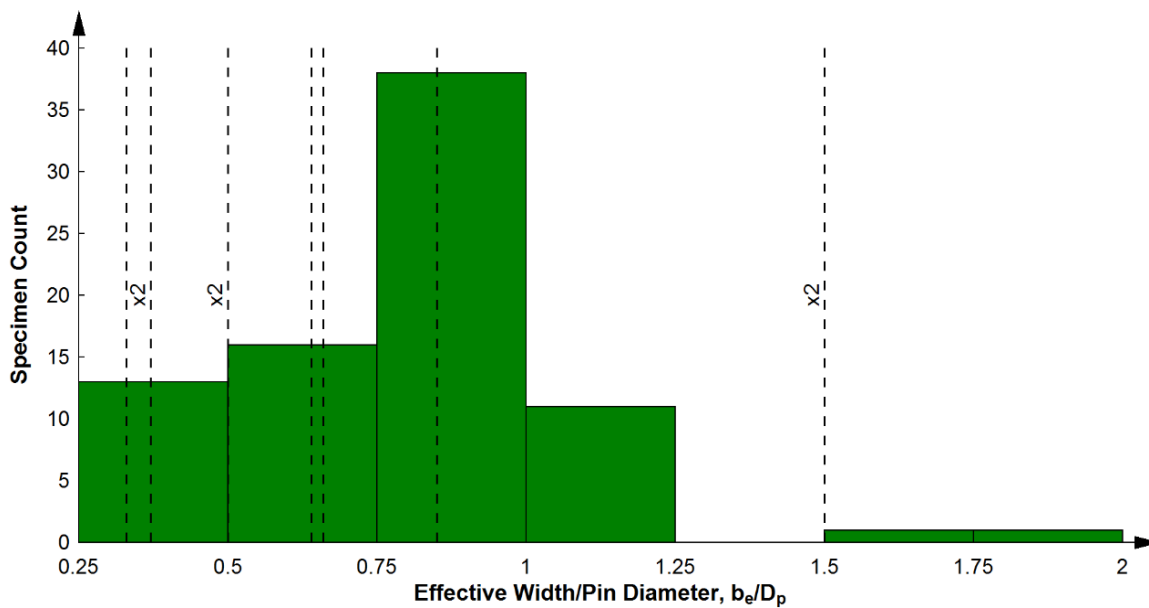


Figure 3-6: Ratio of b_e to D_p of Caltrans' hanger inventory with experimental data.

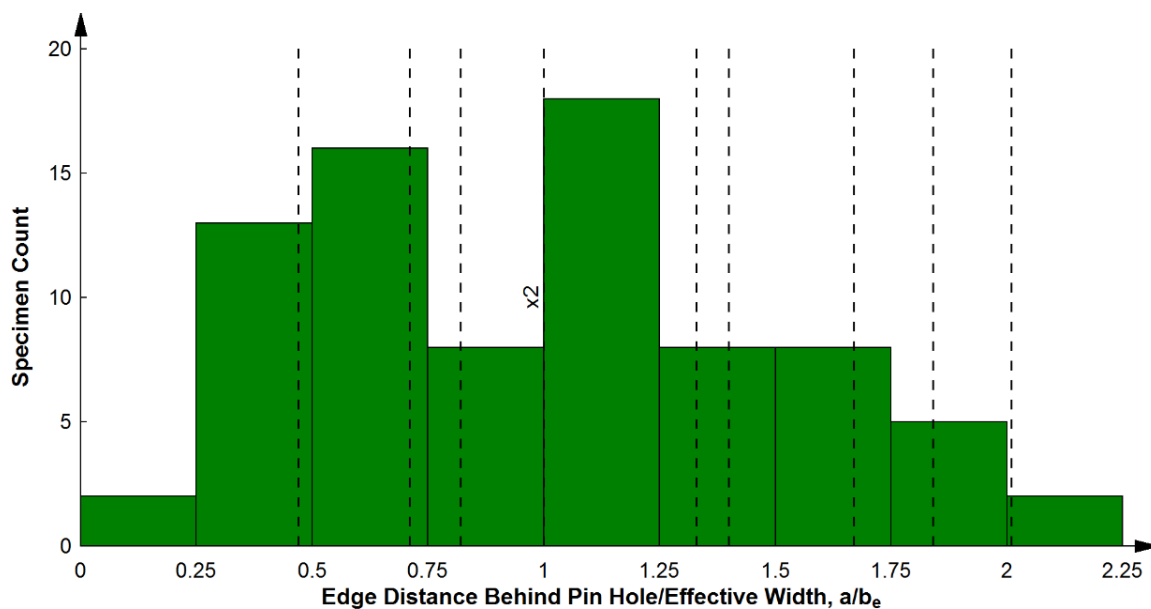


Figure 3-7: Ratio of a to b_e of Caltrans' hanger inventory with experimental data.

A comparison of the yield stress of these two groups, shown in Figure 3-8, shows agreement between Caltrans' inventory and the experimental data. But it is important to note that only a single high-yield strength plate exists in the data considered. Caltrans' inventory contains at least one high yield hanger in service. The bounds of Caltrans' inventory is summarized in Table 3-2.

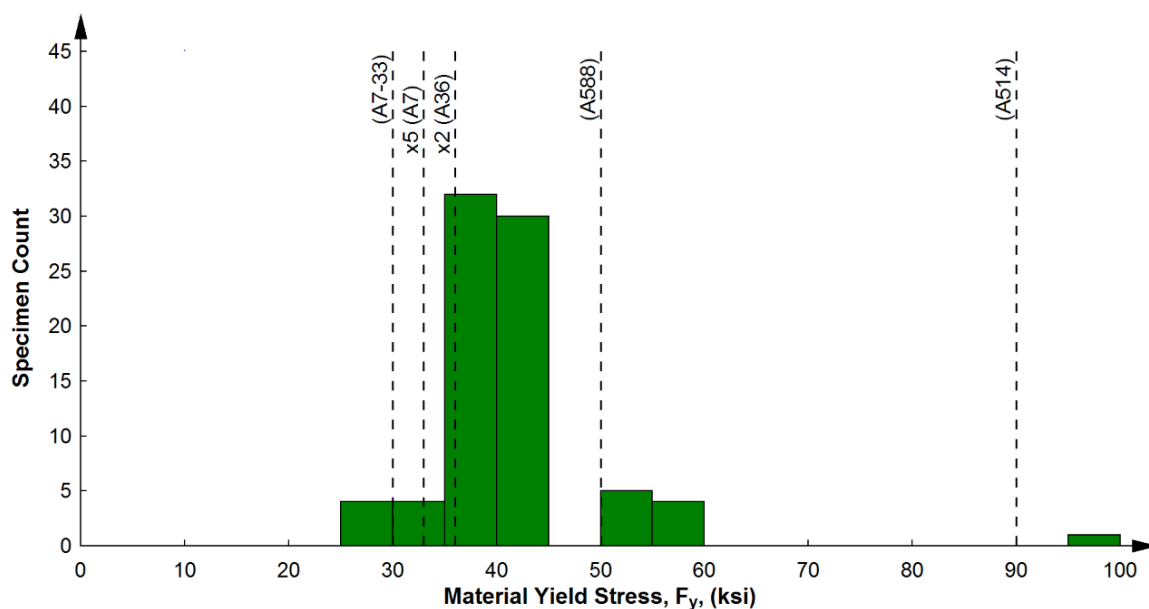


Figure 3-8: Yield stress of Caltrans' hanger inventory with experimental data.

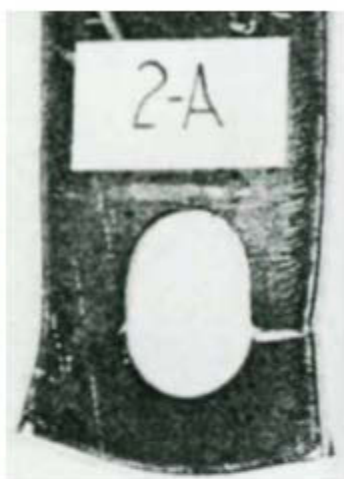
Table 3-2: Range of Caltrans' reported hanger plate inventory.

	b_e (in)	a (in)	D_p (in)	t (in)	F_y (ksi)	F_u (ksi)
Max	16.00	7.98	16	2.25	90	100
Min	1.98	1.98	3	0.375	30	55

3.4 Failure Modes

From the literature review, four (4) hanger plate failure modes were identified. The first of these failure modes was tension fracture across the pin hole. This mode is defined by a fracture across the effective width of the hanger plate perpendicular to the applied load, see Figure 3-9a. The failure modes of splitting behind the pin hole and pin tear out both produce a fracture behind the pin hole at failure. The difference in these two failure modes is in the location of the fracture relative to the pin. For splitting behind the

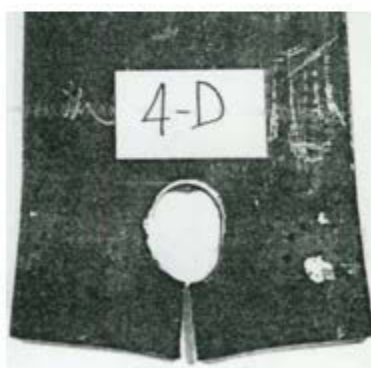
pin hole, the fracture occurs directly behind the center-line of pin as shown in Figure 3-9c. The fracture in the pin tear out failure mode occurs towards the outside of the pin, on one side or both sides, as shown in Figure 3-9d. The failure mode of dishing is due to instability of the material behind the pin hole. Dishing is typified by the section behind the pin curling out of plane as shown in Figure 3-9b.



a) Tension Fracture
Blake (1981)



b) Dishing
Duerr (2006)



c) Splitting Behind the Pin
Blake (1981)



d) Pin Tear Out
Blake (1981)

Figure 3-9: Hanger plate failure modes.

(Note: a, c, and d are front views while b is a side view of plate).

Categorizing the 80 specimens by their respective failure modes produces Table 3-3. A review of this table shows there is minimal data for hangers that failed by pin tear out or splitting behind the pin hole. This lack of data is mostly due to researchers not differentiating between pin tear out and splitting behind the pin (Johnston (1939) and Tolbert (1970)) and, a lack of suitable pictures to enable independent verification of the failure modes.

Table 3-3: Hanger data by failure mode.

Test Series	Splitting	Tear Out	Tension Fracture	Dishing
Quebec Bridge (1919)	1	0	1	4
Johnston (1939)	12*		5	37
Luley (1942)	3	3	6	0
Tolbert (1970)	6*		0	0
Blake (1981)	0	0	0	0
Duerr and Pincus (1985)	0	0	2	0
Rex and Easterling (1996)	0	0	0	0
Total	4	3	14	41
	Combined: 18			

3.5 Review of Caltrans' Rating Methods

The present methods used by Caltrans to evaluate hanger plates were compared against the 80 available data in the literature to assess the current state-of-the-practice. The predicted capacity of each specimen was compared to its experimentally determined ultimate strength. The inputs for rating were the actual reported material properties and

plate geometries. This procedure was performed for both rating methods used by Caltrans: the Load and Resistance Factor Rating (LRFR) and Load Factor Rating (LFR) method. These methods for rating hangers were previously discussed in detail in sections 2.2.2.3 and 2.2.2.4. For clarity, the equations used by Caltrans for each method will briefly be reviewed prior to comparison.

It should be noted that these equations are presented without the resistance factors that are typically found in the LRFR method and occasionally in the LFR method. This was done intentionally because resistance factors are used to achieve a target reliability for the given uncertainties.

3.5.1 Caltrans LFR Method

In Caltrans' LFR method, five checks are used to determine the nominal strength of a hanger plate. In practice, the check that predicts the lowest capacity for the hanger controls the rating and defines the hanger plate capacity. Yield across the pin is checked using:

$$P_{n1} = 2b_e t F_y \quad (kips) \quad [3 - 1]$$

where b_e is the effective width next to the in hole (in), t is the plate thickness (in) and F_y is the plate material yield stress (ksi). Excessive bearing pressure on the pin hole is checked by:

$$P_{n2} = D_p t F_y \quad (kips) \quad [3 - 2]$$

where D_p is the pin diameter (in). Shear yielding behind the pin is checked using:

$$P_{n3} = 0.58 F_y A_{sf} \quad (kips) \quad [3 - 3]$$

where A_{sf} is the area of the pin shear out surface (in) and is described in detail in section 2.2.2.3.4 of this paper. Shear rupture behind the pin is checked using:

$$P_{n4} = 0.58F_u A_{sf} \quad (kips) \quad [3 - 4]$$

where F_u is the ultimate stress of the plate material (ksi). Finally fracture across the pin hole is checked using:

$$P_{n5} = \frac{2b_e t}{1.4} F_u \quad (kips) \quad [3 - 5]$$

When these checks were used to compute the nominal strength of the 80 tight-fit specimens from the literature they were found to be generally conservative with only 2 specimens having capacities above those predicted. Figure 3-10 shows the experimentally determined ultimate load of each specimen divided by its predicted capacity (P_n) using the LFR method. Additionally, the symbol used for each specimen denotes which LFR check controls the rating of the hanger. When a symbol is filled, that denotes that the failure mode of the test specimen corresponds to the predicted failure mode. The checks for yielding across the pin hole, bearing, and shear yield correspond to a limit state which is not necessarily a failure mode.

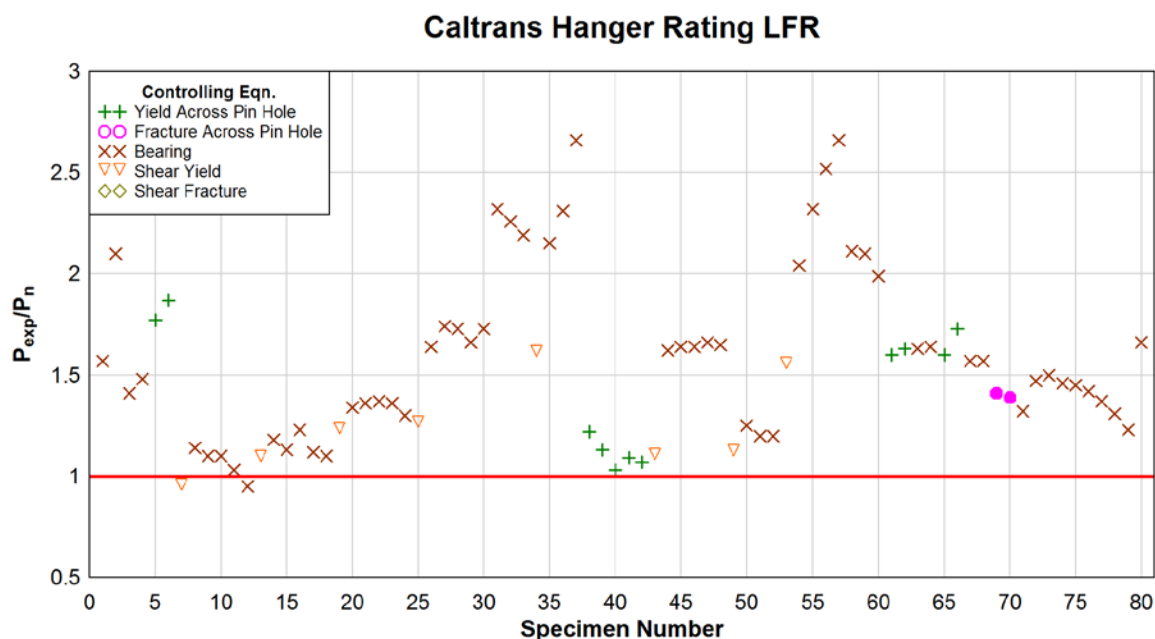


Figure 3-10: Ratio of measured and predicted strength for Caltrans LFR methods across all specimens.

As can be seen in Figure 3-10, this method is generally conservative and produced a high bias with an average P_{exp}/P_n of 1.54 but shows large variability with a coefficient of variation (COV) of 26.5%. Additionally, the checks properly identified the actual failure mode for only two (2) specimens out of the population of 80 specimens.

One possible explanation for the inaccuracy of this rating method is the presence of dishing failures. Of the specimens in the data set, over half failed by dishing. The LFR rating method has no check for this failure mode. Considering only specimens that had failure modes other than dishing the results are shown in Figure 3-11.

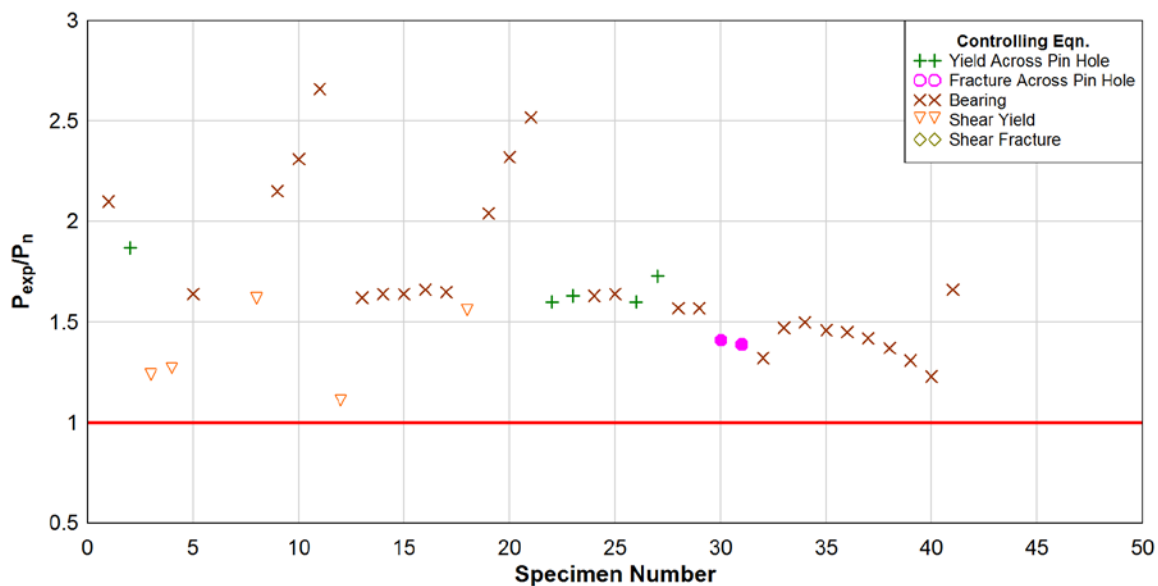


Figure 3-11: Ratio of measured and predicted strength for Caltrans' LFR method with non-dishing specimens.

Removal of the dishing specimens increased the average P_{exp}/P_n to 1.65 and lowered the COV to 21.2%. It is also notable that all predictions are now conservative. The results for these analyses are summarized in Table 3-4.

3.5.2 Caltrans LRFR Method

Caltrans' LRFR method utilizes the same rating equations as the LFR method except that Eqn. 3-5 is replaced with:

$$P_{n5} = W_e t F_u \quad (kips) \quad [3 - 6]$$

where W_e , the effective section, is given by the lesser of:

$$W_e = \frac{2b_e}{1.4} \quad (in) \quad [3 - 7]$$

and

$$W_e = a \quad (in) \quad [3 - 8]$$

Review of this equation shows that it can be used to predict two separate failure modes. When the effective section is controlled by the clearance behind the hole (a), it can be used to predict failure behind the hole. When the effective section is controlled by the effective width (b_e) it is equal to Eqn. 3-5 and checks for fracture across the pin hole.

This method was then used to rate the 80 tight-fit specimens from the literature with the results shown in Figure 3-12. The LRFR method proved to be more conservative than the LFR method and predicted the correct failure mode 21 out of 80 times. But this method produced large bias with an average P_{exp}/P_n of 1.77 and a high coefficient of variation (COV) of 26.6%.

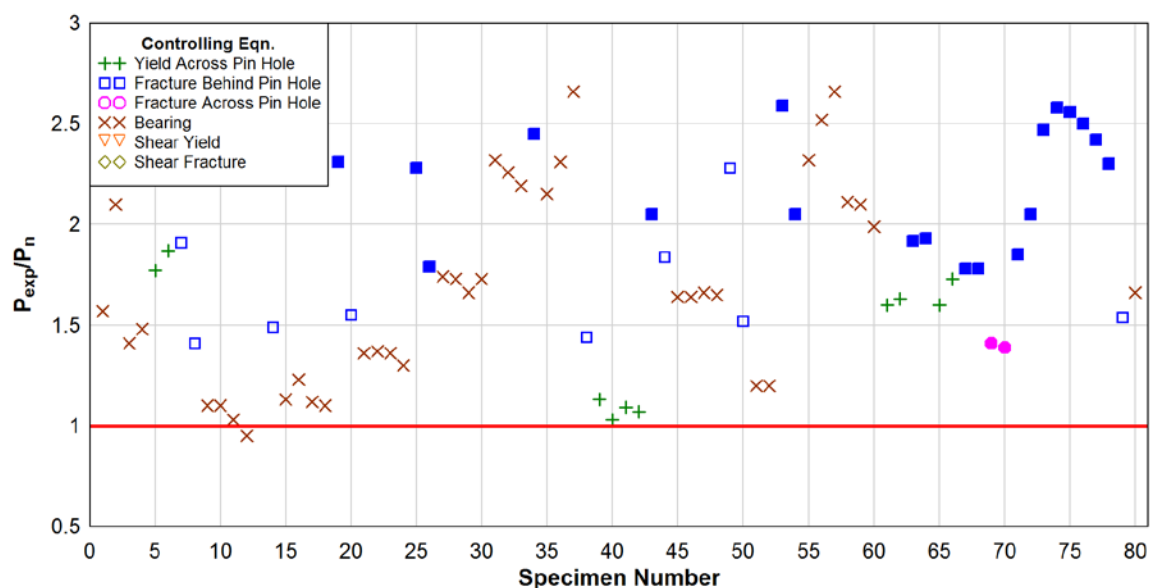


Figure 3-12: Ratio of measured and predicted strength for Caltrans' LRFR methods across all specimens.

When dishing specimens are removed from the analysis, the bias P_{exp}/P_n increased to 2.02, the coefficient of variation decreased to 18.2%, and all the predictions

were conservative. A plot of the LRFR method comparisons without dishing specimens is shown in Figure 3-13. The statistical results from these two methods are summarized in Table 3-4.

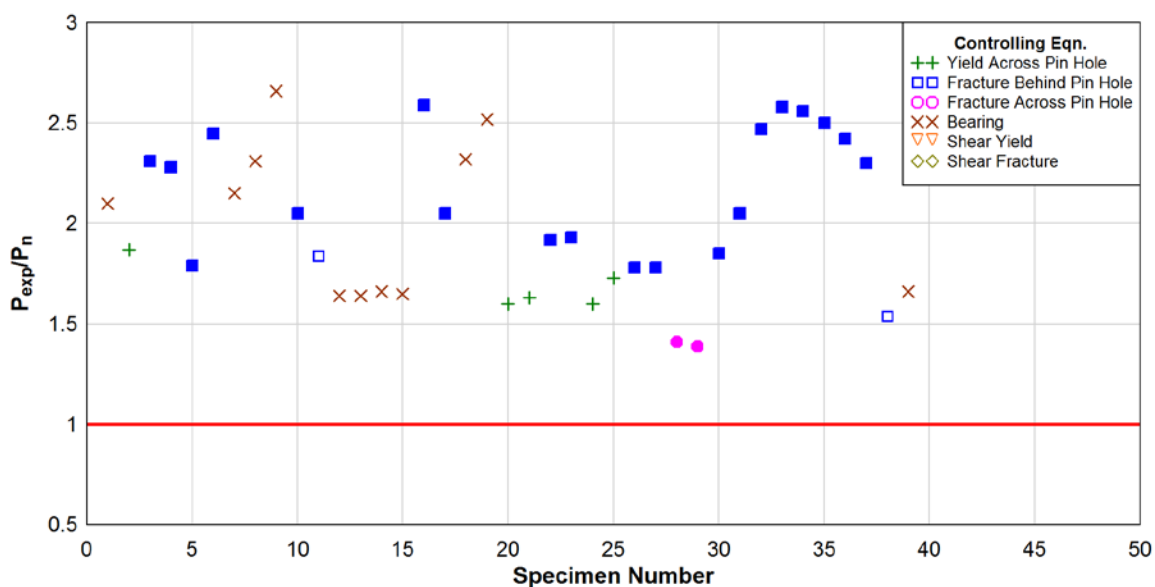


Figure 3-13: Ratio of measured and predicted strength for Caltrans LRFR methods with non-dishing specimens.

Table 3-4: Statistics for Caltrans rating methods.

	Caltrans' Method	P_{exp}/P_n Max	P_{exp}/P_n Min	P_{exp}/P_n Mean	COV	# of Specimens
All Data	LFR	2.66	0.95	1.54	26.5%	80
	LRFR	2.66	0.95	1.77	26.6%	
Dishing Data Excluded	LFR	2.66	1.10	1.65	21.2%	39
	LRFR	2.66	1.39	2.02	18.2%	

3.6 Analysis by Failure Mode

In this section, all of the ultimate strength prediction equations specific to a single failure mode were compared directly to specimens that failed in that failure mode. First, each prediction equation considered is used to predict the ultimate capacity of the applicable specimens. This predicted capacity (P_n) will then be compared to the experimentally determined ultimate capacity (P_{exp}) reported in the literature. The comparison of these two values are then used to determine the bias and COV for each method.

3.6.1 Failure Behind the Pin

For the purpose of this study the failure modes of pin tear out and splitting behind the pin hole were combined into a single failure mode: failure behind the pin. This combination was made for practical reasons, due to the lack of data necessary for them to be treated separately. Additionally, it was noted that these two failure modes seemed to behave very similarly. An example of this common behavior comes from Luley (1942) who conducted tests on two specimens (M7-1 and M7-2) of the same low alloy steel and with near identical dimensions (see Table 3-5). As can be seen in Figure 3-14, specimen M7-1 failed by splitting behind the pin hole while M7-2 failed in pin tear out. Additionally, a comparison of the ultimate load for both plates shows approximately the same maximum strength.

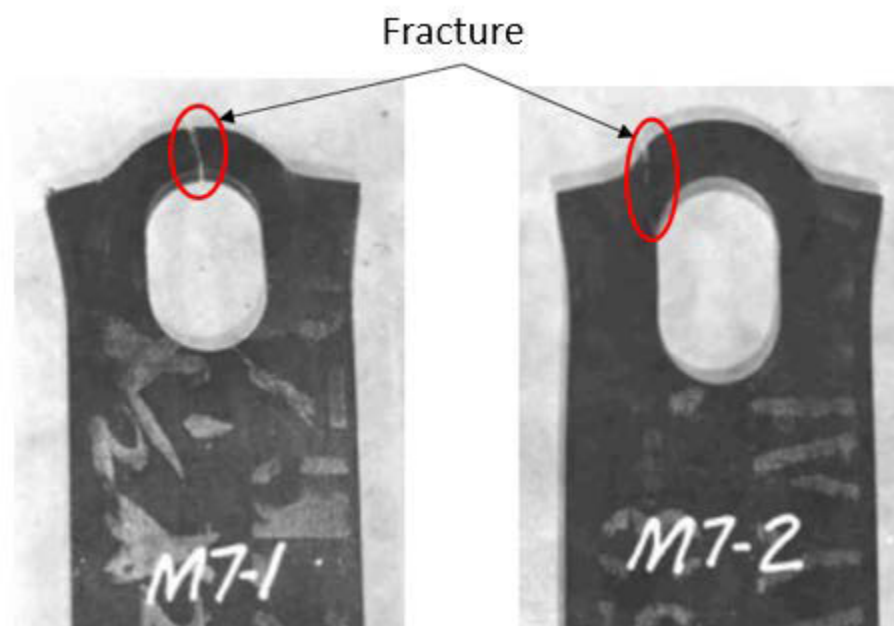


Figure 3-14: Splitting versus shear failure example (Luley, 1942).

Table 3-5: Example of similarity between splitting and shear failure behind the pin hole (Luley, 1942).

Specimen	a (in)	b_e (in)	D_p (in)	t (in)	F_y (ksi)	F_u (ksi)	P_{exp} (kips)
M7-1	1.02	1.49	2.0	0.508	55.5	77.3	82.8
M7-2	1.03	1.49	2.0	0.507	55.5	77.3	82.6

Given that these are only two specimens that may or may not be representative of hangers in general, further investigation was conducted into the other five hangers that were known to have failed in these limit states. Unfortunately, unlike in the example above from Luley (1942), a direct comparison between specimens was not possible given the varying material and dimensions between hanger plates. Instead of direct comparison the equations for splitting behind the pin and pin tear out from Duerr (2006) were used to

calculate the capacities of specimens that failed by splitting behind the hole and shear tear out. The results for this analysis can be seen in Table 3-6 and Table 3-7. This analysis shows that both equations predict ultimate hanger strength with reasonable accuracy, regardless of the whether the hanger failed by splitting behind the hole or pin tear out.

Table 3-6: Splitting specimens compared against splitting and tear out prediction methods.

Test Series	Specimen	P_{exp} (kips)	Duerr Splitting		Duerr Tear Out	
			P_n (kips)	P_{exp}/P_n	P_n (kips)	P_{exp}/P_n
Quebec Bridge (1919)	P5-2	145	176	0.82	199.0	0.73
Luley (1942)	S7-1	82.8	86.7	0.96	92.1	0.90
Luley (1942)	S7-2	82.6	86.6	0.95	91.8	0.90
Luley (1942)	M7-1	74.5	74.9	0.99	79.5	0.94

Table 3-7: Tear out specimens compared against splitting and tear out prediction methods.

Test Series	Specimen	P_{exp} (kips)	Duerr Splitting		Duerr Tear Out	
			P_n (kips)	P_{exp}/P_n	P_n	P_{exp}/P_n
Luley (1942)	C7-1	46.3	45.0	1.03	47.7	0.97
Luley (1942)	C7-2	46.8	45.1	1.04	47.9	0.98
Luley (1942)	M7-2	83.0	74.7	1.11	79.8	1.04

The predictive equations for both splitting and tear out were compared to the available data that are defined here as generally having failed behind the pin hole. The predictive equations analyzed in this section are shear fracture (Eqn. 3-4) and the fracture

behind the pin hole equation used in Caltrans' LRFR method (Eqns. 3-6 and 3-8). As discussed in the literature review, Johnston (1939) and Duerr (2006) both developed equations for failure behind the pin hole. The equations from these studies will be reiterated below for convenience. From Johnston (1939), the empirically derived equation:

$$P_n = F_u D_p t \left[1.13 \left(\frac{a}{D_h} \right) + \frac{0.92 \left(\frac{b_e}{D_h} \right)}{1 + \left(\frac{b_e}{D_h} \right)} \right] \quad (\text{kips}) \quad [3 - 9]$$

was developed to predict failure occurring behind the pin. In Duerr (2006), two (2) equations for failure behind the pin were developed. The first was intended specifically for pin tear out as:

$$P_{nto} = 0.7 A_{sp} F_u \quad (\text{kips}) \quad [3 - 10]$$

where A_{sp} is the area of the shear planes and is described in greater detail in section 2.4.1.8. Duerr's second equation, which was based on Johnston's, was intended specifically for splitting behind the pin as:

$$P_{ns} = F_u C_r t \left[1.13a + \frac{0.92(b_e)}{1 + \left(\frac{b_e}{D_h} \right)} \right] \quad (\text{kips}) \quad [3 - 11]$$

where the coefficient C_r is used to account for pin clearance and is equal to:

$$C_r = 1 - 0.275 \sqrt{1 - \frac{D_p^2}{D_h^2}} \quad [3 - 12]$$

Using these five (5) equations, the nominal capacities were calculated for the 25 specimens that failed behind the pin. The results are shown in Figure 3-15 with the data

sorted by according to their origin of study. The statistics for this analysis are summarized in Table 3-8.

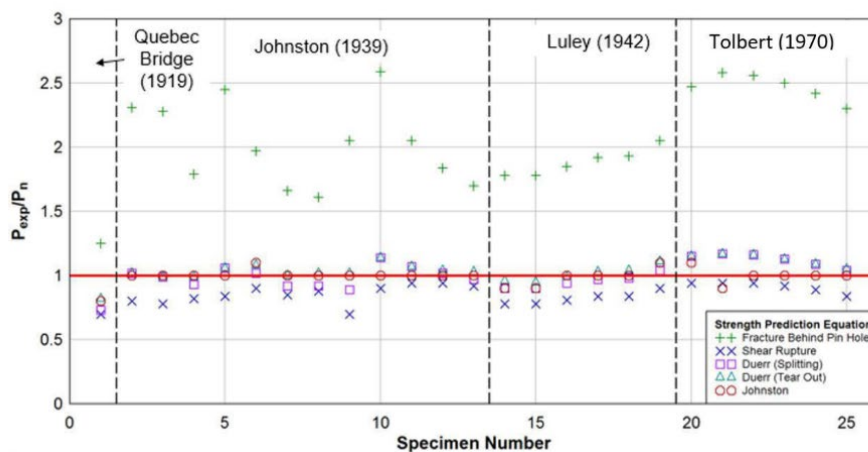


Figure 3-15: Ratio of measured and predicted strength for failure behind the pin prediction methods.

Table 3-8: Statistics for failure behind the pin prediction methods.

Prediction Equation	P_{exp}/P_n	COV
Fracture Behind the Pin Hole (Caltrans)	2.07	15.8%
Shear Rupture (Caltrans)	0.86	7.7%
Johnston	0.99	5.7%
Duerr -Splitting	1.01	5.6%
Duerr -Tear Out	1.01	10.4%

The Johnston and Duerr splitting equations performed the best, with bias close to 1.0 and reasonably low COVs. The shear rupture equation used by Caltrans produced a low COV, but it proves to be unconservative. The fracture behind the pin hole equation

used by Caltrans is very conservative but produced the largest variability of those investigated.

3.6.2 Fracture on Net Section

In this section the predictive equations for fracture across the pin hole are reviewed against the available data. Four equations were considered, including the fracture across the pin hole equation used in both Caltrans' LFR and LRFR methods (Eqn. 3-5). The second equation considered was the net section rupture from the AISC Specification for Structural Steel Buildings (AISC, 2016):

$$P_n = 2b_{e1}tF_u \quad (\text{kips}) \quad [3 - 13]$$

where b_{e1} is an adjusted effective width and given as the lesser of

$$b_{e1} = 2t + 0.63 \text{ in.} \leq b_e \quad (\text{in}) \quad [3 - 14]$$

From Johnston (1939) the equation:

$$P_n = 2b_e t F_u \frac{D_p}{D_h} \quad (\text{kips}) \quad [3 - 15]$$

will be considered. Finally, the equation from Duerr (2006) for net section rupture:

$$P_n = 2b_{e2} t C_r F_u \quad (\text{kips}) \quad [3 - 16]$$

where b_{e2} is an adjusted effective width and is given by:

$$b_{e2} = 0.6b_e \frac{F_u}{F_y} \sqrt{\frac{D_h}{b_e}} \leq b_e \quad (\text{in}) \quad [3 - 17]$$

and C_r is the same coefficient described by Eqn. 3-12. These predictive equations were compared to the fifteen specimens that failed in net section fracture (Figure 3-16 and Table 3-9).

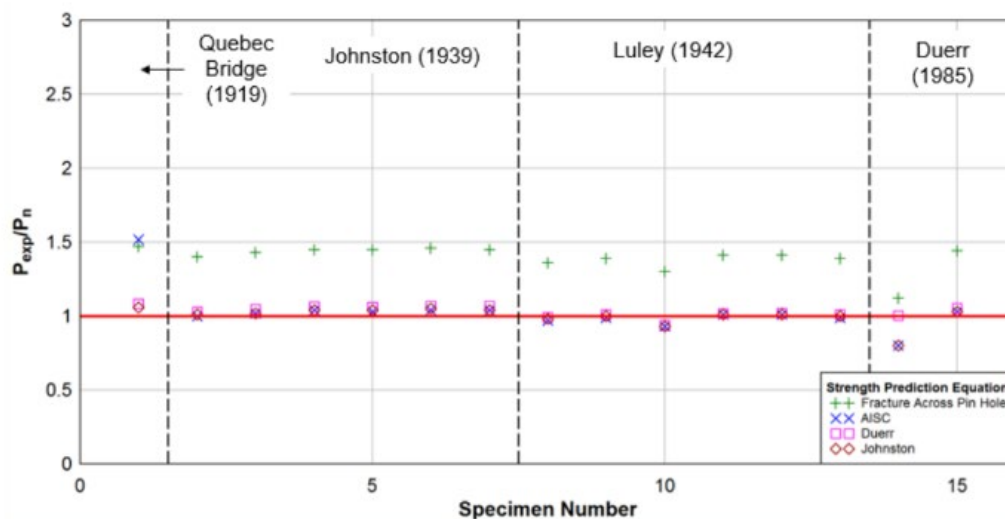


Figure 3-16: Ratio of measured and predicted strength for fracture on net section prediction methods

Table 3-9: Statistics for net section fracture prediction methods.

Prediction Equation	P_{exp}/P_n	COV
Fracture Across the Pin Hole (Caltrans)	1.40	6.4%
AISC	1.03	14.6%
Johnston	1.00	6.5%
Duerr	1.03	3.7%

A brief review of the prediction equations for fracture across the pin hole showed similar formats. Where these equations appear to differ was in the treatment of two variables: pin clearance and the effective net section. Due to the relatively tight pin clearances specified for actual bridge hangers, the treatment of pin clearance is not relevant here. The Caltrans' method divides the capacity of the plate by 1.4 which implies that only about 70% of the net section is considered active at ultimate strength. Figure 3-

16 shows that, in general, this assumption is conservative. For the AISC method, a review of the second specimen in Figure 3-16 (Quebec bridge (1919) specimen #2) provides some further insight. This specimen is the only one that had an effective section (b_{e1}) that was controlled by the plate thickness and was therefore less than b_e . The results for this specimen show that this adjustment to the effective net section may be overly conservative. Another interesting data point in Figure 3-16 was for the 14th specimen (specimen 1-A from Duerr and Pincus (1985), referred to here now as DP 1-A). The main significance of specimen DP-1A is that it is the only sample with steel plate having a high ratio of yield strength (F_y) to ultimate strength (F_u), F_y/F_u of approximately 0.9. Table 3-10 shows the results of DP 1-A compared to the average results for the all 15 specimens. This table shows that for this specimen there is a general drop in the P_{exp}/P_n value for all but the Duerr predictive equation. This is due to Duerr's adjustment to the effective area that takes into account the F_y/F_u ratio. Table 3-10 shows that only the Caltrans method and Duerr's method predict a capacity that is not greater than the experimental result. Given that Duerr developed his equation with consideration of this specimen, more investigation into high-yield plates may be necessary to verify Duerr's adjustment.

Table 3-10: Relative performance of specimen DP 1-A for alternate rating methods.

Prediction Equation	P_{exp}/P_n	$\frac{P_{exp}}{P_n}$	$\frac{P_{exp}/P_n}{\frac{P_{exp}}{P_n}}$
Fracture Across Pin Hole (Caltrans)	1.12	1.39	0.81
AISC	0.80	1.03	0.78
Johnston	0.80	1.00	0.80
Duerr	1.00	1.03	0.97

3.6.3 Dishing

Only two (2) methods for predicting the strength of specimens exhibiting dishing are identified in the literature. The first equation was empirically derived in Johnston (1939) as:

$$P_n = (20 + 315 \left(\frac{t}{D_h}\right) + 75 \left(\frac{tb_e}{D_h^2}\right) + 20 \left(\frac{a}{D_h}\right) - 20 \left(\frac{a}{D_h}\right)^2) D_p t \quad (\text{kip}) \quad [3 - 18]$$

The second was developed in Duerr (2006) and gave the dishing load as:

$$P_n = W_{eff} t F_{cr} \quad (\text{kips}) \quad [3 - 19]$$

where F_{cr} , the critical dishing stress, is equal to

$$F_{cr} = \left[\frac{1 - \frac{(Ka/r)^2}{2c^2}}{1 - \nu^2} \right] * F_y \quad (\text{ksi}) \quad [3 - 20]$$

for inelastic dishing and

$$F_{cr} = \frac{\pi^2 E}{(1 - \nu^2)(KL/r)^2} \quad (\text{kips}) \quad [3 - 21]$$

for elastic dishing. With W_{eff} , the effect dishing width, taken as the lesser of:

$$W_{eff} = D_p + a \quad (\text{in}) \quad [3 - 22]$$

and

$$W_{eff} = D_h + 1.25b_e \quad (in) \quad [3 - 23]$$

These prediction methods were compared to the 41 dishing specimens from the literature (Figure 3-17 and Table 3-11). A review of these results show that Johnston's equation significantly out performs Duerr's method. It is critical to note, however, that the only data considered in this review is either from Johnston's study or from the Quebec bridge study, which Johnston reviewed in his initial study. It should be of no surprise that an empirical equation performs well when compared to the data from which it was derived. Another concern regarding Johnston's equation, as described in Duerr (2006), is its poor performance against the results of Rex and Easterling (1996), whose specimens fall within the allowable proportions for this equation as described by Johnston. While the Rex and Easterling study was not considered in this analysis, due to relatively large pin clearances, the poor performance does raise the concern that Johnston's equation for dishing may not produce good correlation for variables outside the scope of the present data.

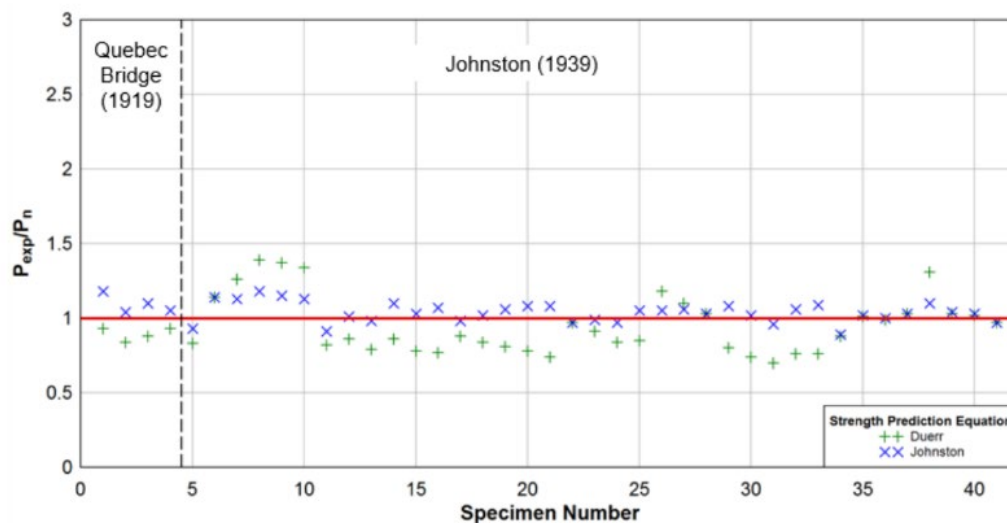


Figure 3-17: Ratio of measured and predicted strength for dishing prediction analysis.

Table 3-11: Statistical results for dishing prediction methods.

Prediction Equation	\bar{P}_{exp}/\bar{P}_n	COV
Johnston	1.04	6.5%
Duerr	0.94	19.7%

3.6.4 Dishing Proportional Limit

An alternative method for checking the dishing limit state is implied by the AASHTO Design provisions and discussed in Duerr (2006). This method involves limiting the proportional thickness of a plate in order to prevent dishing. The first proportional limit discussed was added to the AASHTO Standard Specifications in 1941 (AASHTO, 1941). This limit is directly stated in the specifications and restricts the ratio of the width of the net effective section across the pin hole ($2 * b_e$) to the plate thickness to a value less than or equal to 8:

$$\frac{2b_e}{t} \leq 8 \quad [3 - 24]$$

It should be noted that the specifications do not provide a reason for this limit nor does it mention dishing. But this requirement does limit the slenderness of a plate which appears to be a driving factor for dishing. Additionally, this requirement was added to the AASHTO Standard Specifications in the years immediately following Johnston's test series which investigated dishing extensively.

To investigate the effectiveness of this proportional limit on restricting dishing failure, the ultimate bearing stress of both specimens that failed by dishing and those that failed in other manners were plotted against their ratio of the width of the net effective section across the pin hole to the plate thickness ($2b_e/t$). This results is shown in Figure 3-18. This figure shows that all the specimens that failed in dishing exceeded the proportional limit. What this figure also shows is that many specimens that did not fail in dishing also failed to meet the proportional limit.

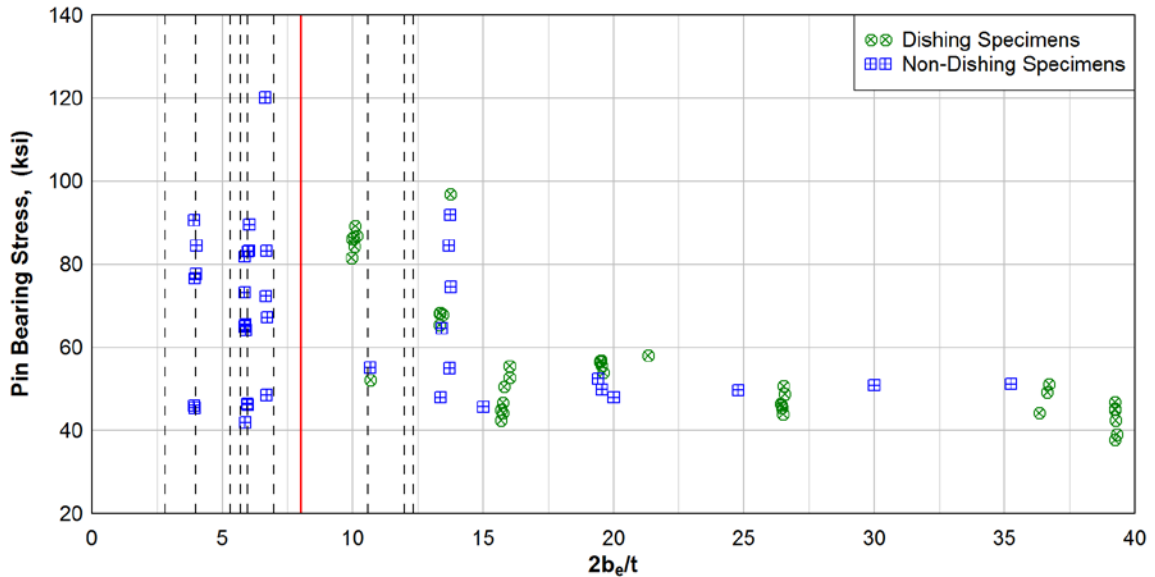


Figure 3-18: Effective width to thickness ratios compared to bearing stresses.

If the proportional limit discussed above is combined with the AASHTO requirement that the net area across the pin hole be equal to 140% of the area behind the pin hole, a proportional limit can be derived relating clearance behind the pin hole to plate thickness as:

$$\frac{a}{t} \leq 5.6 \quad [3 - 25]$$

This limit is appealing because, as noted in Johnston (1939), dishing appears to be more a factor of the section behind the pin rather than across the pin. As seen in Figure 3-19, this limit appears to differentiate better between dishing and non-dishing specimens. Though it is notable that three (3) specimens that met this limit still exhibited dishing.

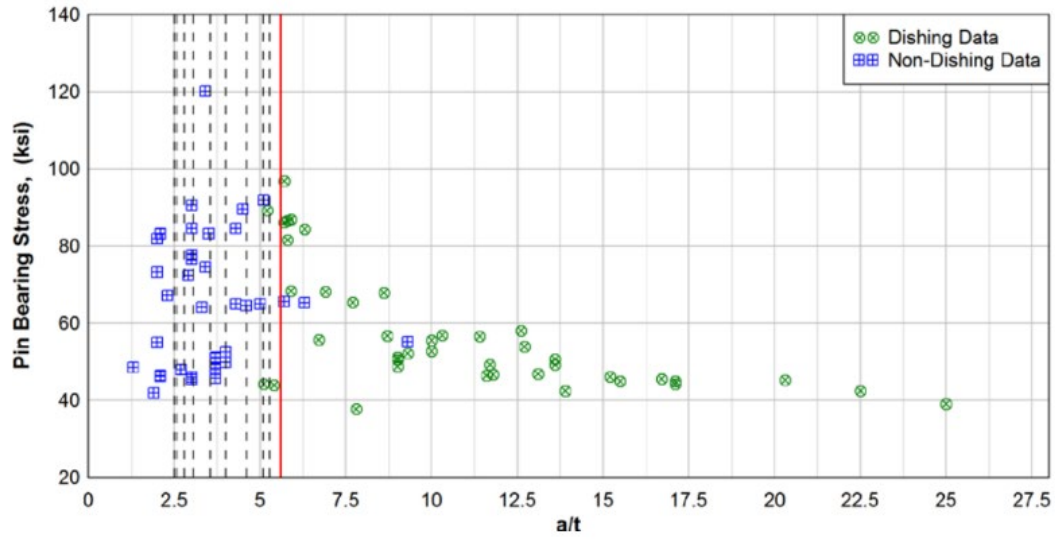


Figure 3-19: Dimension behind the pin to plate thickness ratios compared to bearing stresses.

Duerr (2006) suggest an alternate thickness limit based on the clearance behind the hole:

$$\frac{a}{t} < 0.19 \frac{D_p}{D_h} \sqrt{\frac{E}{F_y}} \quad [3 - 26]$$

This proposed limit is very similar to the implied limit from AASHTO seen above. In fact, if this limit is calculated for a hanger with negligible pin clearance and made from 33 ksi steel, it is found to be equal to the 5.6 implied by AASHTO. The main contribution of this new limit is the ability to account for higher steel plate yield stresses. This update makes this limit comparable to local buckling limits commonly seen for the webs and flanges of compression and flexural members. Figure 3-20 shows the performance of this limit by normalizing it (above 1.0, specimens exceed limit), and as seen here all but one of the specimens that meet the limit (below 1.0) do not exhibit dishing. The sole

specimen that met this limit but still exhibited dishing had a normalized slenderness of 0.99.

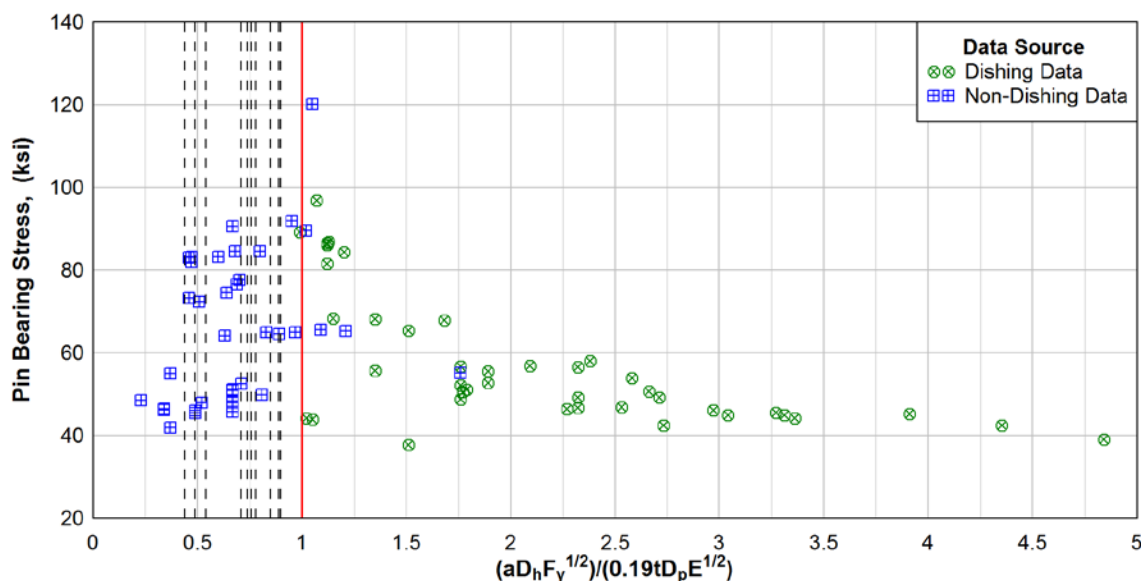


Figure 3-20: Normalized dimensions for plate behind pin from Duerr (2006) with bearing stress.

The vertical dashed lines in Figures 3-18 through 3-20 represent the proportions of the actual hangers representative of bridges in Caltrans inventory. Based on these figures it appears that dishing may not be an issue for the hangers within Caltrans inventory, but the provisions of Eqn. 3-26 can be used to identify potential for dishing in other cases.

3.7 Discussion

Based on this review it was determined that while Caltrans' current methods may be inaccurate and imprecise with regards to actual failure modes, they are consistently conservative for the available test data on hangers not susceptible to dishing. There are

better strength prediction equations for failure behind the pin and net section fracture failure modes.

For predicting failure behind the pin, the most accurate methods were determined to be the splitting equations presented by Johnston (1939) and Duerr (2006). Of the two methods used by Caltrans', the shear rupture (equation 3-4) is reasonably precise but frequently over predicts capacity. Caltrans' fracture behind the pin equation (equation 3-6 and 3-8) is conservative but relatively imprecise and inaccurate.

For prediction of net section fracture, Caltrans' method of reducing the net section by 30% appears overly conservative for most data considered here. However, for the only specimen with a high ratio of F_y to F_u , this reduction appears somewhat appropriate. Duerr (2006) appears to provide the most accurate method for determining net effective area for fracture on the net section.

The current prediction methods for the failure mode of dishing are either inaccurate or uncertain of broad applicability beyond the calibration data set. Proportional limits on the plate dimensions with respect to the material properties appear to be way to identify susceptibility to dishing. Based on the dishing limits described, none of the hanger plates in the inventory provided by Caltrans appear to be susceptible to dishing.

Chapter 4 – Calibration of Resistance Factors for LRFR

4.1 Introduction

In the load and resistance factor design and rating methodology, factors are applied to both the load effects and resistance of the element. The intent of these factors is to account for the uncertainty in these values and provide a uniform level of reliability in design and rating across materials, members, and connections. In order to achieve a specified level of reliability, these factors are calibrated. In this chapter, the process of calibration will be reviewed and resistance factors for the ultimate limit state equations reviewed in Chapter 3 will be calibrated for use in the LRFR methodology. The method of calibration used for this project was a one-sided calibration using a Monte Carlo simulation similar to that described in Ocel (2014). Prior to discussing the specific calibration process used for the present work, background is provided on probabilistic methods used for structural design. Next, the source and treatment of the statistical parameters used in calibration are discussed. Finally, the calibration process is described and the results are presented.

4.2 Load and Resistance as Random Variables

The fundamental assumption in probability-based design methods, such as the AASHTO LRFD, is that the resistance of an element and the load effect seen by that element are not deterministic, but instead are random variables. This assumption recognizes that during design an engineer cannot know exactly the magnitude and

distribution of load applied to the bridge during the lifetime or if a component is constructed with materials or methods so that it may be higher or lower than assumed. The variability of load and resistances can be described by their probability distribution functions (PDFs). An example probability distribution curve is shown in Figure 4-1. The total area under a PDF curve is equal to one as it describes all the possible variation in the population. To describe a PDF, and by extension the random variable, three properties are necessary: a distribution type, a mean value, and the standard deviation. The distribution type describes the shape of the PDF curve. In the example shown in Figure 4-1, the distribution type is a normal distribution, also called a Gaussian Distribution. The standard deviation describes the degree of variation in the parameter. An increased standard deviation, relative to the mean value, will shorten the height of the curve and make the curve wider. Conversely a small standard deviation relative to the mean will make the curve narrower. If the standard deviation were zero, the data would be deterministic. In order to perform a calibration of load and resistance factors, the distribution, mean value, and standard deviation of the random variables of load and resistance must first be identified. The process for identifying these values will be described in the following two sections.

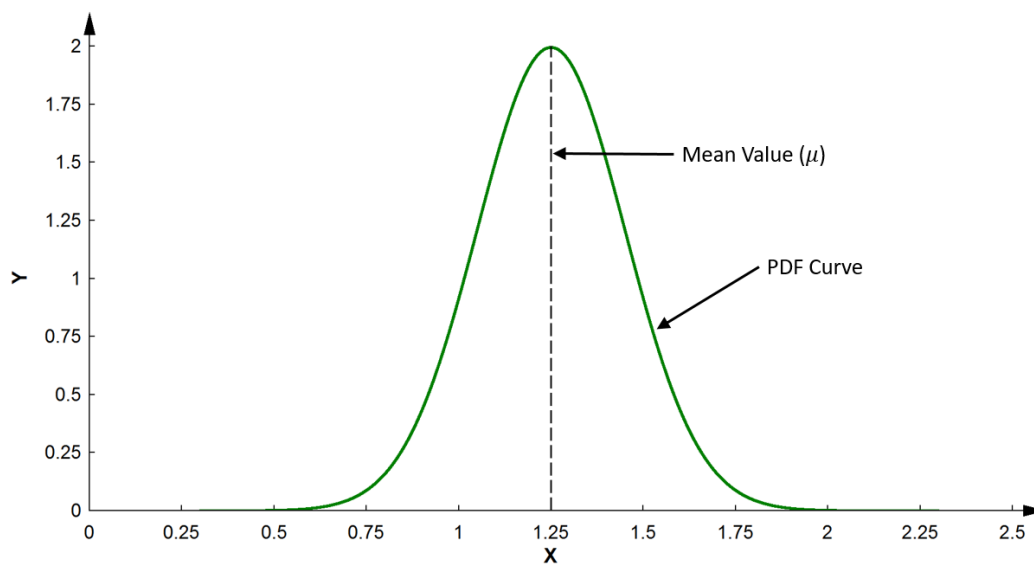


Figure 4-1: Random variable probability density function (PDF).

4.3 Load Variability

To model the load effect random variables, statistical properties that describe these variables were identified in the literature. These properties were used, along with information about the structure, to develop mean values and standard deviations for load effects in the calibration. This process is described in this section.

4.3.1 Load Statistical Properties

The final report for NCHRP Project 20-07, Task 186, referred to here as NCHRP 20-7/186, describes the strength limit-state calibration of the load and resistance factors used in the AASHTO LRFD Bridge Design Specifications (Kulicki et al., 2007). In this report the statistical parameters used for the original specification calibration and their origins are presented. These parameters are presented as biases (λ) and coefficients of

variation (*COV*). The bias of a distribution describes the difference between the nominal value and the mean value, while the coefficient of variation describes the standard deviation of a distribution as a percentage of the mean value. In addition to these values, the report states that these loads are often treated as normally distributed.

NCHRP 20-7/186 presents the biases and coefficients of variations for four types of dead load: factory made members, cast in place members, wearing surface and miscellaneous items. While for any single bridge, the total dead load will be comprised of elements that fall into each of these categories, it is understood that the majority of dead load on a bridge comes from the cast-in-place deck. For this reason, the bias and coefficient of variation for dead load used in this calibration was taken as that equal to the cast-in-place values from NCHRP 20-7/186 and reported in Table 4-1.

For live load, NCHRP 20-7/186 presents multiple ranges of biases that are dependent on the: type of load effect, the number of loaded lanes, and the average daily truck traffic (ADTT). For this project, the bias for the shear load effect was chosen because the connection plates are principally loaded by the end reaction of the suspended span girder which is effectively the end shear of the girder. An ADTT of 5000 was chosen to be consistent with the original LRFD Specification calibration which also used 5000 ADTT. Finally, the two lanes loaded case was chosen because this case typically produces the largest multi-lane bridge loading.

Table 4-1: HL-93 statistical live load parameters (Kulicki et al., 2007).

Moment or Shear	Number of Loaded Lanes	Bias Factor ADTT = 1000	Bias Factor ADTT = 5000	Coefficient of Variation
+ moment	1	1.23-1.36	1.26-1.38	0.12
	2	1.08-1.15	1.10-1.20	0.12
shear	1	1.17-1.28	1.21-1.32	0.12
	2	1.04-1.14	1.08-1.18	0.12
- moment	1	1.20-1.33	1.23-1.36	0.12
	2	1.10-1.22	1.14-1.26	0.12

To account for the addition of impact loading, the coefficient of variation was increased from twelve percent as shown in Table 4-1, to 18% as described in NHCPRP 20-7/186. The load statistical parameters taken from this report are summarized in Table 4-2.

Table 4-2: Load statistics used for calibration.

Factor	Bias (λ)	COV (V)
Dead Load (DL)	1.05	10%
Live Load and Impact ($LL + IM$)	1.13	18%

4.3.2 Load Mean and Standard Deviation

With the bias and COV identified, mean load effect values can be determined as:

$$\mu = \lambda * L_n \quad (kips) \quad [4 - 1]$$

where L_n is the nominal effect of the load under consideration, λ is the bias as described in the previous section and μ is the mean load value for use in calibration. Similarly, the standard deviation can then be determined by:

$$\sigma = \mu * COV \quad (kips) \quad [4 - 2]$$

where COV is the coefficient of variation from the previous section and σ the standard deviation of the load effect for calibration ($kips$).

Based on Eqns. 4-1 and 4-2 it is seen that nominal values for both live load and dead load are required prior to calibration. In the calibration of the original AASHTO LRFD load and resistance factors, nominal load values were determined by performing live load analyses on approximately 200 actual bridge designs (Kulicki et al., 2007). For the calibration of resistance factors for gusset plate connections presented in Ocel (2013), live load to dead load ratios were used to determine nominal load values. The use of live to dead load ratios is an effective method for the purpose of calibration because the value of total nominal load does not affect the reliability level. In calibration, the rating equation is always set so the factored resistance equals the factored load. This means that if the total nominal load is doubled, with load and resistance factors, as well as live to dead ratios held constant, the nominal resistance is also doubled creating no net change to the reliability. A change in the relative proportions of live and dead load on the other hand does affect the reliability due to the different bias, COV, and load factors connected to each type of load.

In this project, similar to Ocel (2013), live load ratios ($r_{LL:Q}$) were used to determine nominal loads for calibration. The live load ratio used in this project is defined as:

$$r_{LL:Q} = \frac{LL_n}{Q_n} \quad [4 - 3]$$

where LL_n is the nominal live load (including impact) (*kips*) and Q_n is the total nominal load (*kips*) and is equal to:

$$Q_n = LL_n + DL_n \quad (\text{kips}) \quad [4 - 4]$$

where DL_n is the nominal dead load (*kips*). For simplicity, the total nominal load was set to unity for all resistance factor calibrations. In an attempt to determine realistic bounds for dead and live load proportions, the ten bridges provided by Caltrans were reviewed to determine their live load ratio. The dead load was taken directly from the rating sheets provided by Caltrans with the wearing surface and miscellaneous dead loads lumped into a single value with the dead load of components. The live load was determined by performing live load analysis on each bridge using the HL-93 load model including impact. Where applicable, distribution factors for this analysis were determined using Table 4.6.2.2.3a-1 of the AASHTO LRFD Bridge Design Specifications (AASHTO, 2014). Where this table was not applicable (mainly for two girder bridges) the lever rule was used. Based on the analysis of these ten bridges, the live load ratios ranged from 0.25 to 0.85. Using the live load ratio discussed above and the assumed total nominal load of one, the nominal live load and dead load were determined through Eqns. 4-3 and 4-4. With the nominal value of both live load and dead load effects determined, the average values and standard deviations of both were determined using Eqns. 4-1 and 4-2, respectively.

4.4 Resistance Statistical Properties

Similar to the load effect produced on a member, the resistance of a member can also be treated as a random variable. Ravindra and Galambos (1978) describe the uncertainty in member resistance as a combination of three separate random variables. Each of these variables represent an independent source of uncertainty for a member. Using this concept, the resistance of a member can be represented using a simple production relationship as:

$$R = R_n * M * F * P \quad (kips) \quad [4 - 5]$$

where R is a random variable representing the actual resistance of a member ($kips$), R_n is the calculated nominal resistance of the member ($kips$), M , the material factor, is a random variable representing the uncertainty due to material properties, F , the fabrication factor, is a random variable representing the dimensional uncertainty due to fabrication tolerances, and P , the professional factor, is a random variable used to represent the uncertainty of the calculations used to estimate the resistance. These three random variables are described in the literature with different biases and COVs. This is convenient for code calibration because when the bias for each factor is inserted into Eqn. 4-5, along with the nominal value for resistance, the mean resistance is known. To determine the nominal resistance for calibration, the rating equation is set so that the factored resistance exactly equals the factored load. This equation can then be solved for R_n to give:

$$R_n = \frac{\gamma_{LL}LL_n + \gamma_{DL}DL}{\phi} \quad (kips) \quad [4 - 6]$$

where ϕ is an assumed resistance factor with a value between 0.05 and 1, though values below 0.6 are not typical.

The coefficient of variation for the member resistance was found using the method by Ravindra and Galambos (1978) as:

$$V_R = \sqrt{V_M^2 + V_F^2 + V_P^2} \quad [4 - 7]$$

where V_R is the coefficient of variation of the member's resistance and V_M , V_F and V_P are the COVs for the material, fabrication and professional factors, respectively.

For this project the fabrication and material factor values for bias and COV were taken from Elingwood (1980). These values are shown in Table 4-3. Because the ultimate strength of steel generally controls in these equations, the variability of ultimate strength was used for the material factor. For the fabrication factor a single set of statistics are given for hot rolled steel elements, because it is assumed that these plates are hot rolled these values were used. The bias and COV for the professional factor were developed by comparison of predicted strength to actual values as reported in Chapter 3 in Tables 3-8, 3-9 and 3-11.

Table 4-3: Resistance statistics used for calibration.

Factor	Bias	COV
Fabrication (F)	1.00	5%
Material (I)	1.05	11%

With the mean and COV defined for the resistance of an element, the remaining piece of information required for the resistance side of calibration is the distribution of resistance. In this study, the resistance distribution was assumed to be lognormal, a common assumption for resistance (Kulicki et al., 2007).

4.5 Reliability Index

While several methods exist to conduct calibration of load and resistance factors, the method used in this project was the Monte Carlo method. The calibration procedure was one-sided resistance factor calibration, similar to that conducted in Ocel (2013). This method calibrates resistance factors using the existing load factors in the specification. This method is advantageous because it prevents the development of additional, unnecessary load cases. The ultimate goal of this calibration is to produce resistance factors that provide uniform reliability with the remainder of the code. The level of reliability is typically described by the reliability index (β), which is defined as the number of standard deviations between the mean margin of safety and failure. An example of this is shown in Figure 4-2. Margin of safety is a random variable defined as:

$$Y = R - Q \quad (\text{kips}) \quad [4 - 8]$$

where R and Q are the random variables of resistance and total load effect, respectively.

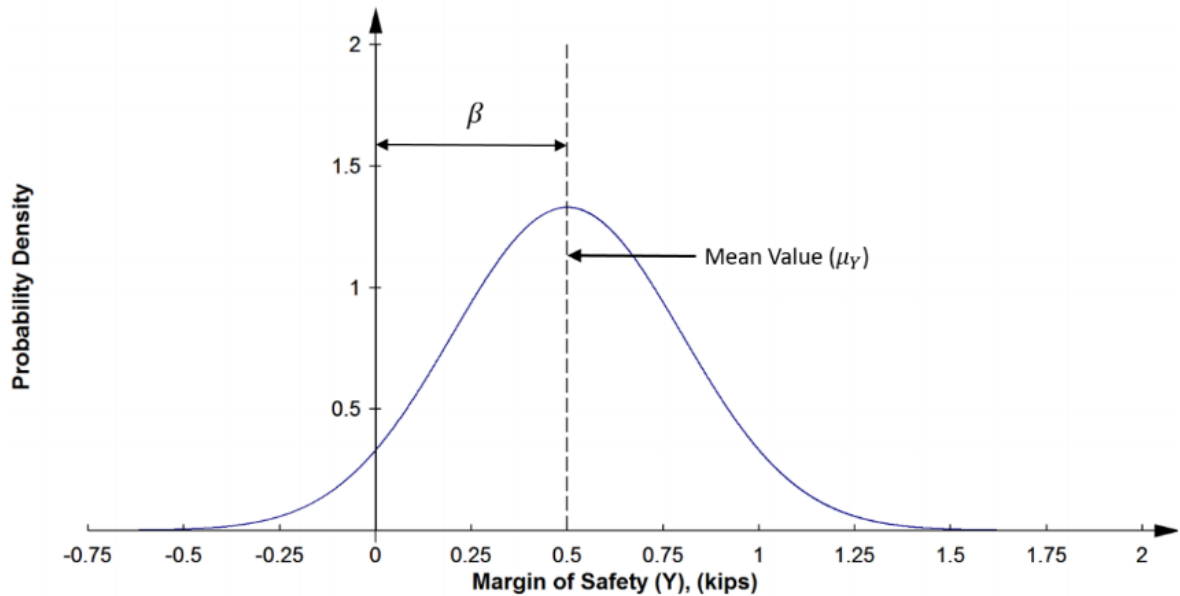


Figure 4-2: Example reliability index for a normal PDF.

The simplest method for determining the reliability index is to use the closed-form solution:

$$\beta = \frac{\mu_R - \mu_Q}{\sqrt{\sigma_R^2 + \sigma_Q^2}} \quad [4 - 9]$$

where μ_Q and μ_R are the mean values of load and resistance respectively, and σ_Q and σ_R are the standard deviations of load and resistance. This method proves only to be applicable if the load and resistance variables are both normally distributed or both lognormally distributed (Kulicki et al., 2007). Because both variables are not defined using the same distribution in the present case, a more robust method such as the Monte Carlo method is required.

4.6 Monte Carlo Simulation

In this section, the actual process of the Monte Carlo simulation technique is described. This process is based on that described in the NCHRP 20-7/186 (Kulicki et al., 2007). The first step in the Monte Carlo process is to define the nominal values for the resistance and loads. As discussed in Section 4.3.2, the nominal total load was set equal to one. Using Eqns. 4-3 and 4-4, the nominal live load and dead load were determined. The resistance factor was assumed and the nominal resistance was found using Eqn. 4-6. Next the average resistance was found using Eqn. 4-5.

Three (3) normally distributed random values X_1 , X_2 and X_3 were generated. In this project, these values were created using the two Excel functions RAND and NORMSINV. The first function creates evenly distributed random values between one and zero, and the second function converts these values into a standard normal distribution with a mean of zero and a standard deviation of one. Using one of these values a simulated value of dead load was determined as:

$$DL_1 = DL_n + \sigma_{DL}X_1 \quad [4 - 11]$$

Similarly, a value for the simulated live load was determined as:

$$LL_1 = LL_n + \sigma_{LL}X_2 \quad [4 - 12]$$

Because the member resistance is taken as lognormally distributed, the mean and standard deviation had to first be converted to lognormal values prior to using them in the calibration. The lognormal mean was determined as:

$$\mu_{lnR} = \ln(\mu_R) - \frac{1}{2} \sigma_{lnR}^2 \quad [4 - 13]$$

where σ_{lnR} is the lognormal standard deviation of resistance that is given by:

$$\sigma_{\ln R} = (\ln(COV_R^2 + 1))^{\frac{1}{2}} \quad [4 - 14]$$

Using Eqns. 4-13 and 4-14, a single value of simulated member resistance was determined as:

$$R_1 = e^{(\mu_R + \mu_R X_3)} \quad [4 - 15]$$

From these simulated load and resistance values, a margin of safety was calculated as:

$$Y_1 = R_1 - (LL_1 + DL_1) \quad [4 - 16]$$

A set of sample calculations was conducted for a single simulation and can be found in Appendix B.

This process was then repeated 100,000 times for each of the predictive equations at each live load ratio. These 100,000 values of Y were then ranked in ascending order and a Z value was calculated as:

$$Z = \frac{Rank}{\# \text{ of Simulations} + 1} \quad [4 - 17]$$

This Z value was then inserted into the inverse normal distribution function, NORMSINV, to calculate the standard normal value (Z_n). The margins of safety for these 100,000 simulations are plotted against their respective standard normal variables to produce a normal probability plot as shown in Figure 4-3. As describe in Allen et al. (2005) the value of Z_n when the Y equals zero is the negative value of the reliability index (β).

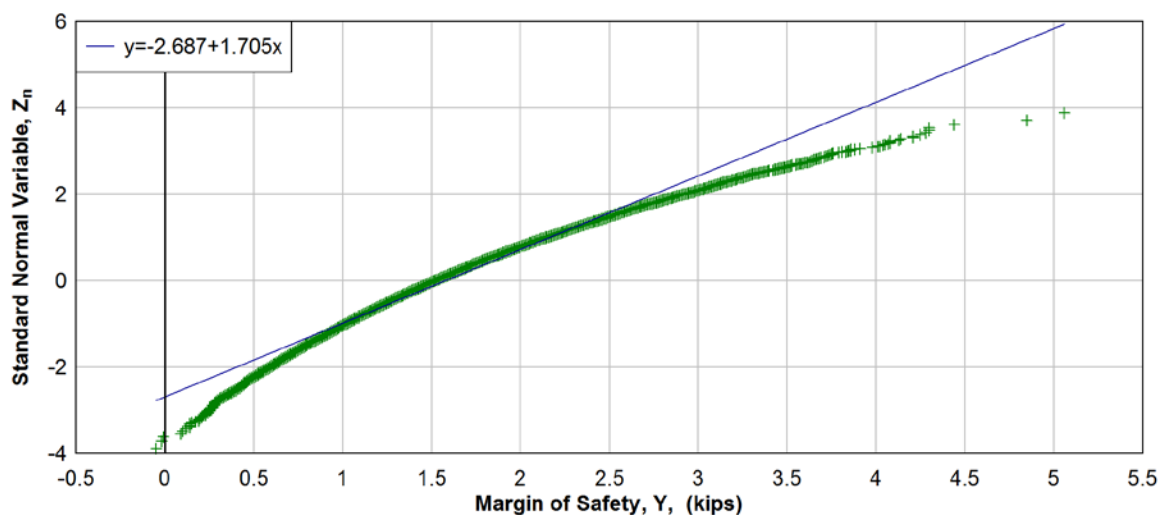


Figure 4-3: Example calibration probability plot using 100,000 simulations.

As can be seen in Figure 4-3 the values for the probability plot show a definitive curve and only a few values exist near failure ($Y = 0$). The curve in this plot is due to the contribution of the lognormal variable, had all variables been normally distributed, the points in this plot would be distributed in an approximately linear fashion. As discussed previously, the intent of producing this plot is to determine the approximate value of Z_n where $Y = 0$. Unfortunately, there are very few values in this tail of the graph and the values available show greater scatter. In order to determine a β without conducting excessive additional simulations, the lower ten percent of values were isolated from Figure 4-3. This lower tail was assumed to be approximately linear and a linear curve was fit to the data. The negative value of the y-intercept of this best fit line was then taken to be β . As can be seen in Figure 4-4 produces slightly conservative results.

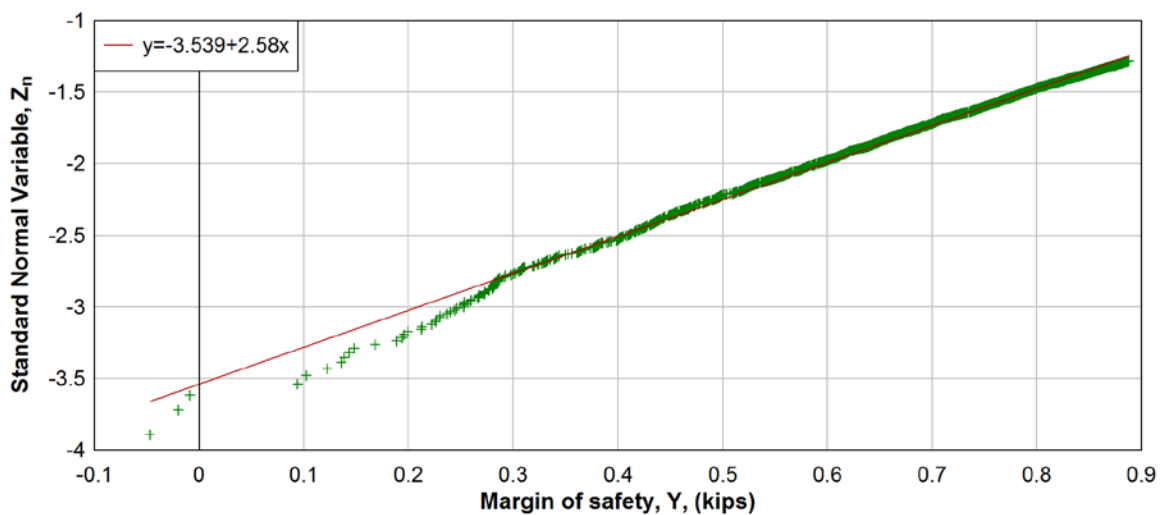


Figure 4-4: Example of best-fit line using lower 5% of data from Monte Carlo simulations.

If this analysis produced a reliability index near the target of 3.5, the assumed resistance factor was deemed acceptable and recorded. If the reliability index produced was deemed unacceptable, the resistance factor was changed and the process in this section was repeated until the reliability factor achieved near the target of 3.5.

4.7 Calibration Results

The process discussed in Section 4.6 was then conducted twice (once for each live load ratio) for each predictive equation considered. The resistance factors were chosen based on producing an average (between each live load ratio) reliability index of approximately 3.5. The calibrated resistance factors for each predictive equation are shown in Tables 4-4 through 4-6; additionally in these tables, the reliability indices are noted for each live load ratio along with the average.

Table 4-4: Calibrated resistance factors for failure behind the pin.

Prediction Equation	Resistance Factor (ϕ)		Reliability Index (β)		
	Existing	Calibrated	85% LLR	25% LLR	Avg.
Shear Rupture (Eqn. 3-4)	0.80	0.70	3.57	3.30	3.44
Fracture Behind The Pin Hole (Eqn. 3-6&8)	0.80	1.00	4.67	4.39	4.53
Johnston (Eqn. 3-9)	N/A	0.80	3.70	3.43	3.57
Duerr –Splitting (Eqn. 3-11)	N/A	0.80	3.84	3.66	3.75
Duerr -Tear out (Eqn. 3-10)	N/A	0.75	3.75	3.45	3.60

Table 4-5: Calibrated resistance factors for fracture on net section.

Prediction Equation	Resistance Factor (ϕ)		Reliability Index (β)		
	Existing	Calibrated	85% LLR	25% LLR	Avg.
Fracture Across Pin Hole (Eqn. 3-5)	0.80	1.00	4.21	4.07	4.14
AISC (Eqn. 3-13)	0.75*	0.70	3.66	3.39	3.53
Johnston (Eqn. 3-15)	N/A	0.80	3.72	3.48	3.60
Duerr (Eqn. 3-16)	N/A	0.85	3.72	3.52	3.62

*Resistance factor is based off of separate load factors, shown for reference only.

Table 4-6: Calibrated resistance factors for dishing.

Prediction Equation	Resistance Factor (ϕ)		Reliability Index (β)		
	Existing	Calibrated	85% LLR	25% LLR	Avg.
Johnston (Eqn. 3-18)	N/A	0.85	3.60	3.33	3.47
Duerr (Eqns. 3-19)	N/A	0.55	3.65	3.40	3.53

A review of these calibrated resistance factors brings up a few points. First, the AISC net section rupture equation has the smallest resistance factor for the fracture on net section equations. This low resistance factor is due to the relatively high COV for the professional factor, from the conservative treatment of the effective net section for wide plates. Outside of this treatment of effective net area, this equation is very similar to Johnston's. This highlights the influence of variability on the calibration process and the need to ensure that an analytical model is properly describing the strength across the relevant parameters rather than being applied to cases for which it was not intended.

As can be seen in Tables 4-4 and 4-5, fracture across the pin hole and behind the pin hole, both used by Caltrans, have reliability indices greater than 3.5. The high reliability indices for these equations are due to their resistance factors being capped at one. To achieve a reliability index of 3.5, these resistance factors would have to be larger than unity. These were artificially capped here because traditionally such factors are not taken greater than one.

Finally, the very low resistance factor for Duerr's dishing equation (Eqn. 3-19) shows that the present formulation is not sufficiently robust to be an used in bridge rating.

The better approach is to test for susceptibility to dishing based on the plate material and geometry, as described in Chapter 3. If the plate is susceptible to dishing, then further analysis would be needed.

Chapter 5 – Conclusion and Recommendations

5.1 Summary and Conclusions

In this study, the literature regarding pin and hanger connections for steel bridges was reviewed and summarized. Included in this literature review were current and historic design and materials specifications, reports describing assembly field performance, experimental studies on different elements within these assemblies, and material behavior related to mechanical wear. From this literature review the following conclusions are drawn:

- There is a lack of previous testing on large diameter pins to support the pin interaction equation given in the AASHTO LRFD Specifications.
- The provisions available in the AASHTO Specifications for the analysis of girder ends in pin and hanger assemblies are based on Euler-Bernoulli beam theory. Based on the complex and non-uniform stresses created by the concentrated load exerted by the pin, the application of these equations is questionable.
- There is a large body of information on hanger plates in the literature. This information includes data from several test series, identified failure modes, and ultimate strength prediction equations. There appears to be enough experimental data on hanger plates to evaluate and calibrate rating methods.

Based on the literature review, it was determined that there was only sufficient data on hanger plates for further analysis. The experimental data from the hanger plate

literature was then reduced to eliminate data that lacked sufficient details or had pin hole clearances exceeding AASHTO tolerances. There were 80 test results that satisfied the requirements for further use in the study. The experimental data were then compared to Caltrans reported representative inventory of bridge hanger plates. The data set was used to investigate the sufficiency of Caltrans' current LFR and LRFR methods for rating hangers. Alternative strength predictions from AISC (2016), Johnston (1939), Duerr (2006) and Caltrans's methods were evaluated relative to the empirical data for each failure mode. Finally, geometrical proportion and material properties were used to determine the susceptibility to dishing failure. From this analysis the following conclusions are drawn:

- The empirical data were smaller in size, but had relative proportions that were representative of in-service hanger plates. The materials also covered those of the in-service bridges. The available experimental data were regarded as representative of Caltrans' hanger plate inventory.
- There is limited experimental data for specimens with high ratios of F_y to F_u .
- Current Caltrans rating methods using LFR and LRFR were not able to predict the controlling failure mode, produced large bias and high variation. However, when dishing specimens are not considered, both methods provided conservative ratings.
- There are currently available methods that better predicted the ultimate strength for the failure modes of net section fracture and failure behind the pin.

- The current prediction methods for dishing failure produce high variability or may not apply beyond the limited data for which they were developed. They should not be used for bridge rating.
- The use of proportional limits based on the edge distance behind the pin relative to the plate thickness and material yield stress appear to effectively identify if a hanger is susceptible to dishing.

Resistance factors were calibrated for all of the prediction equations that described the failure modes identified in the literature. This calibration was conducted through Monte Carlo simulation using statistical information gathered from the literature and from the professional factors determined for each of the analysis methods considered. From this calibration the following conclusions are drawn:

- The calibration factors can be used for rating bridge hanger plates that is more fully consistent with the AASHTO calibration to provide uniform levels of reliability.
- New LRFR calibrated equations provide rating for the failure modes of net section fracture and failure behind the pin as a single failure mode at prescribed target reliability indices.
- The resistance factors were calibrated for inventory levels with target reliability indices of 3.5, and achieved target reliability indices near 2.5 for the operating level.
- The low resistance factor calibrated for dishing failure further indicated that it should not be used for bridge rating.

5.2 Recommendations for Future Work

For future studies, it is recommended that experimental studies be conducted on large diameter pins and beam ends with riveted pin plates. These tests should be instrumented to identify stress distribution throughout these elements. For large diameter pins, the study should be conducted in a manner to compare to the current specification interaction equation as described in Kulicki, (1983).

For hangers, further investigation is required to develop a robust prediction for dishing failures. For this development, finite element analyses could be used to analytically simulate buckling behind the pin. Due to the lack of data for high yield plates, additional experimental tests on hanger plates with high ratios of F_y to F_u is recommended if these are commonly encountered in practice. These would be particularly useful in evaluating the material property influence on net section fracture. Finally, while this study focused on the ultimate strength evaluation of these components, it was noted in the literature that hanger plates can undergo significant plastic deformation prior to failure (Johnston, 1939). Limited work has been conducted on this subject since Johnston's original study. Further investigation may be warranted if it is desired to make changes to Eqns. 3-1, 3-2, 3-3.

A recommended order for this work would be to investigate pins first, beam ends second, and develop dishing models as the final phase of research.

References

- Aalberg, A. (2015). "Experimental and numerical parametric study on the capacity of coped beam ends." *Journal of Constructional Steel Research*, 113, 146–155.
- AASHO (1931). *AASHO Standard Specifications for Highway Bridges and Incidental Structures*, 1st Ed., American Association of State Highway Officials, Washington, DC.
- AASHO (1935). *AASHO Standard Specifications for Highway Bridges*, 2nd Ed., American Association of State Highway Officials, Washington, DC.
- AASHO (1941). *AASHO Standard Specifications for Highway Bridges*, 3rd Ed., American Association of State Highway Officials, Washington, DC.
- AASHO (1944). *AASHO Standard Specifications for Highway Bridges*, 4th Ed., American Association of State Highway Officials, Washington, DC.
- AASHO (1949). *AASHO Standard Specifications for Highway Bridges*, 5th Ed., American Association of State Highway Officials, Washington, DC.
- AASHO (1953). *AASHO Standard Specifications for Highway Bridges*, 6th Ed., American Association of State Highway Officials, Washington, DC.
- AASHO (1957). *AASHO Standard Specifications for Highway Bridges*, 7th Ed., American Association of State Highway Officials, Washington, DC.
- AASHO (1961). *AASHO Standard Specifications for Highway Bridges*, 8th Ed., American Association of State Highway Officials, Washington, DC.
- AASHO (1965). *AASHO Standard Specifications for Highway Bridges*, 9th Ed., American Association of State Highway Officials, Washington, DC.
- AASHO (1969). *AASHO Standard Specifications for Highway Bridges*, 10th Ed., American Association of State Highway Officials, Washington, DC.
- AASHO (1973). *AASHO Standard Specifications for Highway Bridges*, 11th Ed., American Association of State Highway Officials, Washington, DC.
- AASHTO (2002). *AASHTO Standard Specifications for Highway Bridges*, 17th Ed., American Association of State Highway and Transportation Officials, Washington, DC.
- AASHTO (2011). *AASHTO Manual for Bridge Evaluation*, 2nd Ed., American Association of State Highway and Transportation Officials, Washington, DC.

- AASHTO (2014). *AASHTO LRFD Bridge Design Specifications*, 7th Ed., American Association of State Highway and Transportation Officials, Washington, DC.
- AISC (2016). *Specification for Structural Steel Buildings*, ANSI/AISC 360-16, American Institute of Steel Construction, Chicago, IL.
- AISC (2017). *Steel Construction Manual*, 15th Ed., American Institute of Steel Construction, Chicago, IL.
- Allen, T.M., Nowak, A.S., Bathurst, R.J., (2005). “Calibration to Determine Load and Resistance Factors for Geotechnical and Structural Design.” *Transportation Research Circular*, E-C079.
- Archard, J.F. (1953). “Contact and rubbing of flat surfaces.” *Journal of Applied Physics*, 24(8), 981-988
- Archard, J.F. (1980). “Wear theory and mechanisms.” *Wear Control Handbook*, edited by M.B Peterson and W.O. Winer, ASME, New York, N.Y., 35-80.
- AREMA (2015). *Manual for Railway Engineering*, 2015, American Railway Engineering and Maintenance-of-Way Association, Lanham, MD.
- Askeland D.R., Kisslinger F., Wolf W.R. (1987) “Investigation of Bridge Pin Failures”, Report number 87-1, Missouri Highway and Transportation Commission, Jefferson City, MO
- ASME (2006). *Design of below-the-hook lifting devices*, BTH-1-2005, American Society of Mechanical Engineers, New York, N.Y.
- ASTM (2009). G98-02 Standard Test Method for Galling Resistance of Materials, 2009, ASTM International, West Conshohocken, PA, 2009, <https://doi.org/10.1520/G0098-02R09>
- ASTM (2015). G40-15: Standard Terminology Relating to Wear and Erosion, ASTM International, West Conshohocken, PA, 2015. <https://doi.org/10.1520/G0040-15>
- ASTM (2016). G196-08 Standard Test Method for Galling Resistance of Material Couples, 2016, ASTM International, West Conshohocken, PA, <https://doi.org/10.1520/G0196-08R16>
- Blake, A. (1974). “Structural pin design.” *Des. News*, 29(2), 88–94.
- Blake, G.T. (1981), “Structural tests of large pin-connected links”, U.S. Steel Research, Monroeville, Pa.
- Brockenbrough, R.L. (2002). *Design Guide 15: Rehabilitation and Retrofit Guide*, American Institute of Steel Construction, Chicago, IL.

- Caltrans, (2004). *Bridge Design Specifications*. California Department of Transportation, Sacramento, CA.
- CEN. (2005). *Eurocode 3: Design of steel structures*. EN 1993-1-8, European Committee for Standardization (CEN), Brussels, Belgium, Part 1-8: Design of Steel Joints.
- Cheng J.J., Yura J.A, Johnson C.P (1984) “Design and Behavior of Coped Beams” PMFSEL Report No. 84-1, University of Texas at Austin, Austin, TX.
- Duerr, D. (2006), “Pinned connection strength and behavior.” *Journal of Structural Engineering*, 2006; 132 (2), 182-194.
- Duerr, D. (2008). “ASME BTH-1 Pinned Connection Design Provisions.” *Practice Periodical on Structural Design and Construction*, 13(2), pp.53-58.
- Duerr, D. and Pincus G. (1988), Deformation Behavior of Pinned Connections with Large Pin Clearance”, *Journal of Structural Engineering*, 114 (12), 2803-2807.
- Duerr, D., and Pincus, G. (1985). “Experimental Investigation of Pin Plates.” Research Rep. No. UHCE 85-3, Univ. of Houston, Houston, TX.
- Drucker, D.C., (1956). “The effect of shear on the plastic bending of beams.” *Journal of Applied Mechanics*, Dec. 1956, American Society of Mechanical Engineers, New York, N.Y.
- Ellingwood, B., Galambos, T.V., MacGregor, J.G., Cornell C.A., (1980). “Development of a Probability Based Load Criterion for American National Standard A58.” NBS Special Publication 577. U.S. Department of Commerce, Washington, DC
- Finch, K.J., Freeman, M.P. (1994). “NDT (UT) Inspection and Data Management for Bridge Pins and Trunnions” *Structural Material Technology: An NDT Conference.*, Scancelli R.J., Callahan M.E., Technomics, Chicago, IL, 257-260.
- Government Board of Engineers (1919). “The Quebec Bridge over the St. Lawrence River.” Vol. 1, Rep. of the Government Board of Engineers, Canada Department of Railways and Canals, Canada.
- Hodge, P.G. (1957). “Interaction curves for shear and bending of plastic beams.” Sept. 1957, American Society of Mechanical Engineers, New York, N.Y.
- Jansson, P.O. (2008), “Analysis of Stress Distribution in Link Plates Used for Suspended Bridge Beams” Research Report No. R-1517, Michigan Department of Transportation, Lansing, MI
- Johnston, B. G. (1939). “Pin-connected plate links.” *Transactions of American Society of Civil Engineers*, 104, 314–339.

- Juntunen, D. (1998), "Study of Michigan's Link Plate and Pin Assemblies", Research Report No. R-1358, Michigan Department of Transportation, Lansing, MI.
- Kulicki, J.M., (1983). "Load Factor Design Applied to Truss Members in Design of Greater New Orleans Bridge No. 2" *Transportation Research Record*, 903, Chicago, IL., 22-26.
- Kulicki, J.M., Prucz, Z., Sorgenfrei, D.F., Mertz, D.R., Young, W.T. (1990). *Guidelines for Evaluating Corrosion Effects in Existing Steel Bridges*, NCHRP Report 333, Transportation Research Board, Washington D.C.
- Kulicki, J.M., Prucz, Z., Clancy, C.M., Mertz, D.R., Nowak, A.S., (2007). "Updating the Calibration Report for AASHTO LRFD Code", NCHRP 20-7/186, Transportation Research Board, Washington D.C.
- Ludema, K.C., (1990). "Sliding and adhesive wear." *ASM Handbook: Volume 18 Friction, Lubrication, and Wear Technology*, ASM International, Materials Park, OH., 236-241.
- Luley, H. G. (1942), "Pin-connected plates, BSCE Thesis, Lehigh University, 1942." *Fritz Laboratory Reports*. Paper 1220.
- Melcon, M. A., and Hoblit, F. M. (1953). "Developments in the analysis of lugs and shear pins." *Prod. Eng. N.Y.*, 24(6), 160–170.
- Madsen, W.M., (1990). "Corrosive Wear." *ASM Handbook: Volume 18 Friction, Lubrication, and Wear Technology*, ASM International, Materials Park, OH., 271-279.
- Miller W.J. and M.K. Chaney (1994). "NDT of Bridge Pins on PennDOT Structures." *Structural Material Technology: An NDT Conference.*, Scancellia R.J., Callahan M.E., Technomics, Chicago, IL, 252-256.
- Moore, M., Phares, B.M., Washer, G.A. (2004). *Guidelines for Ultrasonic Inspection of Hanger Pins*, FHWA-HRT-04-042, Federal Highway Administration, Washington, D.C.
- NTSB, (1984). "Highway Accident Report – Collapse of a suspended Span of Interstate Route 95 Highway Bridge over the Mianus River" NTSB/HAR-84/03, National Transportation Safety Board, Washington, D.C.
- Ocel, J.M. (2013). "Guidelines for the Load and Resistance Factor Design and Rating of Riveted and Bolted Gusset-Plate Connections for Steel Bridges." National Academy of Sciences, Washington ,D.C.
- Ravindra, M.K., Galambos T.V. (1978). "Load and Resistance Factor Design for Steel." *Journal of the Structural Division*, Vol. 104, No. ST9, 1337-1353.

- Rex C.O., Easterling, (1996). S.W. "Behavior and Modeling of A single Plate Bearing on A Single Bolt." Report No. CE/VPI-ST 96/14, Virginia Tech University, Blacksburg, VA.
- Rigney, D. (1997). "Comments on the sliding wear of metals." *Tribology International*, 30(5), pp.361-367.
- South, J. M., Hahin C., Telford R.O., (1992) "Analysis, Inspection, and Repair Methods for Pin Connections of Illinois Bridges", Illinois Department of Transportation, Report No. FHWA/IL/PR-107. 1992.
- Suh, N.P., Jahamir, S., Abrahamson, E.P. (1974). The Delamination Theory of Wear Progress Report, AD/A-003 583, Office of Naval Research, Arlington, VA.
- Tolbert, R.N. (1970). "A Photoelastic Investigation of Lug Stresses and Failures." Vanderbilt University, Nashville, TN.
- Tolbert, R.N., and Hackett, R.M. (1974). "Experimental Investigation of Lug Stresses and Failures." *AISC Engineering Journal*, Vol. 11, No.2, 34-37.
- Trausmuth, A., Rodríguez Ripoll, M., Zehethofer, G., Vogl, T., and Badisch, E. (2015). "Impact of corrosion on sliding wear properties of low-alloyed carbon steel". *Wear*, 328-329, 338-347.
- Welsh, N. (1965). "The Dry Wear of Steels II. Interpretation and Special Features." *Philosophical Transactions of the Royal Society A: Mathematical, Physical and Engineering Sciences*, 257(1077), pp.51-70.
- Yam, M., and Chung, K. (2013). "A numerical study of the strength and behavior of reinforced coped beams". *Journal of Constructional Steel Research*, 80, 224-234.
- Yam, M., Lam, A., Iu, V. and Cheng, J. (2003). "Local Web Buckling Strength of Coped Steel I Beams." *Journal of Structural Engineering*, 129(1), pp.3-11.
- Yam, M., Fang, C., Lam, A. and Cheng, J. (2014). "Local failures of coped steel beams — A state-of-the-art review." *Journal of Constructional Steel Research*, 102, pp.217-232.

Appendices

Appendix A – Historic Steel Specification (Brockenbrough, 2002)

Appendix B – Example Calibration Simulation